

INFORMATION TO USERS

This reproduction was made from a copy of a manuscript sent to us for publication and microfilming. While the most advanced technology has been used to photograph and reproduce this manuscript, the quality of the reproduction is heavily dependent upon the quality of the material submitted. Pages in any manuscript may have indistinct print. In all cases the best available copy has been filmed.

The following explanation of techniques is provided to help clarify notations which may appear on this reproduction.

1. Manuscripts may not always be complete. When it is not possible to obtain missing pages, a note appears to indicate this.
2. When copyrighted materials are removed from the manuscript, a note appears to indicate this.
3. Oversize materials (maps, drawings, and charts) are photographed by sectioning the original, beginning at the upper left hand corner and continuing from left to right in equal sections with small overlaps. Each oversize page is also filmed as one exposure and is available, for an additional charge, as a standard 35mm slide or in black and white paper format.*
4. Most photographs reproduce acceptably on positive microfilm or microfiche but lack clarity on xerographic copies made from the microfilm. For an additional charge, all photographs are available in black and white standard 35mm slide format.*

***For more information about black and white slides or enlarged paper reproductions, please contact the Dissertations Customer Services Department.**

U·M·I Dissertation
Information Service

University Microfilms International
A Bell & Howell Information Company
300 N. Zeeb Road, Ann Arbor, Michigan 48106

8617442

Ganapathy, Nirmala

VOLUME CONDUCTED CURRENTS AND POTENTIALS FROM EXCITABLE
CELLS OF CYLINDRICAL GEOMETRY

Rice University

Ph.D. 1986

University
Microfilms
International 300 N. Zeeb Road, Ann Arbor, MI 48106

RICE UNIVERSITY

VOLUME CONDUCTED CURRENTS AND POTENTIALS FROM EXCITABLE CELLS
OF
CYLINDRICAL GEOMETRY

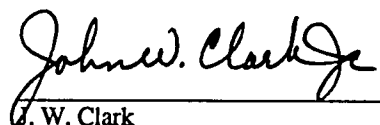
by

NIRMALA GANAPATHY

A THESIS SUBMITTED
IN PARTIAL FULFILLMENT OF THE
REQUIREMENTS FOR THE DEGREE

DOCTOR OF PHILOSOPHY

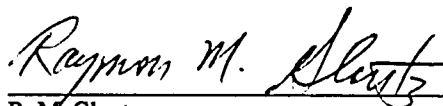
APPROVED, THESIS COMMITTEE:



J. W. Clark
Professor of Electrical & Computer
Engineering, Chairman



R. J. P. deFigueiredo
Professor of Electrical & Computer
Engineering & Mathematical Sciences



R. M. Glantz
Professor of Biology

HOUSTON, TEXAS

APRIL, 1986

ABSTRACT

Volume Conducted Currents and Potentials from Excitable Cells of Cylindrical Geometry

by

Nirmala Ganapathy

The dissertation deals with the evaluation of currents and potentials from a variety of excitable cells of cylindrical geometry. Specifically, the cells considered are the unmyelinated and myelinated nerve fibers and the active skeletal muscle. The electrical behavior of these cylindrical cells is modeled in terms of a distributed parameter network resulting in a parabolic partial differential equation describing the propagation of electrical activity along the cell. The partial differential equation is numerically integrated using an implicit, finite difference technique, the Crank-Nicholson method. The immediate environment of the cell is characterized by an electromagnetic field theory model, the result of solving Laplace's equation in the medium around the cell. The field theory model is treated as an equivalent filtering problem, the one and two dimensional Fourier transforms being used to perform the resulting linear convolution. Conduction under normal and diseased states is investigated for the myelinated nerve fiber, and attempts are also made to simulate complex motor unit action potentials from motor units consisting of several individual skeletal muscle fibers.

A rigorous evaluation of the core conductor model of a single active nerve fiber and its distributed electrical equivalent circuit is undertaken, based on principles of electromagnetic field theory. The core conductor model is found to be a fairly inaccurate representation of events in the extracellular medium except in cases where the volume conductor is extremely small in extent. On the other hand, the core conductor model is a very good representation of electrical events occurring in the intracellular medium.

It is possible to reconstruct the extracellular currents and potentials of the myelinated nerve fiber as functions of time using a simple and efficient filter theory approach. The resulting currents and potential waveform correspond well with experimental values in literature. The effects of slowed con-

duction are seen in the transmembrane potential, the transmembrane current, the external longitudinal current and the calculated extracellular potential waveforms. Also simulated is the experimental technique that is used to measure currents in practice. The results of the simulation indicate that electrode separation and placement are critical factors when such measurements are made. Decreasing the extent of volume conductor makes these factors less critical.

A technique for evaluating extracellular potentials from either a single active muscle fiber or an active motor unit, located in a finite, anisotropic volume conductor is also demonstrated in this work. The motor unit may also have an arbitrary distribution of component fibers, and these fibers may be activated either synchronously or asynchronously with an arbitrary excitation pattern. The model is shown useful in the prediction of surface electromyographic (EMG) waveforms due to the activity of bioelectric sources lying within the anisotropic muscle medium that comprises the volume conductor. As such, this field theoretic model represents a first approximation to the study of multifiber activity and its contribution to surface EMG.

ACKNOWLEDGEMENTS

I wish to express my sincere thanks to Dr. John Clark without whose constant guidance and supervision this work would never have been accomplished. I also wish to thank Dr. Sidney Burrus, Chairman of the Electrical and Computer Engineering department whose timely help was of great value to me. My thanks are also due to the many professors and students of the Electrical and Computer Engineering department who were always ready to answer my questions and lend me their help. Most specially, I am very grateful to Dr. Owen Wilson and Ms. Keri Hicks, discussions with whom proved very valuable.

I also wish to express my gratitude to Ms. Nora Quioco, Ms. Idalia Cuellar, Ms. Victoria Benson and Mr. Donald Schroeder for all the help they have given me from time to time. Most of all my heartfelt gratitude go to my parents, Mr. and Mrs. Ganapathy and my sister, Ms. Prabha Ganapathy for all the love, patience, hope and encouragement they have always bestowed on me and without which I would never have accomplished anything.

Table of Contents

Introduction	1
CHAPTER 1 : Mathematical Formulation of the Problem	
1.1 Introduction	5
1.2 Potential Field of the Single Active Fiber centrically located in a finite volume conductor	7
1.3 Volume Conductor Currents Associated with the Core Conductor Model	12
1.4 Discrete Fourier Methods of Solution for Cable Equation Variables	18
1.5 Models for the Active Source Fiber	19
1.6 Summary	23
CHAPTER 2 : Evaluation of the Core Conductor Model for Active Nerve Fibers	
2.1 Introduction	24
2.2 Modeling Aspects	24
2.3 Computational Aspects	28
2.4 Results	35
2.5 Discussion of Results	47
CHAPTER 3 : Currents and Potentials of the Active Myelinated Nerve Fiber	
3.1 Introduction	54
3.2 Modeling Aspects	55
3.3 Computational Aspects	58
3.4 Results	60
3.5 Discussion of Results	81
CHAPTER 4 : Extracellular Potentials from Skeletal Muscle	
4.1 Introduction	83
4.2 Modeling Aspects	83
4.21 Potential in a finite volume conductor	83

4.22 Discrete Fourier Methods of Solution	91
4.3 Computational Aspects	92
4.4 Results	100
4.41 Single Fiber Studies	100
4.42 Multiple Fiber Studies	106
4.5 Discussion of Results	115
CHAPTER 5 : Conclusions and Future Extensions of the Model	116
APPENDIX I : An Improved Source Description of the Active Myelinated Nerve	118
A1.1 A modified network model for the myelinated fiber	120
A1.2 A compartmental model for the myelinated fiber	127
APPENDIX II : Source Code of Major Computer Programs	131
BIBLIOGRAPHY	159

Introduction

It is a well established fact that all living creatures are made up of cells. The simplest organisms of our world are unicellular while higher organisms such as mammals are the result of a complex interaction between several types of cells, each of which is assigned a specific task to perform. Cells can communicate with each other by subtly altering the environment around them either chemically or electrically. Cells that are capable of generating action currents around them may be termed "excitable cells". Such cells fall into two broad categories namely nerve cells and muscle cells. As early as 1786 Galvani's famous experiments on frog legs had demonstrated the presence of electric currents around nerve and muscle fibers [Green, 1953]. Galvani wrongfully attributed his findings to animal electricity stored in the muscles. It was only fifty years or more later that experiments were performed that showed a correlation between changes in the cell membrane resting potential and the changes in the currents flowing in the fluid around the cell [Bernstein, 1871]. In 1879 Hermann proposed what is now the celebrated core conductor model in an attempt to account for the electrical phenomena in excitable cells in terms of a mathematical model.

The cells that can be modeled using the core conductor model are elongated cells, cells that have one dimension which is considerably larger than their other dimensions. These cells may be viewed as cylindrical structures where the length of the cylinder is nearly infinite when compared with the radius of the cylinder. Long muscle and nerve cells may be justifiably approximated by this geometrical abstraction. The classical core conductor model assumes that these cylindrical cells possess a uniform, homogeneous, isotropic core of intracellular fluid, whose electrical properties are completely defined by its specific conductivity (S/cm). The conductive fluid core is enclosed within a surface membrane whose electrical description is in terms of a specific capacity in $\mu F/cm^2$ and specific conductivity in S/cm^2 . The uniform, homogeneous and isotropic medium outside the cell, the so called volume conductor medium, is also characterized by its specific conductivity. Such a characterization of the cell leads to a cable-like network of the cell where the intra- and extracellular media are represented by

lumped resistances whose value is only dependent on the geometry and specific conductivity of the media, with the membrane forming the shunt element between the resistances representing the two regions. One such network is illustrated in fig. 1.1 of chapter 1. Implicit in this characterization of the intra- and extracellular media by lumped resistances, depending only on the volume and resistivity of the region being characterized, is the assumption that the current flow both inside and outside the cell is purely axial.

In the first quarter of the twentieth century a powerful electronic device was invented which made it possible to experimentally record action potentials and their spread in volume conductors. This device was the vacuum tube amplifier which enabled researchers to extract and amplify small biological signals emanating from nerve and muscle cells. Craib and Canfield (1927) pioneered such work by studying heart and skeletal muscle immersed in a saline solution. Their results showed the tri-phasic nature of the action potential in the volume conductor. Several investigators followed in their wake, studying different experimental preparations under a variety of experimental conditions. Lorente de No (1947) studied the frog sciatic nerve in situ, Tasaki and Tasaki (1950) recorded action potentials from a toad motor nerve fiber in a thin layer of Ringer, Buchthal and his group (1957, 1962, 1966) did an extensive study of small bundles and single fibers of human muscle, and the list goes on and on.

The explanations that were given to account for the experimental results made use of the core conductor model and the resulting cable equations. Another quantitative description of the spread of the action potential was the classical account of Lorente de No (1947) that modeled the biological source as a dipole generator. A more elegant formulation of a mathematical description of the cylindrical equivalent cell and its immediate environment can be obtained on applying the principles of electromagnetic field theory. Such a formulation is the analysis of Clark and Plonsey (1966, 1968) for the single unmyelinated axon. A drawback of this formulation is the necessity of specifying all potential distributions as functions of the spatial variable z rather than in the conventional manner as functions of time. This could be difficult in situations where the action potential does not propagate with a constant propagation velocity. The present work seeks to rectify this drawback and to investigate the

effects of the various assumptions implicit in the different forms of mathematical models used to provide explanations for experimentally observed phenomenon in excitable cells that could be said to conform to a cylindrical geometry.

This thesis is an investigation of the volume conducted currents and potentials from three types of excitable cylindrical cells, namely the unmyelinated nerve fiber, the myelinated nerve fiber and the skeletal muscle fiber. First, a detailed analysis of the core conductor model is performed for both myelinated and unmyelinated nerve fibers. This is done using a three dimensional field theory description of the currents and potentials around a cylindrical cell in a finite volume conductor. The spatial distributions of the potentials are explicitly calculated by solving the partial differential equations describing propagation along a fiber and Chapter 1 provides a detailed description of the mathematical techniques used in this process. Chapter 2 contains the analysis of the one dimensional core conductor model where the effects of the volume conductor extent on the assumptions of the core conductor model are also examined. The time waveforms for the currents and potentials may also be reconstructed from the values calculated by the field theory model. This is done in chapter 3 for the myelinated fiber where the velocity of propagation is definitely non-uniform and this necessitates the utilization of special temporal reconstruction techniques. Also in chapter 3, experimental techniques of measuring extracellular currents and potentials are simulated and possible sources of error are pointed out. In the same chapter a brief investigation is also carried out on the effects of slowed conduction induced by the demyelination of a single node, on the extracellular currents and potentials.

Chapter 4 is an investigation of the extracellular potentials from skeletal muscle. The field theory model employed, is one that permits an arbitrary location of the source within a cylindrical volume conductor. Here an attempt is made to simulate a surface electromyogram recorded from a muscle containing a single active motor unit consisting of nine identical skeletal muscle fibers. The effects of anisotropy of the medium and the results of synchronized and desynchronized firing of the individual fibers of the motor unit are also investigated. Chapter 5 both summarizes the work done here and suggests feasible extensions. Finally, an initial attempt to postulate a more complete mathematical model describing the myelinated nerve fiber is also made, the proposed form of the

model along with the mathematical equations that describe it being specified in Appendix I. Such a model would be required before a detailed study into topics such as slowed conduction in the myelinated nerve could be undertaken.

CHAPTER 1

Mathematical Formulation of the Problem

1.1 Introduction

The classical core conductor model of Hermann (1879) and its distributed electrical equivalent circuit model are very fundamental concepts in the area of nerve electrophysiology, where they are used to explain both the passive and active properties of a cable-like nerve fiber lying within a cylindrical volume conductor. Theoretician and experimentalist alike, have called upon the logic of this model in many practical situations to explain observed phenomena. In this project the core conductor model and the celebrated cable equations that are derived from its electrical equivalent circuit are revisited, for a rigorous evaluation of these equations based on the principles of electromagnetic field theory; a procedure that is greatly facilitated by the Fourier transform approach introduced earlier by Clark and Plonsey (1966) and made fast, efficient and practical by means of the discrete Fourier Transform (DFT) approach of Greco and Clark (1977). The associated volume conductor field problem is viewed as an equivalent filter problem, so that many variables of interest in the core conductor model may be easily calculated using the DFT approach, including those that are not frequently measured such as transmembrane current per unit length ($i_m(z)$) and total longitudinal current ($I_L(z)$). An earlier mathematical analysis of the core conductor model was made by Clark and Plonsey (1966), however the computational methods employed were laborious, the external bathing medium of the fiber was assumed to be of infinite extent and only the case of the unmyelinated nerve fiber was investigated. These conditions are rectified in the present study and conclusions are drawn regarding the accuracy of the cable equations, particularly as they are applied to the extracellular medium of the fiber. The DFT approach greatly simplifies the calculation of all field quantities involved, making it a useful tool in problems where a cable equation analysis is justifiably performed.

The study of currents and potentials in and around active myelinated nerve fibers is also a subject of great interest in electrophysiology. The effects of demyelination on the nerve fiber's ability to conduct an action potential and the nature of conduction after the myelin sheath grows back some days after the nerve fiber is demyelinated, are but a few of the many aspects of myelinated nerve fiber conduction that are studied using extracellular current and potential measurements from an excised fiber situated in a finite volume conductor (Paintal (1965), Paintal (1966), Rasminsky & Sears (1972), Bostock & Sears (1978), Bostock (1983)). As stated before, the model based on the principles of electromagnetic field theory, can be utilized to rapidly and accurately calculate the potential and current density distribution, everywhere in the finite cylindrical volume conductor bathing the active nerve fiber. The input data required for the calculation consists of the transmembrane potential distribution $\Phi_m(z)$ and the specific conductivities of the intra- and extracellular media. Simulated transmembrane potential data, the result of solving the partial differential equations associated with the distributed parameter model of the myelinated nerve fiber is employed in this theoretical study into the nature of the potentials and currents flowing around the single myelinated fiber under conditions of normal and abnormal conduction.

The study of extracellular potentials from an active muscle fiber in a muscle bundle is of considerable interest in the area of electromyography. In this project an active skeletal muscle fiber is also modeled as a distributed parameter model of resistive and capacitive elements, and the transmembrane potential distribution across the cell membrane of the fiber is obtained using an implicit numerical integration technique for the solution of the parabolic partial differential equation associated with the cable-like model of the fiber. Once again the extracellular potentials are evaluated using a field theory model. In this case however, the fiber is treated as lying eccentrically in a finite muscle medium volume conductor and a two-dimensional Fourier transform technique is employed.

More than one fiber may be active in the muscle at any time and the resulting potential at a field point on the surface of the muscle may be evaluated using principles of superposition. Variation in the time of activation of the various muscle fibers within the muscle would lead to desynchronization of the components of the compound action potential recorded at the surface of the muscle. The effects of

multiple fibers being active at slightly different times are studied in this work using a muscle consisting of nine individual muscle fibers. The muscle fibers considered are all assumed to be characterized by the same geometrical and electrical parameters and belong to the same motor unit.

1.2 Potential Field of the Single Active Fiber centrically located in a finite volume conductor

In the core conductor model an idealized, infinite circular cylindrical axon of radius a and specific axoplasmic conductivity σ_i , is located centrically in a finite, homogeneous volume conductor of radius b and specific conductivity σ_o . This is shown in fig. 1.1. The general form of the solutions to Laplace's equation in the intracellular and extracellular media under conditions of quasistationarity are :

$$\Phi^i(\rho, z) = \frac{1}{2\pi} \int_{-\infty}^{\infty} A(k) I_0(|k|\rho) e^{-jkz} dk \quad \rho < a \quad (1.1)$$

$$\Phi^o(\rho, z) = \frac{1}{2\pi} \int_{-\infty}^{\infty} [B(k) I_0(|k|\rho) + C(k) K_0(|k|\rho)] e^{-jkz} dk \quad a < \rho < b \quad (1.2)$$

where I_n and K_n are modified Bessel functions of the first and second kind order n . Since axial symmetry ($\partial/\partial\phi = 0$) is assumed, only order $n = 0$ is of interest here. The coefficients $A(k)$, $B(k)$ and $C(k)$ can be solved for by applying the following boundary conditions at $\rho = a$ and $\rho = b$.

At $\rho = a$

$$-\sigma_i \left. \frac{\partial \Phi^i}{\partial \rho} \right|_a = -\sigma_o \left. \frac{\partial \Phi^o}{\partial \rho} \right|_a \quad (1.3)$$

$$\Phi^i(a^-, z) = \Phi_{si}(z) \quad (1.4)$$

$$\Phi^o(a^+, z) = \Phi_{so}(z) \quad (1.5)$$

where $\Phi_{si}(z)$ and $\Phi_{so}(z)$ are potential distributions in z along the inner and outer surfaces of the membrane, respectively.

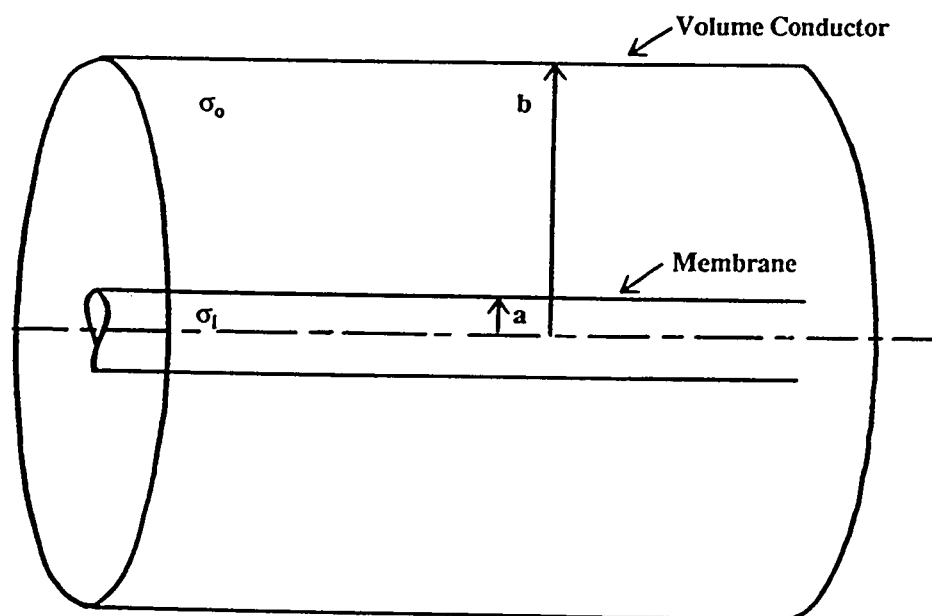


Figure 1.1 Fiber geometry. The external medium is considered uniform, homogeneous and isotropic with a specific conductivity σ_o (S/cm); the internal medium is assumed to be uniform, homogeneous and isotropic and is characterized by a specific conductivity σ_i . The fiber radius is denoted by a and the volume conductor radius is b .

At $\rho = b$, the sheath-like boundary may be either conductive or non-conductive. In our consideration of the core conductor model we will consider it to be non-conductive, that is

$$\left. \frac{\partial \Phi^o}{\partial \rho} \right|_b = 0 \quad . \quad (1.6)$$

Applying the boundary condition expressed in (1.6), $C(k)$ can be solved for in terms of $B(k)$ as :

$$C(k) = \frac{I_1(|k|b)}{K_1(|k|b)} B(k) \quad . \quad (1.7)$$

Thus, expression for external potential $\Phi^o(\rho, z)$ may be rewritten as

$$\Phi^o(\rho, z) = \frac{1}{2\pi} \int_{-\infty}^{\infty} \left[I_0(|k|\rho) + \frac{I_1(|k|b)}{K_1(|k|b)} K_0(|k|\rho) \right] B(k) e^{-jkz} dk \quad (1.8)$$

Similarly, upon considering the boundary conditions at $\rho = a$ we have the following relations :

(a) at the inner membrane surface ($\rho = a^-$) :

$$\Phi_{si}(z) = \frac{1}{2\pi} \int_{-\infty}^{\infty} A(k) I_0(|k|a) e^{-jkz} dk \equiv \frac{1}{2\pi} \int_{-\infty}^{\infty} F_{si}(k) e^{-jkz} dk \quad (1.9)$$

where $F_{si}(k)$ is the Fourier transform of the inner membrane surface potential, $\Phi_{si}(z)$. Thus,

$$A(k) = \frac{F_{si}(k)}{I_0(|k|a)} \quad (1.10)$$

(b) at the outer membrane surface ($\rho = a^+$) :

$$\Phi_{so}(z) = \frac{1}{2\pi} \int_{-\infty}^{\infty} \left[I_0(|k|a) + \frac{I_1(|k|b)}{K_1(|k|b)} K_0(|k|a) \right] B(k) e^{-jkz} dk \equiv \frac{1}{2\pi} \int_{-\infty}^{\infty} F_{so}(k) e^{-jkz} dk \quad (1.11)$$

where $F_{so}(k)$ is the Fourier transform of the outer membrane surface potential, $\Phi_{so}(z)$.

Thus,

$$B(k) = \frac{F_{so}(k)}{I_0(|k|a) \left[1 + \frac{I_1(|k|b) K_0(|k|a)}{I_0(|k|a) K_1(|k|b)} \right]} \quad (1.12)$$

It may also be shown via the current continuity condition at $\rho = a$, namely equation (1.3) that

$$B(k) = \frac{\sigma_i}{\sigma_o} \frac{A(k)}{1 - \frac{I_1(|k|b)K_1(|k|a)}{I_1(|k|a)K_1(|k|b)}} \quad (1.13)$$

From (1.10), $B(k)$ may also be expressed as :

$$B(k) = \frac{\sigma_i}{\sigma_o} \frac{F_{si}(k)}{I_0(|k|a) \left[1 - \frac{I_1(|k|b)K_1(|k|a)}{I_1(|k|a)K_1(|k|b)} \right]} \quad (1.14)$$

Letting

$$\eta(|k|) \equiv \frac{\sigma_o}{\sigma_i} I_0(|k|a) \left[1 - \frac{I_1(|k|b)K_1(|k|a)}{I_1(|k|a)K_1(|k|b)} \right] \quad (1.15)$$

it follows that

$$B(k) = \frac{F_{si}(k)}{\eta(|k|)} \quad (1.16)$$

Thus, from equations (1.11) and (1.16), the extracellular potential at an arbitrary field point (ρ, z) may be expressed as :

$$\Phi^o(\rho, z) = \frac{1}{2\pi} \int_{-\infty}^{\infty} \left[I_0(|k|\rho) + \frac{I_1(|k|b)}{K_1(|k|b)} K_0(|k|\rho) \right] \frac{F_{si}(k)}{\eta(|k|)} e^{-jkz} dk \quad (1.17)$$

The transmembrane potential $\Phi_m(z)$ may be defined according to

$$\Phi_m(z) = \Phi_{si}(z) - \Phi_{so}(z) \quad (1.18)$$

and taking the Fourier transforms of each of these terms, it follows that

$$F_m(k) = F_{si}(k) - F_{so}(k) \quad (1.19)$$

where $F_m(k)$ is the Fourier transform of $\Phi_m(z)$ defined in a fashion similar to (1.9) and (1.11). Consequently, using the two relations for $B(k)$ seen in equations (1.12) and (1.14) it can be shown that

$$F_m(k) = \frac{F_m(k)}{\Delta(|k|)} \quad (1.20)$$

where $\Delta(|k|)$ is defined as

$$\Delta(|k|) \equiv 1 - \frac{\sigma_i}{\sigma_o} \frac{1 + \frac{I_1(|k|b)K_0(|k|a)}{I_0(|k|a)K_1(|k|b)}}{1 - \frac{I_1(|k|b)K_1(|k|a)}{I_1(|k|a)K_1(|k|b)}} \quad (1.21)$$

The final expressions for intra- and extracellular potential in terms of the Fourier transform of the transmembrane potential are therefore obtained from equations (1.1), (1.2), (1.10), (1.15), (1.17) and (1.21) as :

$$\Phi^i(\rho, z) = \frac{1}{2\pi} \int_{-\infty}^{\infty} \frac{I_0(|k|\rho)}{I_0(|k|a)\Delta(|k|)} F_m(k) e^{-jkz} dk \quad \rho \leq a^- \quad (1.22)$$

and

$$\Phi^o(\rho, z) = \frac{1}{2\pi} \int_{-\infty}^{\infty} \left[I_0(|k|\rho) + \frac{I_1(|k|b)}{K_1(|k|b)} K_0(|k|\rho) \right] \frac{F_m(k)}{\Delta(|k|)\eta(|k|)} e^{-jkz} dk \quad a^+ \leq \rho \leq b, \quad (1.23)$$

respectively.

A set of filter functions may be defined as :

$$W_i(|k|\rho, a) \equiv \frac{I_0(|k|\rho)}{I_0(|k|a)\Delta(|k|)} \quad (1.24)$$

$$W_o(|k|\rho, b) \equiv \left[I_0(|k|\rho) + \frac{I_1(|k|b)}{K_1(|k|b)} K_0(|k|\rho) \right] \frac{1}{\eta(|k|)\{1 - \Delta(|k|)\}} \quad (1.25)$$

$$M(|k|) \equiv \frac{1}{\Delta(|k|)} - 1 \quad (1.26)$$

where $W_i(|k|\rho, a)$ and $W_o(|k|\rho, b)$ are the medium filter functions for the intra- and extracellular media respectively and $M(|k|)$ is called the membrane filter function.

Using the filter functions defined above the expressions for potential may be rewritten as :

$$\Phi^i(\rho, z) = \frac{1}{2\pi} \int_{-\infty}^{\infty} W_i(|k|, \rho, a) F_m(k) e^{-jkz} dk \quad \rho \leq a^- \quad (1.27)$$

and

$$\Phi^o(\rho, z) = \frac{1}{2\pi} \int_{-\infty}^{\infty} W_o(|k|, \rho, b) M(|k|) F_m(k) e^{-jkz} dk \quad a^+ \leq \rho \leq b \quad (1.28)$$

1.3 Volume Conductor Currents Associated with the Core Conductor Model

The electrical equivalent network that characterizes a unit segmental length (Δz) of an active nerve fiber in a homogeneous cylindrical volume conductor, consistent with the core conductor model of Hermann (1879) is shown in figure 1.2. The fiber is characterized as an iterative structure of this same basic form. The axial resistance per unit length r_i , accounts for the resistive electrical properties of the axoplasm, while r_o is the resistance per unit length that characterizes the lumped resistive properties of the extracellular medium. The shunt elements represent the electrical properties of the membrane. Applying Kirchoff's laws to the electrical network in fig. 1.2, the following cable equations result

$$i_m(z) = \frac{\partial I_L^o(z)}{\partial z} \quad (1.29)$$

$$I_L^o(z) = -I_L^i(z) \quad (1.30)$$

$$\frac{\partial V^o(z)}{\partial z} = -r_o I_L^o(z) \quad (1.31)$$

$$\frac{\partial V^i(z)}{\partial z} = -r_i I_L^i(z) \quad (1.32)$$

where $I_L^o(z)$ and $I_L^i(z)$ are the total longitudinal currents in the extra- and intracellular media respectively, $i_m(z)$ is the transmembrane current per unit length and $V^o(z)$ and $V^i(z)$ are the extra- and intracellular potential distributions respectively, (Clark and Plonsey, (1966)). At this point we will derive expressions for the transmembrane and total longitudinal currents.

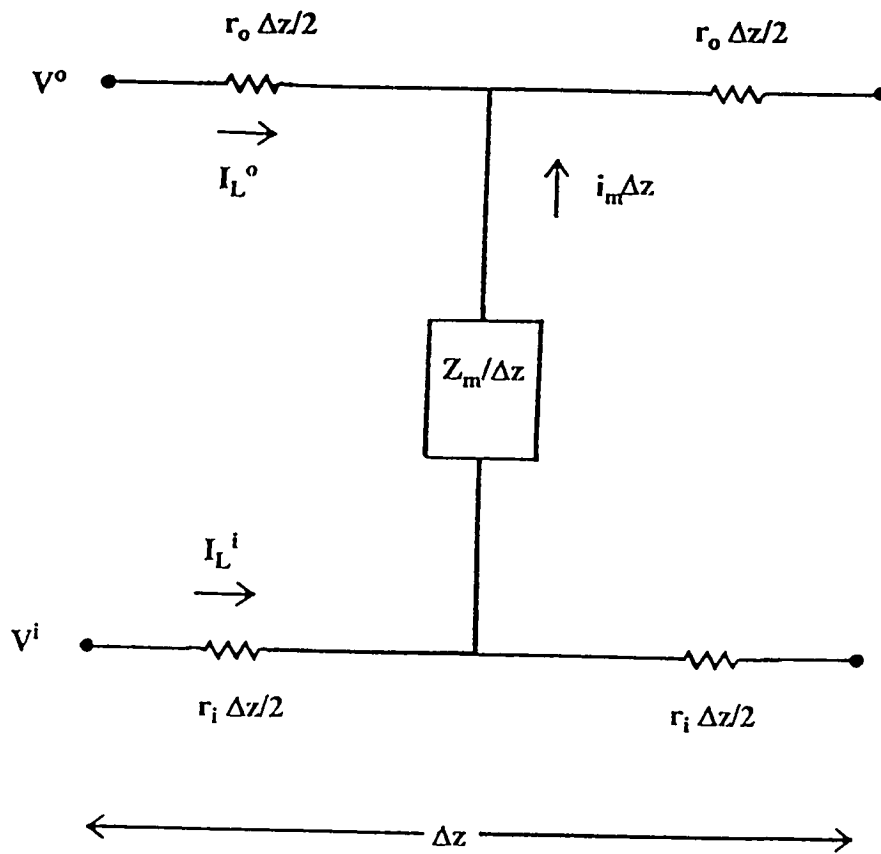


Figure 1.2 The electrical equivalent network of an active nerve fiber in a homogeneous cylindrical volume conductor, consistent with the classical core conductor model of Hermann (1879).

Utilizing the definition of the extracellular field potential (1.23) the expression for transmembrane current per unit length $i_m(z)$ may be expressed as :

$$i_m(z) = -2\pi a \sigma_o \left. \frac{\partial \Phi^o}{\partial \rho} \right|_a = -\sigma_o a \int_{-\infty}^{\infty} \left[I_1(|k|a) - \frac{I_1(|k|b)}{K_1(|k|b)} K_1(|k|a) \right] \frac{|k| F_m(k)}{\Delta(|k|) \eta(|k|)} e^{-jkz} dk \quad (1.33)$$

An alternate expression for $i_m(z)$ may be obtained using the expression for intracellular potential $\Phi^i(\rho, z)$ given by (1.22) :

$$i_m(z) = -2\pi a \sigma_i \left. \frac{\partial \Phi^i}{\partial \rho} \right|_a = -\sigma_i a \int_{-\infty}^{\infty} \frac{I_1(|k|a)}{J_0(|k|a) \Delta(|k|)} |k| F_m(k) e^{-jkz} dk \quad (1.34)$$

The derived expressions for potential given by equations (1.22) and (1.23), allow one to determine the potential everywhere in the intra- and extracellular media. Based on these expressions, it is possible to compute the current density field anywhere in these media and hence the total longitudinal currents $I_L^i(z)$ and $I_L^o(z)$, associated with the cable equations. In general, the current density field \bar{J} in each of these media consists of a radial and axial component, that is

$$\bar{J}^o(\rho, z) = J_\rho^o(\rho, z) \bar{a}_\rho + J_z^o(\rho, z) \bar{a}_z \quad (1.35)$$

$$\bar{J}^i(\rho, z) = J_\rho^i(\rho, z) \bar{a}_\rho + J_z^i(\rho, z) \bar{a}_z \quad (1.36)$$

where

$$J_\rho^o(\rho, z) \equiv -\sigma_o \frac{\partial \Phi^o(\rho, z)}{\partial \rho} \quad (1.37)$$

$$J_z^o(\rho, z) \equiv -\sigma_o \frac{\partial \Phi^o(\rho, z)}{\partial z} \quad (1.38)$$

$$J_\rho^i(\rho, z) \equiv -\sigma_i \frac{\partial \Phi^i(\rho, z)}{\partial \rho} \quad (1.39)$$

$$J_z^i(\rho, z) \equiv -\sigma_i \frac{\partial \Phi^i(\rho, z)}{\partial z} \quad (1.40)$$

and \bar{a}_ρ and \bar{a}_z are the unit directional vectors.

The expressions for total longitudinal current in each of these media is :

$$I_L^o(z) = \int_a^b 2\pi\rho J_z^o(\rho, z) d\rho = -2\pi\sigma_o \int_a^b \rho \frac{\partial \Phi^o(\rho, z)}{\partial z} d\rho \quad (1.41)$$

$$I_L^i(z) = \int_0^a 2\pi\rho J_z^i(\rho, z) d\rho = -2\pi\sigma_i \int_0^a \rho \frac{\partial \Phi^i(\rho, z)}{\partial z} d\rho \quad (1.42)$$

We proceed by utilizing the expressions for potential (1.22) and (1.23), differentiating them with respect to z and interchanging the order of integration. The result is :

$$I_L^o(z) = j\sigma_o \int_{-\infty}^{\infty} \frac{kF_m(k)}{\Delta(|k|)\eta(|k|)} e^{-jkz} \left[\int_a^b \left\{ I_0(|k|\rho) + \frac{I_1(|k|b)}{K_1(|k|b)} K_0(|k|\rho) \right\} \rho d\rho \right] dk \quad (1.43)$$

and

$$I_L^i(z) = j\sigma_i \int_{-\infty}^{\infty} \frac{kF_m(k)}{I_0(|k|a)\Delta(|k|)} e^{-jkz} \left[\int_0^a I_0(|k|\rho) \rho d\rho \right] dk \quad (1.44)$$

In each case the integration in ρ is a relatively simple one, wherein the following identities for the modified Bessel functions of order n are employed (Abramowitz and Stegun, 1965)

$$\int_{x_1}^{x_2} x^n K_{n-1}(x) dx = - \left[x^n K_n(x) \right]_{x_1}^{x_2} \quad (1.45)$$

$$\int_{x_1}^{x_2} x^n I_{n-1}(x) dx = \left[x^n I_n(x) \right]_{x_1}^{x_2} \quad (1.46)$$

The results for the total longitudinal currents are :

$$I_L^o(z) = -\sigma_o \int_{-\infty}^{\infty} \frac{jkF_m(k)}{\Delta(|k|)\eta(|k|)} \left[I_1(|k|a) - \frac{I_1(|k|b)}{K_1(|k|b)} K_1(|k|a) \right] \frac{a}{|k|} e^{-jkz} dk \quad (1.47)$$

and

$$I_L^i(z) = \sigma_i \int_{-\infty}^{\infty} \frac{jkF_m(k)}{I_0(|k|a)\Delta(|k|)} \left[\frac{aI_1(|k|a)}{|k|} \right] e^{-jkz} dk \quad (1.48)$$

A set of filter functions may now be defined as

$$C_{mo}(|k|a,b) \equiv \left\{ I_1(|k|a) - \frac{I_1(|k|b)}{K_1(|k|b)} K_1(|k|a) \right\} \frac{|k|}{\Delta(|k|)\eta(|k|)} \quad (1.49)$$

$$C_{mi}(|k|a) \equiv \frac{|k|I_1(|k|a)}{\Delta(|k|)I_0(|k|a)} \quad (1.50)$$

$$C_{Lo}(|k|a,b) \equiv \left\{ I_1(|k|a) - \frac{I_1(|k|b)}{K_1(|k|b)} K_1(|k|a) \right\} \frac{1}{\Delta(|k|)\eta(|k|)} \quad (1.51)$$

$$C_{Li}(|k|a) \equiv \frac{I_1(|k|a)}{\Delta(|k|)I_0(|k|a)} \quad (1.52)$$

where $C_{mo}(|k|a,b)$ and $C_{mi}(|k|a)$ are two forms of the transmembrane current filter function. Here $C_{mi}(|k|a)$ is the form used when the potential inside the fiber is known while $C_{mo}(|k|a,b)$ is the form used when the potential outside the fiber is specified. Similarly $C_{Lo}(|k|a,b)$ is the external and $C_{Li}(|k|a)$ the internal longitudinal filter function.

Using the filter functions defined above the expressions for transmembrane current per unit length $i_m(z)$ may be written as either :

$$i_m(z) = -\sigma_o a \int_{-\infty}^{\infty} F_m(k) C_{mo}(|k|a,b) e^{-jkz} dk \quad (1.53)$$

or

$$i_m(z) = -\sigma_i a \int_{-\infty}^{\infty} F_m(k) C_{mi}(|k|a) e^{-jkz} dk \quad (1.54)$$

while the expressions for total longitudinal current ($I_L^o(z)$, $I_L^i(z)$) are written as :

$$I_L^o(z) = -a\sigma_o \int_{-\infty}^{\infty} j F_m(k) C_{Lo}(|k|a,b) e^{-jkz} dk \quad (1.55)$$

and

$$I_L^i(z) = a\sigma_i \int_{-\infty}^{\infty} j F_m(k) C_{L_i}(|k|a) e^{-jkz} dk \quad . \quad (1.56)$$

At this point we define the following Fourier transform pairs for the transmembrane current per unit length :

$$i_m(z) = -2\pi\sigma_o a \left[\frac{1}{2\pi} \int_{-\infty}^{\infty} I_m(k) e^{-jkz} dk \right] \quad (1.57)$$

$$I_m(k) = \frac{1}{2\pi\sigma_o a} \int_{-\infty}^{\infty} i_m(z) e^{jkz} dz = F_m(k) C_{m_o}(|k|a, b) \quad (1.58)$$

and

$$i_m(z) = -2\pi\sigma_i a \left[\frac{1}{2\pi} \int_{-\infty}^{\infty} I'_m(k) e^{-jkz} dk \right] \quad (1.59)$$

$$I'_m(k) = \frac{1}{2\pi\sigma_i a} \int_{-\infty}^{\infty} i_m(z) e^{jkz} dz = F_m(k) C_{m_i}(|k|a) \quad (1.60)$$

A similar Fourier transform pair for the external total longitudinal current is defined as :

$$I_L^o(z) = -2a\sigma_o \pi \left[\frac{1}{2\pi} \int_{-\infty}^{\infty} F_L^o(k) e^{-jkz} dk \right] \quad (1.61)$$

$$F_L^o(k) = \frac{1}{2a\sigma_o \pi} \int_{-\infty}^{\infty} I_L^o(z) e^{jkz} dz = jF_m(k) C_{L_o}(|k|a, b) \quad (1.62)$$

while the Fourier transform pair for the internal total longitudinal current is similarly defined as :

$$I_L^i(z) = 2a\sigma_i \pi \left[\frac{1}{2\pi} \int_{-\infty}^{\infty} F_L^i(k) e^{-jkz} dk \right] \quad (1.63)$$

$$F_L^i(k) = \frac{1}{2a\sigma_i \pi} \int_{-\infty}^{\infty} I_L^i(z) e^{jkz} dz = jF_m(k) C_{L_i}(|k|a) \quad (1.64)$$

In each case, the Fourier transforms may be rapidly evaluated once they are discretized into discrete Fourier transforms (DFTs) and then evaluated using the fast Fourier transform (FFT) algorithm.

1.4 Discrete Fourier Methods of Solution for Cable Equation Variables

In the preceding sections, Fourier integral expressions have been developed for a number of variables including extracellular potential $\Phi^o(\rho, z)$, transmembrane current per unit length $i_m(z)$, and the total intracellular and extracellular longitudinal current, $I_L^i(z)$ and $I_L^o(z)$ respectively. Computation of these quantities is greatly facilitated by reformulation of these integral expressions in terms of the methodology of the discrete Fourier Transform (DFT) technique. Reformulation of these equations for representation in the discrete spatial (z) and spatial frequency (k) domains will be illustrated using the transmembrane current per unit length as an example

$$I_m(Pq) = -\frac{1}{2\pi\sigma_o a} \sum_{n=0}^{N-1} i_m(Zn) e^{j2\pi nq/N} = -\frac{1}{2\pi\sigma_o a} \text{DFT}[i_m(Zn)] \quad (1.65)$$

$$I_m(Zn) = -2\pi\sigma_o a \frac{1}{N} \sum_{q=0}^{N-1} I_m(Pq) e^{-j2\pi nq/N} = -2\pi\sigma_o a \text{IDFT}[I_m(Pq)] \quad (1.66)$$

where

$$P = \frac{2\pi}{NZ} \quad (1.67)$$

Here Z and P are the sampling intervals in the z - and k -domains, respectively, and n and q are integers. The function $i_m(z)$ is normally limited in both the z - and k -domains, meaning that $i_m(z)$ is nonzero for a small finite range of z values ($-Z_1 < z < Z_2$) and essentially zero outside this range. Similarly, $i_m(z)$ is limited with respect to frequency content; therefore $I_m(k)$ is nonzero only within a small range $|k| < M$ (a constant) and zero elsewhere. Thus, the discrete functions $i_m(Zn)$ and $I_m(Pq)$ approach zero as Zn and Pq , respectively, become large. The sampling interval Z is chosen to be small enough so that no aliasing occurs in the k -domain, and the number of samples or sampling duration, NZ , is chosen to include the entire signal. Relationships similar in form to the DFT pair of equa-

tions (i.e., (1.65) and (1.66)) exist for $I_L^o(z)$ and $F_L^o(k)$ as well as $I_L^i(z)$ and $F_L^i(k)$.

Thus the various cable equations can be evaluated as products of DFTs (equivalent to linear convolution). Once again the transmembrane current is given as an example.

$$I_m(Pq) = F_m(Pq)C_{mo}(Pq, a, b) \quad (1.68)$$

where $q = 1, \dots, N$.

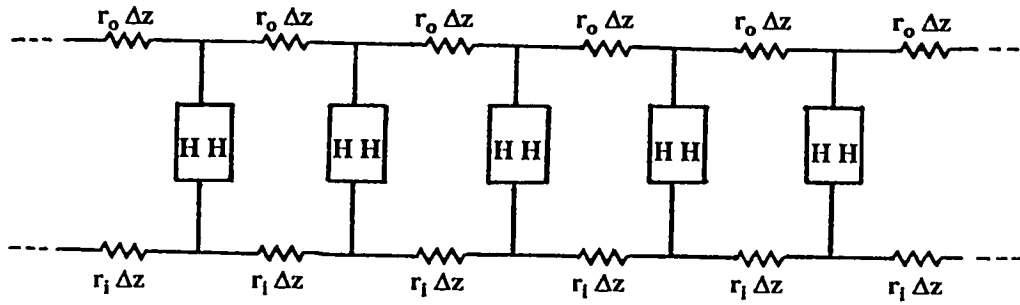
The transmembrane current itself is given by

$$i_m(Zn) = -2\pi\sigma_o a \text{IDFT}[I_m(Pq)] \quad (1.69)$$

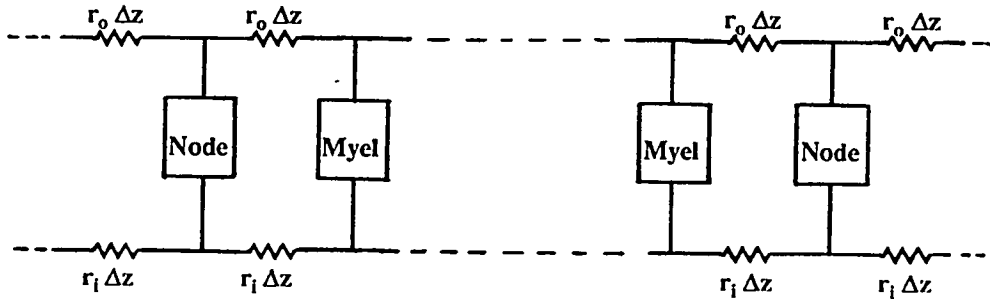
The other cable equations are also evaluated in a similar fashion using FFTs.

1.5 Models for the Active Source Fiber

Our study involves an investigation of the nature of the potential and current density fields in a cylindrical volume conductor surrounding an active nerve fiber. In previous studies of Clark and Plonsey (1966, 1968), rather simple simulated action potential distributions were used as membrane source potential waveforms for the volume conductor problem. In the present study, spatial distributions of transmembrane potential $\Phi_m(z)$ are obtained from a distributed parameter model simulation of active unmyelinated and myelinated nerve fibers. These simulations yield much more realistic action potentials and the model parameters may be conveniently varied so as to represent a variety of experimental conditions. Figures 1.3a and b show the equivalent circuit model for the representative unmyelinated and myelinated nerve fiber, respectively. The equivalent circuit model for the representative skeletal muscle fiber is identical to that of the unmyelinated nerve fiber in fig. 1.3a. The model is characterized by patches of membrane, coupled by resistances $r_i\Delta z$ and $r_o\Delta z$, where Δz represents a unit segment along the fiber; r_i and r_o are resistances per unit length. In the case of the unmyelinated fiber, the shunt elements in the network model, representing membrane patches, are characterized by Hodgkin-Huxley models of the squid giant axon (Hodgkin et al, 1952). The shunt elements of the skeletal muscle fiber model are characterized by Adrian-Peachey models of frog skeletal muscle fiber (Adrian et al, 1973), a model that is identical in form to that used for the squid axon by Hodgkin and Huxley but with dif-



(a)



(b)

Figure 1.3 The distributed parameter models of the (a) unmyelinated and (b) myelinated nerve fibers.

The patches of membrane in (a) are characterized by Hodgkin-Huxley models of the squid giant axon while in (b) a modified Frankenhaeuser-Huxley model is used to describe the nodes and a parallel RC network describes the internodal region.

ferent model parameter values. The shunt elements representing nodes of Ranvier are characterized by the Frankenhaeuser-Huxley model of the myelinated nerve (Frankenhaeuser et al, 1964), with an additional shunt element to account for the myelin sheath adjoining the node of Ranvier on either side. The internodal region between two nodes of Ranvier is represented by a parallel RC circuit. The conductance and capacitance values used are those in accordance with the specific conductance and the specific capacitance of the myelin sheath. This representation of the myelinated nerve fiber is based on the work of Goldman and Albus (1968). The network models are discussed in more detail in chapter 2.

The parabolic partial differential equation describing the propagation of a nerve impulse along these distributed parameter networks is given as :

$$\frac{\partial^2 V_m(z,t)}{\partial z^2} = 2\pi a(r_i + r_o) \left[C_m \frac{\partial V_m(z,t)}{\partial t} + i_{ion} \right]. \quad (1.70)$$

where V_m is the transmembrane voltage, C_m is the membrane capacitance and i_{ion} the total ionic current. The parabolic partial differential equation is numerically integrated by a stable, implicit technique known as the Crank-Nicholson method (Crank, 1947). In accordance with this scheme, the finite difference representation of (1.70) about the point $(i, j+1/2)$ is

$$\frac{1}{2(\Delta z)^2} [V_{i-1,j+1} - 2V_{i,j+1} + V_{i+1,j+1} + V_{i-1,j} - 2V_{i,j} + V_{i+1,j}] = 2\pi a(r_i + r_o) \left[\frac{C_m}{\Delta t} (V_{i,j+1} - V_{i,j}) + i_{ion}(i,j) \right] \quad (1.71)$$

where the indices in the time and z domain are j and i respectively. The terms with an index $j+1$ can therefore be considered to be the unknowns, denoting as they do, values at the next time instant. Equation (1.71) may be rearranged in such a manner as to have all terms representing unknown quantities appear on the left side of the equation. Certain quantities are defined, in order to facilitate this rearrangement of terms, as follows.

$$\alpha \equiv 4\pi a(r_i + r_o) C_m \frac{(\Delta z)^2}{\Delta t} \quad (1.72)$$

$$\gamma_{i,j} \equiv 4\pi a(r_i + r_o) (\Delta z)^2 i_{ion}(i,j) \quad (1.73)$$

$$\theta \equiv -(2 + \alpha) \quad (1.74)$$

The resulting rearrangement yields

$$V_{i-1,j+1} + \theta V_{i,j+1} + V_{i+1,j+1} = \phi_{i,j} \quad (1.75)$$

where

$$\phi_{i,j} \equiv -V_{i-1,j} + (2 - \alpha)V_{i,j} - V_{i+1,j} + \gamma_{i,j} \quad (1.76)$$

The result is a set of linear algebraic equations for each time instant j . The formulation must include boundary conditions at either ends of the fiber, and in this case the ends are considered to be sealed, representing an infinite resistance to longitudinal current flow and hence,

$$\frac{\partial V_m}{\partial z}(0,t) = \frac{\partial V_m}{\partial z}(L,t) = 0 \quad (1.77)$$

where L is the length of the fiber.

In discrete form the differential boundary conditions become

$$-3V_{0,j+1} + 4V_{1,j+1} - V_{2,j+1} = 0 \quad (1.78)$$

$$3V_{N,j+1} - 4V_{N-1,j+1} + V_{N-2,j+1} = 0 \quad (1.79)$$

The resulting set of $N+1$ equations for a cable with N segments is reproduced in matrix form, thus

$$\begin{bmatrix} -2 & 4+\theta & 0 & 0 & 0 & 0 & 0 & 0 \\ 1 & \theta & 1 & 0 & 0 & 0 & 0 & 0 \\ 0 & 1 & \theta & 1 & 0 & 0 & 0 & 0 \\ \cdot & \cdot & \cdot & \cdot & \cdot & \cdot & \cdot & \cdot \\ \cdot & \cdot & \cdot & \cdot & \cdot & \cdot & \cdot & \cdot \\ \cdot & \cdot & \cdot & \cdot & \cdot & \cdot & \cdot & \cdot \\ 0 & 0 & 0 & 0 & 0 & 1 & \theta & 1 \\ 0 & 0 & 0 & 0 & 0 & 0 & 4+\theta & -2 \end{bmatrix} \begin{bmatrix} V_{0,j+1} \\ V_{1,j+1} \\ V_{2,j+1} \\ \cdot \\ \cdot \\ \cdot \\ V_{N-1,j+1} \\ V_{N,j+1} \end{bmatrix} = \begin{bmatrix} \phi_{1,j} \\ \phi_{1,j} \\ \phi_{2,j} \\ \cdot \\ \cdot \\ \cdot \\ \phi_{N-1,j} \\ \phi_{N-1,j} \end{bmatrix} \quad (1.80)$$

The tri-diagonal form of the matrix on the left hand side of (1.80) may be easily inverted to solve for the vector V , which is the transmembrane voltage at every point along the fiber, for each instant of time.

1.6 Summary

In this chapter an introduction to the nature of the problem which is considered in this study has been provided, together with the mathematical model which is used to characterize the different kinds of cells studied. All the expressions developed here will be used in the succeeding chapters, each of which is devoted to a particular aspect of the present study. The next chapter deals with the thorough analysis of the core conductor model that is undertaken for the nerve fibers, and following chapters deal with the reconstruction of the extracellular currents and potentials of the myelinated fiber as functions of time and the investigation of extracellular potentials from an eccentric skeletal muscle fiber located in a finite volume conductor.

CHAPTER 2

Evaluation of the Core Conductor Model for Active Nerve Fibers

2.1 Introduction

In this chapter a detailed evaluation of the core conductor model and the cable equations associated with it, is undertaken for the myelinated and unmyelinated nerve fibers. The mathematical expressions developed in the previous chapter are used to perform the evaluation. As described in the previous chapter, the active nerve fiber is characterized by a distributed parameter model of the form shown in fig. 1.3 and the associated parabolic partial differential equations are solved using the Crank-Nicholson numerical integration technique.

2.2 Modeling Aspects

The distributed parameter models for the unmyelinated and myelinated nerve fibers were introduced in the previous chapter. The patches of membrane that are represented by the shunt elements of the cable in fig. 1.3a are characterized by Hodgkin-Huxley models of the squid giant axon (Hodgkin et al, 1952). The network model is shown in detail in fig. 2.1 where C_M is the membrane specific capacity in $\mu\text{F}/\text{cm}^2$, g_{Na} , g_K and g_L are the specific conductances (mS/cm^2) of the sodium, potassium and leak channels respectively and E_{Na} , E_K and E_L are the Nernst potentials (mV) of the sodium, potassium and the leak channel, respectively. The propagation of electrical activity along the myelinated nerve fiber is simulated using the distributed parameter model based on the work done by Goldman and Albus (1968). The model in turn incorporates a nodal membrane model attributed to Frankenhaeuser-Huxley (1964). The Frankenhaeuser-Huxley model consists of three ionic currents and one leak current that are assumed to be present in the nodal membrane of the myelinated fiber. The three ionic currents consist of a fast inward sodium current, a delayed outward potassium current and a very small inward current that is considerably slower than the fast sodium current. This later current is said to be due to non-specific ions but is characterized in the model as a sodium current. Since experimental

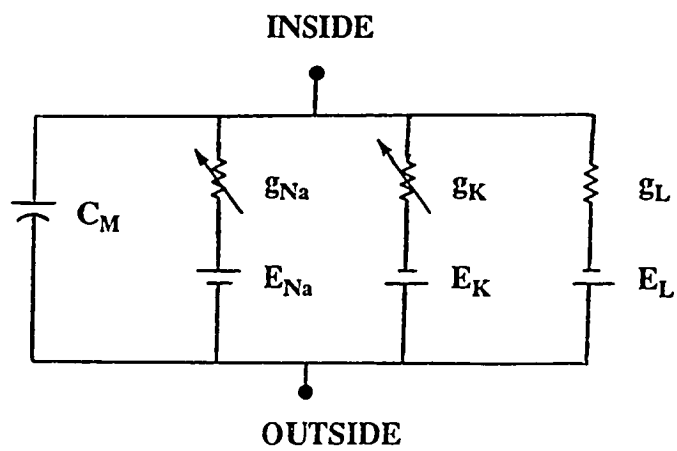


Figure 2.1 The electrical network describing the membrane patches in the distributed parameter models for the unmyelinated fiber.

evidence (Horakova, Nonner & Stampfli (1968); Chiu, Ritchie, Rogart & Stagg (1979); Brismar (1980); Kocsis & Waxman (1980)) has proved the existence of potassium channels in the paranodal region and their almost complete absence in the node, it was decided to associate the potassium and the non-specific inward current in the membrane model with the paranodal region. The segments in the internodal region of the fiber are characterized by lumped parallel resistive capacitive elements as in Goldmann and Albus (1968). An equivalent circuit model of the nodal, paranodal and internodal regions of the myelinated nerve fiber is shown in fig. 2.2. In fig. 2.2 E_p and g_p denote the Nernst potential and specific conductance of the non-specific channel, respectively, while the nodal, paranodal and internodal regions are the regions labeled as a , b , and c respectively, on the drawing of the myelinated fiber.

As stated in the chapter 1, the technique employed to numerically integrate the partial differential equation describing the propagation of the electrical impulse along the fiber, results in a set of equations that may be written in matrix form as :

$$\underline{A} \underline{V} = \underline{B} \quad (2.1)$$

where the matrix on the left hand side of (2.1), \underline{A} is a tridiagonal matrix, \underline{V} and \underline{B} both being vectors. Recalling the form of the tridiagonal matrix \underline{A} from equation (1.80), it can be noticed that the diagonal element of the matrix is the term defined as θ in equation (1.74). In the present study using the various parameter values specified in tables 2.1 through 2.3, the resulting value of θ is approximately 12, a number which is always an order of magnitude greater than the off diagonal elements in the matrix \underline{A} . The tridiagonal matrix \underline{A} is of the following form.

$$\underline{A} = \begin{bmatrix} b_1 & -c_1 & 0 & 0 & 0 & 0 & 0 & 0 \\ -a_2 & b_2 & -c_2 & 0 & 0 & 0 & 0 & 0 \\ 0 & -a_3 & b_3 & -c_3 & 0 & 0 & 0 & 0 \\ \vdots & \vdots & \vdots & \vdots & \vdots & \vdots & \vdots & \vdots \\ \vdots & \vdots & \vdots & \vdots & \vdots & \vdots & \vdots & \vdots \\ 0 & 0 & 0 & 0 & 0 & -a_N & b_N & -c_N \\ 0 & 0 & 0 & 0 & 0 & 0 & -a_{N+1} & b_{N+1} \end{bmatrix} \quad (2.2)$$

The set of equations represented by the matrix equation (1.80) and (2.1) can therefore be written in a very general form as :

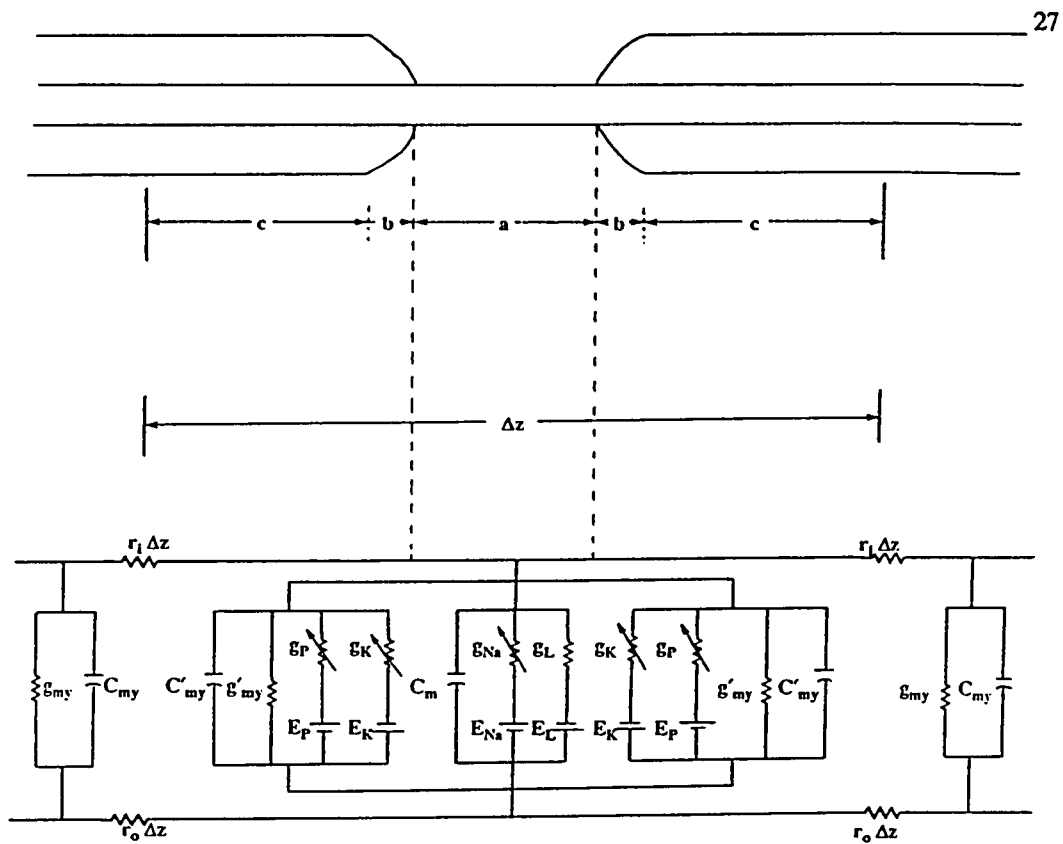


Figure 2.2 The electrical network describing the membrane patches in the distributed parameter models for the nodal, paranodal and internodal regions of the myelinated fiber. The myelinated fiber is shown on top where the regions are labeled as a for the nodal region, b for the paranodal region and c for the internodal region.

28

(ii) $b_i > a_i + c_i$ for $i = 1, 2, \dots, N+1$

2.3 Computational Aspects

The two types of fiber considered in this study are the myelinated nerve fiber, that uses the myelinated nerve model due to Frankenhaeuser and Huxley (1964) as the membrane model, and the unmyelinated nerve fiber that follows the development of Hodgkin and Huxley (1952). The values of the model parameters in both cases are listed in tables 2.1 through 2.3. Table 2.1 is a list of the geometric parameters needed in the two models, table 2.2 lists the values of the parameters in the network models shown in figures 1.3, 2.1 and 2.2, and table 2.3 gives the different forms of the terms defined in equations (1.72) through (1.76). Typical transmembrane potential spatial distributions $\Phi_m(z)$ for the unmyelinated and myelinated fibers described in terms of the parameters given in tables

2.1, 2.2 and 2.3 are shown in figure 2.3a and b, respectively. These transmembrane potential distributions $\Phi_m(z)$ then serve as input to the volume conductor equations for potential and current.

Table 2.1 : Geometric Model Parameters

	Myelinated Fiber	Unmyelinated Fiber
Fiber radius (a)	0.0005 cm	0.0238 cm
Myelin thickness (at)	0.0002 cm	
Length of a node of Ranvier (NL)	0.0004 cm	
Volume conductor radius (b)	n.a	n.a

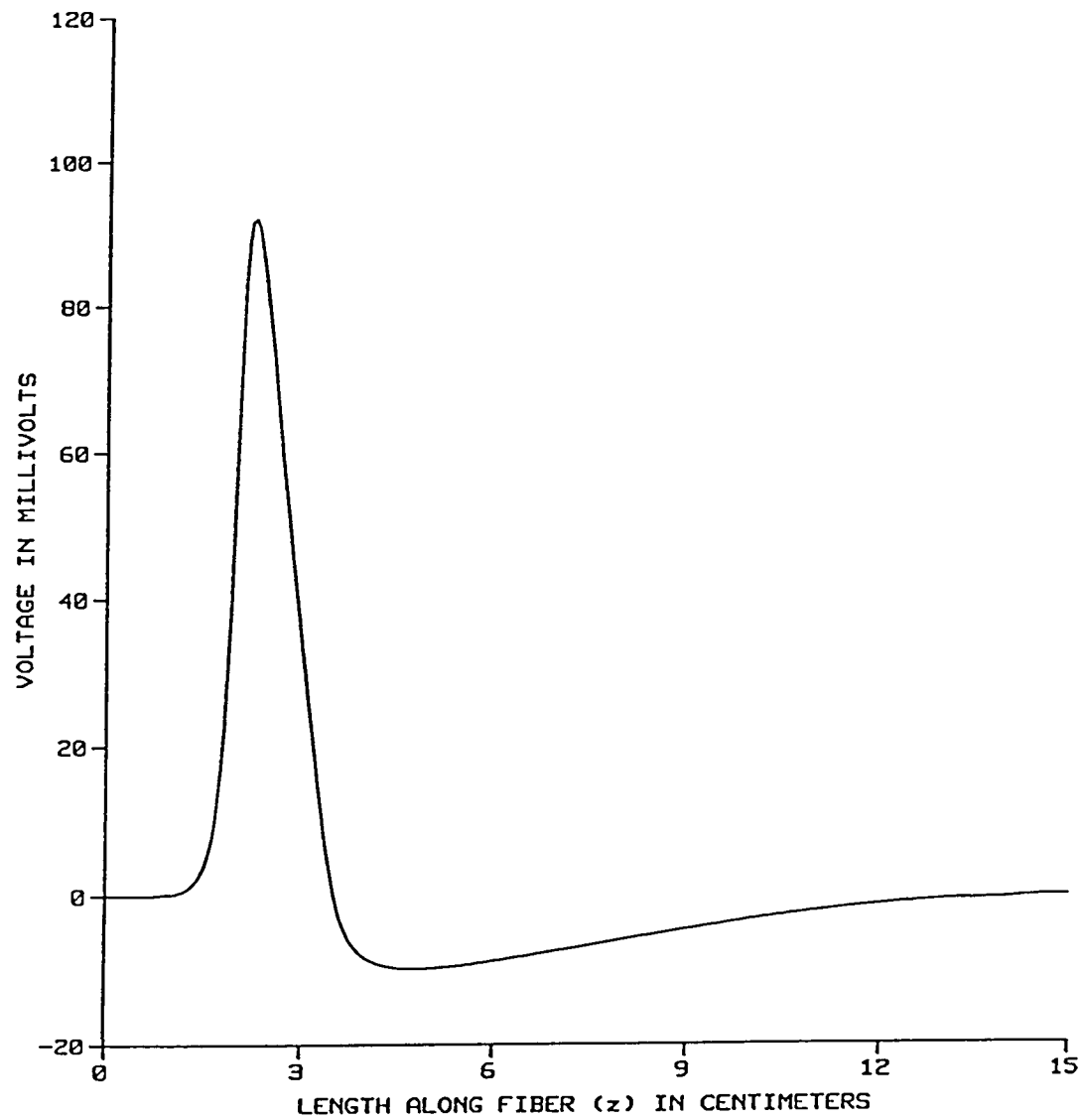


Figure 2.3 a Typical action potential distribution $\Phi_m(z)$ for the unmyelinated nerve fiber generated by the distributed Hodgkin-Huxley model for squid axon.

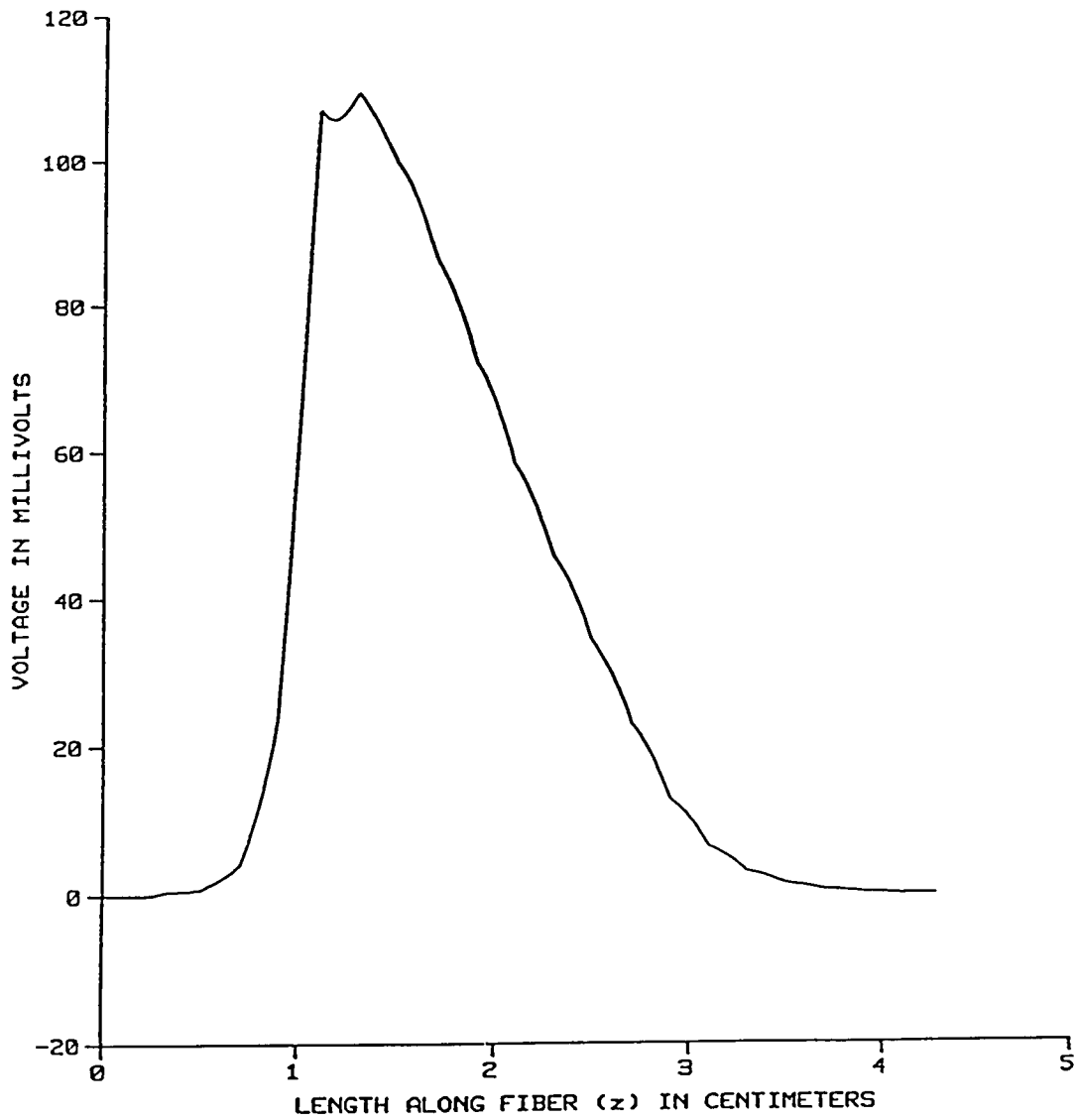


Figure 2.3 b Typical action potential distribution $\Phi_m(z)$ for the myelinated nerve fiber generated by the distributed Frankenhaeuser-Huxley model for a myelinated nerve fiber.

Table 2.2 : Electrical Model Parameters

	Myelinated Fiber	Unmyelinated Fiber
External resistivity (R_o)	70 Ω cm	70 Ω cm
Internal resistivity (R_i)	100 Ω cm	110 Ω cm
External resistance per unit length (r_o)	$R_o/\{\pi a^2(n^2-1)\}$	$R_o/\{\pi a^2(n^2-1)\}$
Internal resistance per unit length (r_i)	$R_i/\pi a^2$	$R_i/\pi a^2$
Membrane Capacitance (C_m)	2 $\mu\text{F}/\text{cm}^2$	1 $\mu\text{F}/\text{cm}^2$
Myelin Capacitance (C_{my})	0.00387 $\mu\text{F}/\text{cm}^2$	
Myelin Conductance (g_{my})	0.083308 $\mu\text{mho}/\text{cm}^2$	
Sodium Nernst Potential (E_{Na})		115 mV
Potassium Nernst Potential (E_K)		-12 mV
Leak Potential (E_l)	0.026 mV	10.6 mV
Sodium conductance constant (\bar{g}_{Na})		120 m mho/ cm^2
Potassium conductance constant (\bar{g}_K)		36 m mho/ cm^2
Leak conductance (g_l)	30.3 m mho/ cm^2	0.3 m mho/ cm^2
Sodium permeability constant (P_{Na})	0.008 cm/sec	
Potassium permeability constant (P_K)	0.0012 cm/sec	
Non-specific permeability constant (P_p)	0.00054 cm/sec	
External Sodium concentration ($[Na^+]_o$)	114.5 mM	
Internal Sodium concentration ($[Na^+]_i$)	13.74 mM	
External Potassium concentration ($[K^+]_o$)	2.5 mM	
Internal Potassium concentration ($[K^+]_i$)	120.0 mM	

Table 2.3 : Crank-Nicholson Parameter Values

	Myelinated Fiber	Unmyelinated Fiber
Step size in time (Δt)	0.005 msec	0.03 msec
Step size in space (Δz)	0.02 cm	0.05 cm
α for unmyelinated node	$[C_m K_1 NL + (\Delta z - NL) C_{my} K_2] / (\Delta z \Delta t)$	$4\pi a(r_i + r_o) C_m (\Delta z)^2 / \Delta t$
α' for the myelinated node	$K_2 C_{my} / \Delta t$	
$i_{ion(i,j)}$	$(i_{Na} + i_K + i_p + i_l)(NL/\Delta z)$	$i_{Na} + i_K + i_l$
i'_{my} for unmyelinated node	$V \cdot g_{my} (\Delta z - NL) / \Delta z$	
i_{my} for myelinated node	$V \cdot g_{my}$	
$\gamma_{i,j}$ for the unmyelinated node	$K_1 i_{ion(i,j)} + K_2 i'_{my}$	$4\pi a(r_i + r_o) (\Delta z)^2 i_{ion(i,j)}$
$\gamma_{i,j}$ for myelinated node	$K_2 i_{my}$	
θ for unmyelinated node	$-(2 + \alpha)$	$-(2 + \alpha)$
θ' for myelinated node	$-(2 + \alpha')$	

$$K_1 = 4\pi a[r_i + (n^2 - 1)r_o](\Delta z)^2$$

$$K_2 = 4\pi(a + at)[r_i + (n^2 - 1)r_o](\Delta z)^2$$

Using the potential filter functions defined in equations (1.24) through (1.26) the volume conductor problem may be viewed as an equivalent filter problem as shown in figure 2.4a. The input to the membrane filter is $F_m(k)$ the Fourier transform of the transmembrane potential distribution, and its output is $F_{so}(k)$ which is the Fourier transform of the potential distribution along the outer surface of the membrane. $F_{so}(k)$ in turn is input to the medium filter and the final output is $F^o(\rho, k)$, the Fourier transform of the potential distribution at a specified field point $P(\rho, z)$ in the extracellular medium calculated in accordance with (1.24).

Utilizing the filter function definitions in equations (1.49) through (1.52), the equivalent filter problem may also be formulated for the core conductor model currents, namely the transmembrane

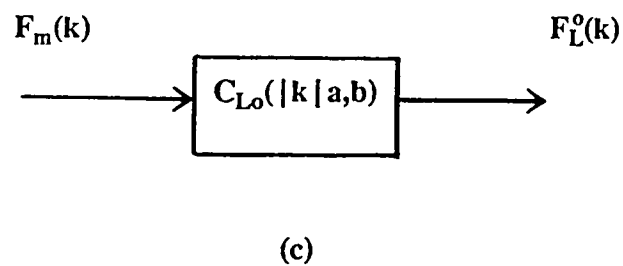
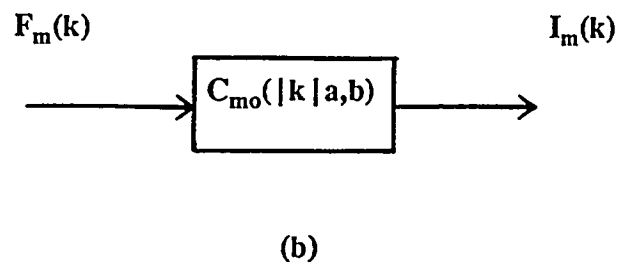
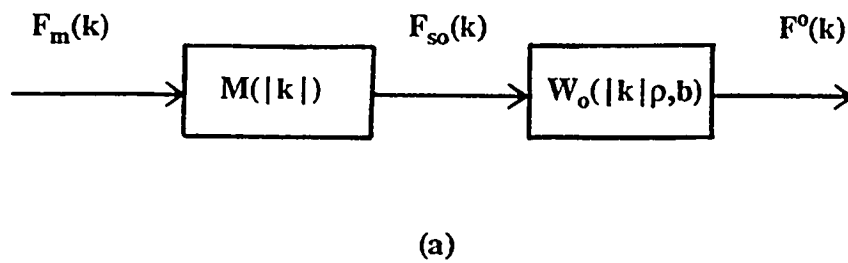


Figure 2.4 Representation of the volume conductor problem as an equivalent filtering problem for the (a) extracellular potential (b) transmembrane current and the (c) total external longitudinal current.

current and the total longitudinal current in the intra- and extracellular media. Figure 2.4b illustrates this procedure using one form of the transmembrane current filter function $C_{mo}(|k|, a, b)$ while figure 2.4c depicts the problem for the total external longitudinal current filter function $C_{Lo}(|k|, a, b)$. The input in both cases is the Fourier transform of the transmembrane potential distribution $F_m(k)$. The output in fig. 2.4b is $I_m(k)$ the Fourier transform of the transmembrane current defined in equation (1.58) while the output in fig. 2.4c is $F_L^o(k)$ the Fourier transform of the external longitudinal current defined in equation (1.62).

Figure 2.5 shows the characteristics of the membrane and medium filter functions when the volume conductor radius is varied. The membrane acts as a second derivative filter and so the shape of the membrane filter characteristic is a family of parabolas as seen from fig. 2.5a. As the outer boundary of the volume conductor is decreased, the membrane filter characteristic no longer approaches zero as the spatial frequency k tends to zero, as in the infinite medium case. Rather as b becomes smaller the membrane filter gain at low spatial frequencies increases (see insert fig. 2.5a). The medium filter characteristic shown in fig. 2.5b is computed at a field radius $\rho = 7a$ and has the nature of a low pass filter whose cut off frequency decreases as the volume conductor radius is increased.

2.4 Results

With the source waveforms shown in fig. 2.3 as input to the model, the volume conductor potentials and currents may be calculated for different values of the various model parameters. For a very large value of volume conductor radius b (e.g. $b=3000\mu$) approximating an infinite volume conductor, the calculated extracellular potential $\Phi^o(\rho, z)$ is triphasic and falls off in magnitude and frequency content with increasing values of ρ . This is clearly seen in fig. 2.6a for the unmyelinated axon where potential is evaluated at $\rho=a, 7a$ and $15a$, as well as for the myelinated fiber shown in fig. 2.6b. The general form of the extracellular potential distribution in axial distance z is triphasic for both types of axons, however the myelinated fiber has high frequency "spikes" superimposed on it, with the spikes appearing spatially at regular intervals equal to the internodal distance. These spikes correspond to potential changes associated with current entering or leaving the nodes of Ranvier. The fall-off in fre-

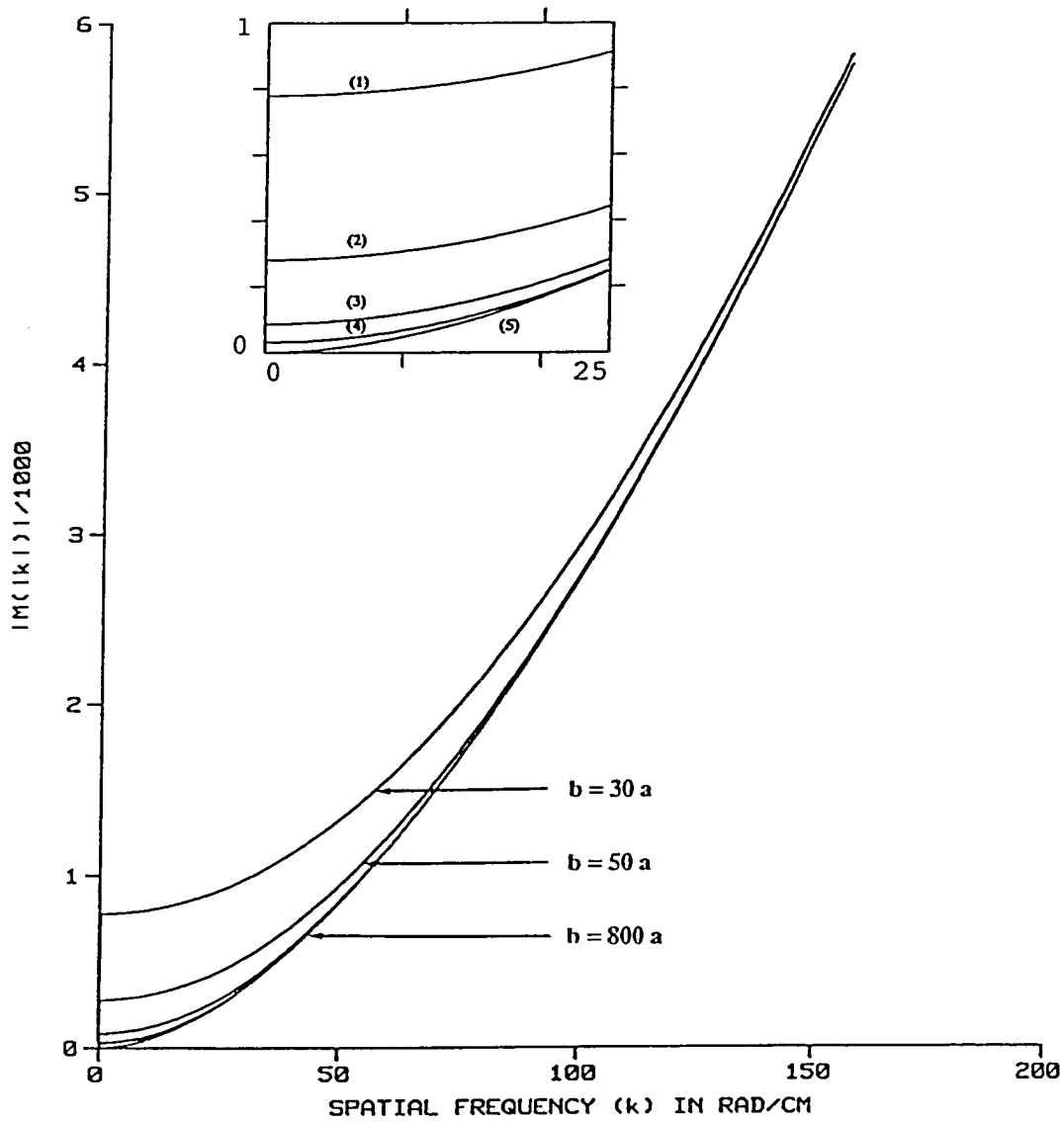


Figure 2.5 a The characteristics of the membrane filter function $M(|k|)$ vs. k for various values of the volume conductor radius b . The case chosen is for a cylindrical myelinated fiber having a radius of $5 \mu\text{m}$. In fig. 2.5 a the characteristics are labeled in the insert as (1) for $b = 30 a$, (2) for $b = 50 a$, (3) for $b = 90 a$, (4) for $b = 150 a$ and (5) for $b = 800 a$.

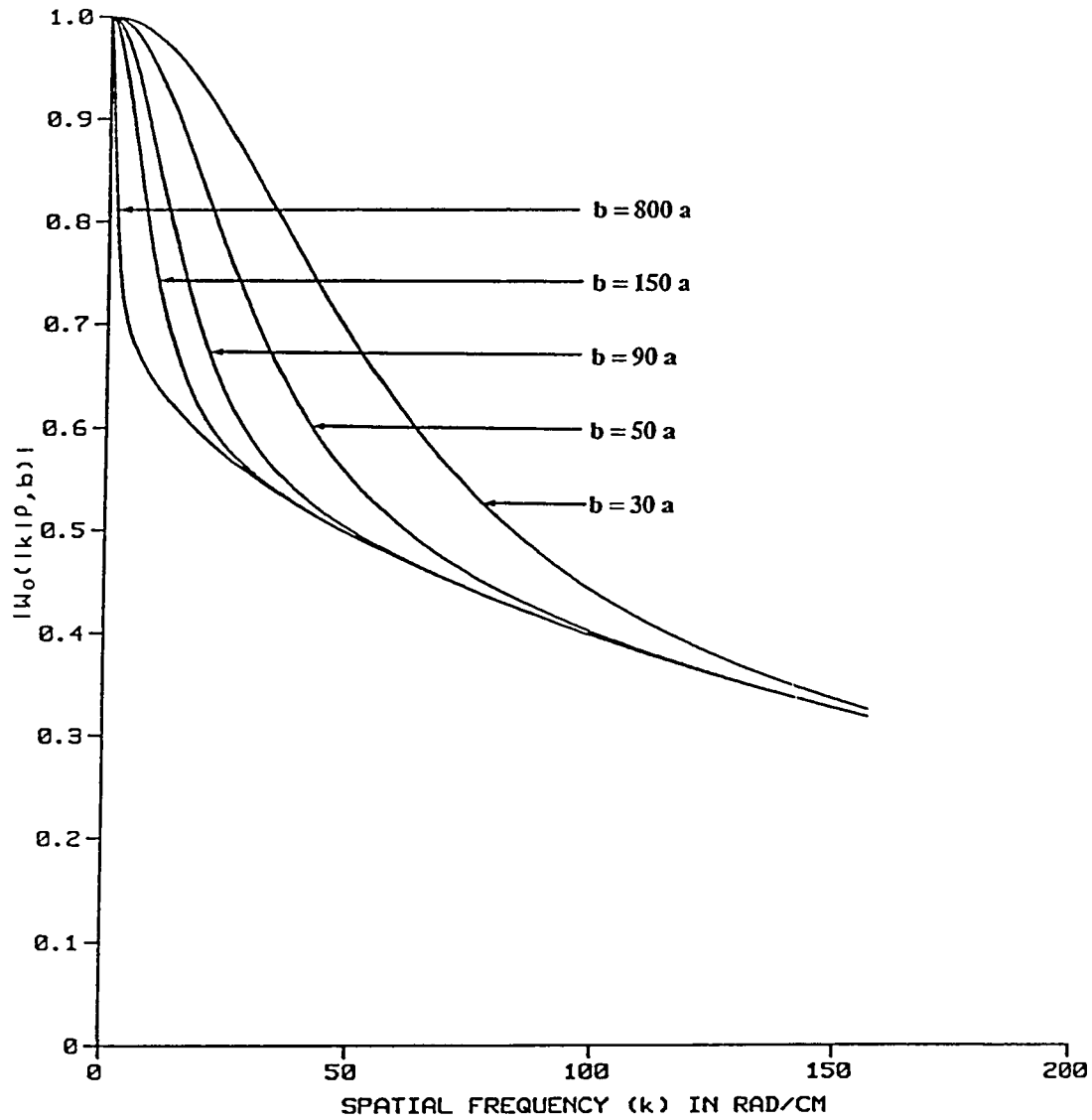


Figure 2.5 b The characteristics of the medium filter function $W(k|\rho, b)$ vs. k for various values of the volume conductor radius b . The case chosen is for a cylindrical myelinated fiber having a radius of $5 \mu\text{m}$. The medium filter is evaluated at a field radius $\rho = 7 a$.

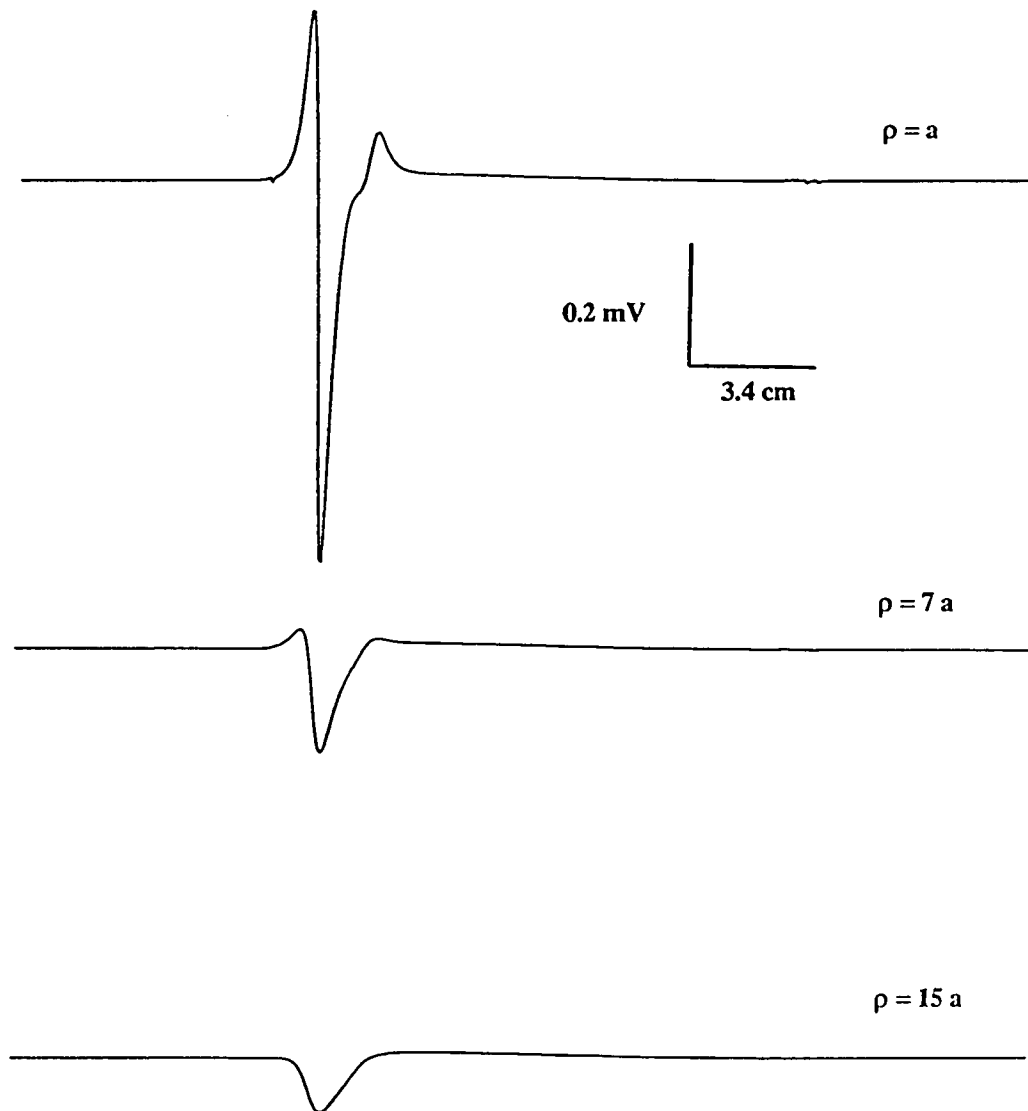


Figure 2.6 a Computed extracellular potential waveforms at several radial distances from the fiber ($\rho = a$, $7a$, and $15a$) for the unmyelinated fiber.

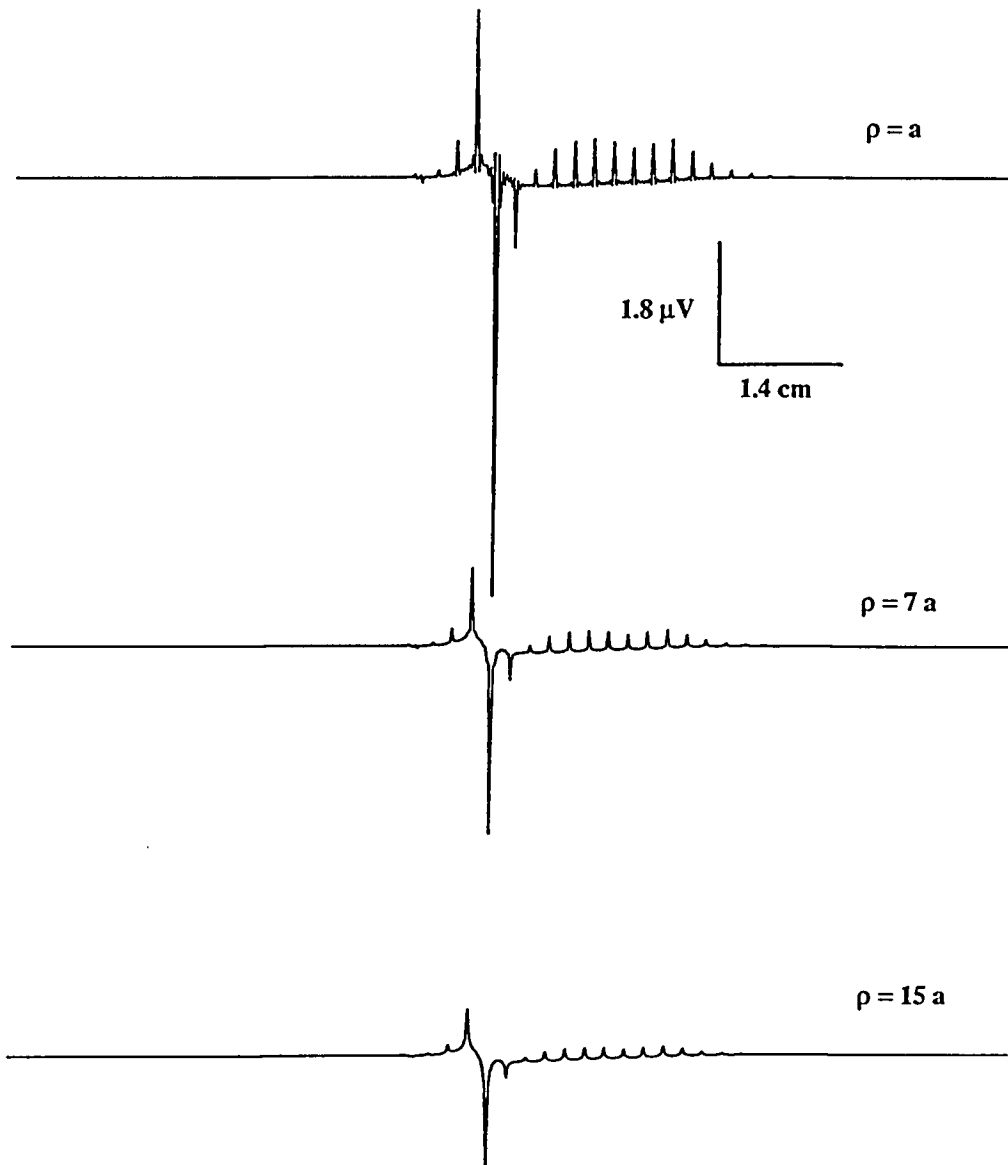


Figure 2.6 b Computed extracellular potential waveforms at several radial distances from the fiber ($\rho = a$, $7a$, and $15a$) for the myelinated fiber.

quency content with potential evaluated at increasing distances from the surface of the fiber is especially well seen in the attenuation of the current related spikes in fig. 2.6b.

The general shape of the extracellular potential waveform is significantly influenced by the value of the model parameter b , the radius of the volume conductor medium. As the outer boundary at $\rho=b$ is made to approach the surface of the fiber, the extracellular potential $\Phi^o(\rho, z)$ increases in spatial extent and undergoes a change in shape. This is illustrated for the case of the outer surface potential distribution $\Phi_{so}(z)$ for the unmyelinated axon in fig. 2.7a and the myelinated axon in fig. 2.7b. When the extent of the volume conductor is very small i.e. when the outer boundary is very close to the surface of the fiber, the extracellular potential is fairly large in magnitude. In the case of the myelinated fiber, the spikes are almost obscured by the relatively slow triphasic potential; the magnitude of this slow potential decreases as the value of b increases.

The peak to peak magnitude of the extracellular potential and the field extent in the volume conductor also depend on the fiber radius a . This variation of peak to peak magnitude at the fiber surface, for the unmyelinated fiber in an infinite volume conductor, is shown in fig. 2.8a as a function of fiber radius. The variation is certainly not linear, and a family of curves can be obtained upon varying the ratio of conductivities σ_o/σ_i , and thereby changing the gain of the membrane filter function in accordance with equations (1.21) and (1.26). The peak to peak magnitude is further increased when the fiber is enclosed in a finite volume conductor of an extent comparable to the size of the fiber. Fig. 2.8b shows the fall off in peak to peak magnitude as a function of absolute distance from the fiber surface for several values of the fiber radius. Once again the nature of the fall off is illustrated for the unmyelinated fiber. The general nature of the fall off is the same for fibers of different radii but the field extent is much smaller for a small fiber, representing a weaker source, than it is for a large axon.

The transmembrane current per unit length $i_m(z)$ is shown in fig. 2.9a for the unmyelinated axon and in fig. 2.9b for the myelinated fiber. Testing has shown that this current is essentially invariant in magnitude and spatial extent for different values of the volume conductor radius b , a result which justifies the assumption that the nerve fiber behaves essentially as a constant current source under a variety of load conditions. The myelinated fiber transmembrane current $i_m(z)$ shown in fig. 2.9b

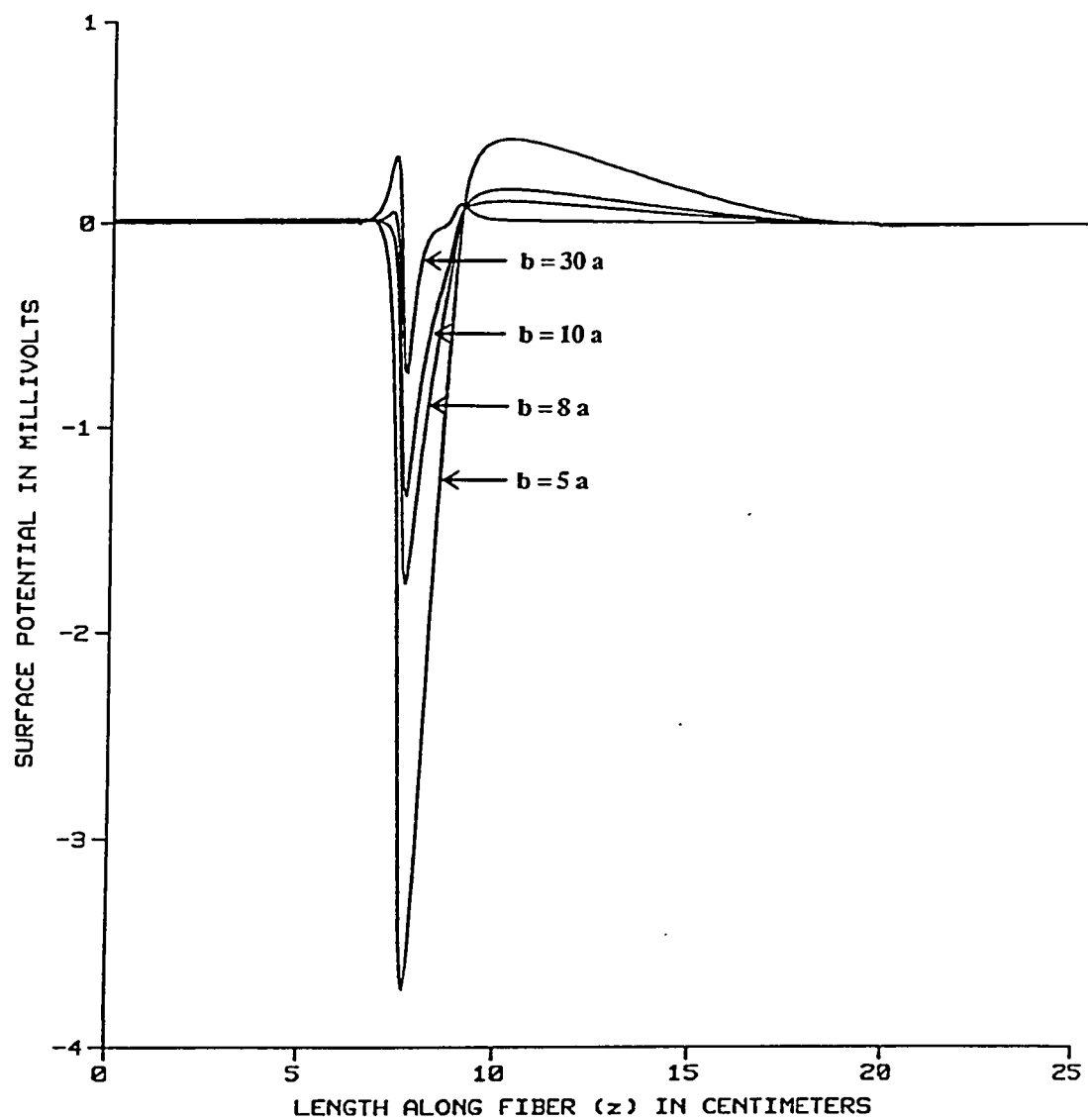


Figure 2.7 a Computed surface potential waveforms $\Phi_{so}(z)$ for different values of the volume conductor radius b in the case of the unmyelinated fiber.

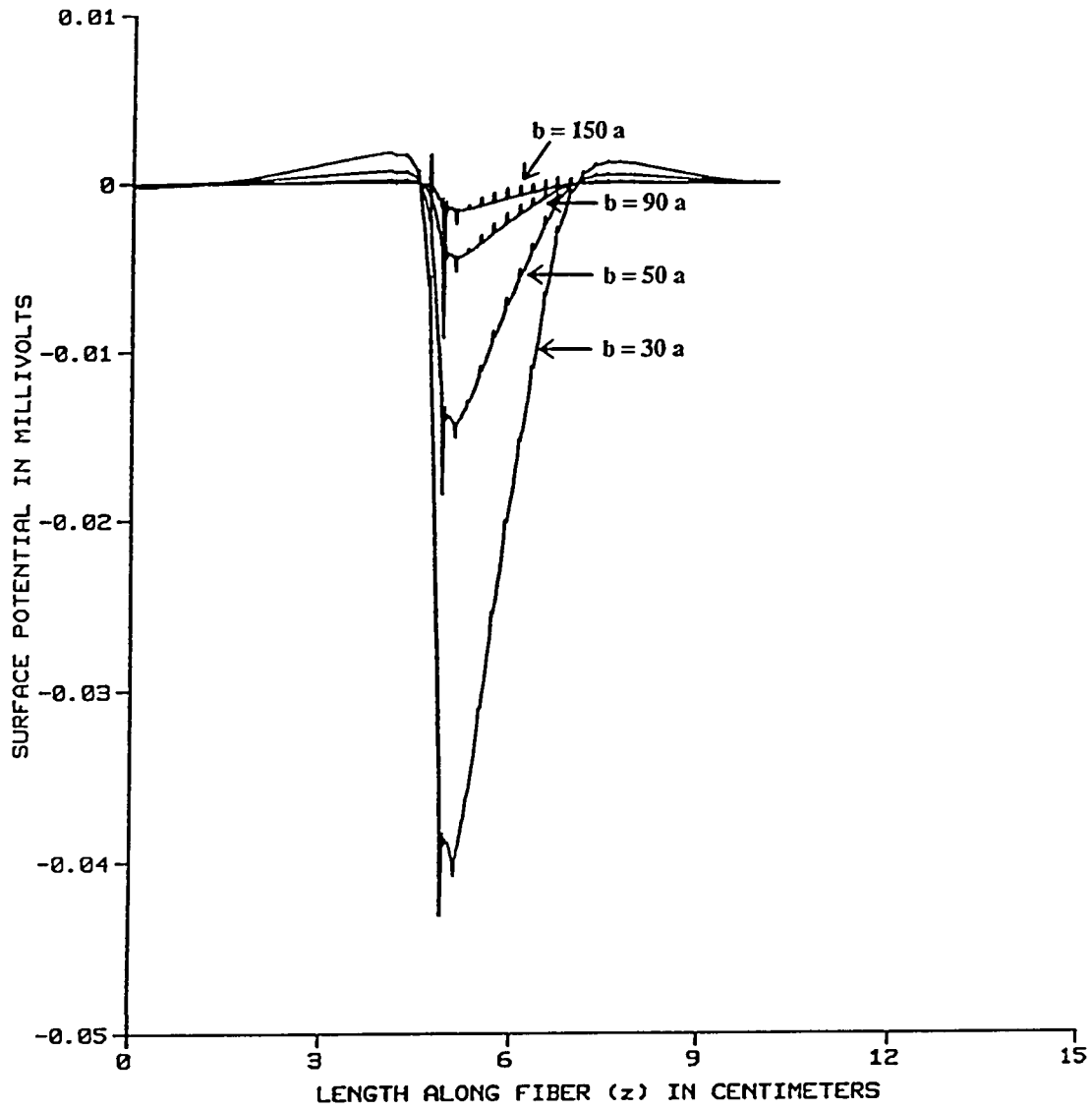


Figure 2.7 b Computed surface potential waveforms $\Phi_{s0}(z)$ for different values of the volume conductor radius b in the case of the myelinated fiber.

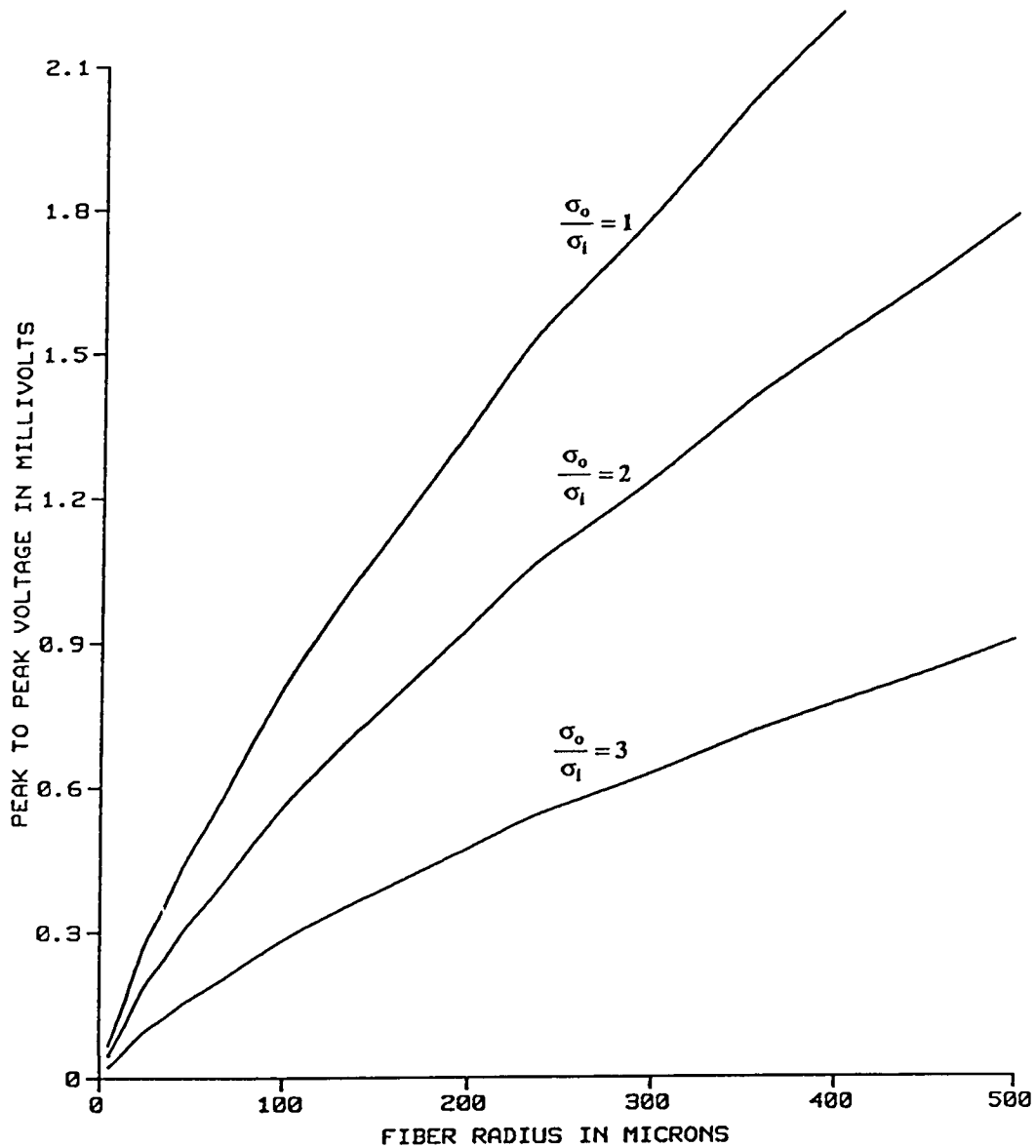


Figure 2.8 a Variation in peak to peak magnitude of the extracellular potential with different fiber radii.

The peak to peak magnitude considered in is at the fiber surface and the family of curves is obtained upon varying the ratio of conductivity outside the fiber σ_o to conductivity inside the fiber σ_i .

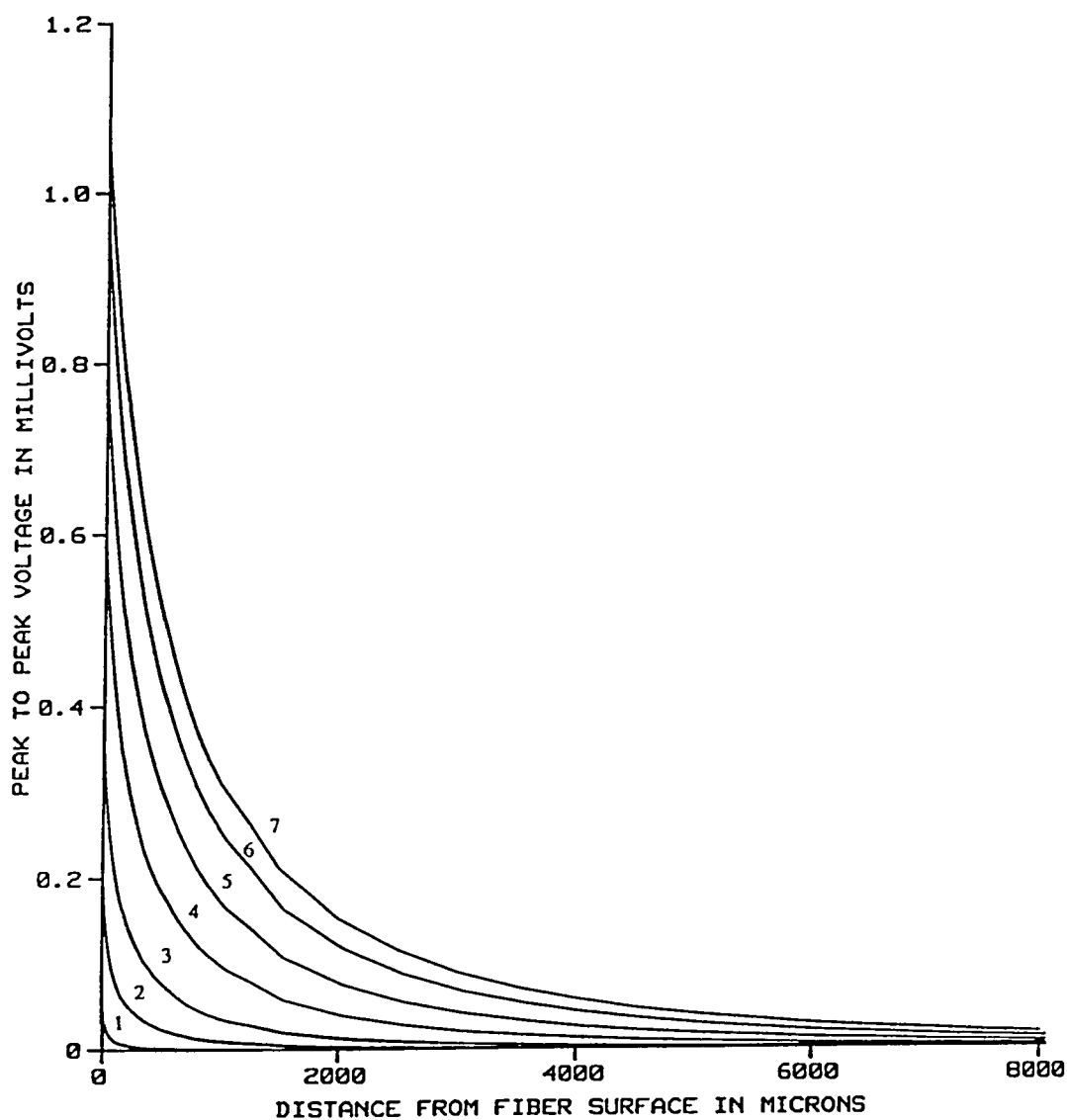


Figure 2.8 b Variation in field extent of the extracellular potential with different fiber radii. The curves in are labeled as (1) for $a = 5 \mu$, (2) for $a = 25 \mu$, (3) for $a = 55 \mu$, (4) for $a = 105 \mu$, (5) for $a = 155 \mu$, (6) for $a = 205 \mu$ and (7) for $a = 238 \mu$.

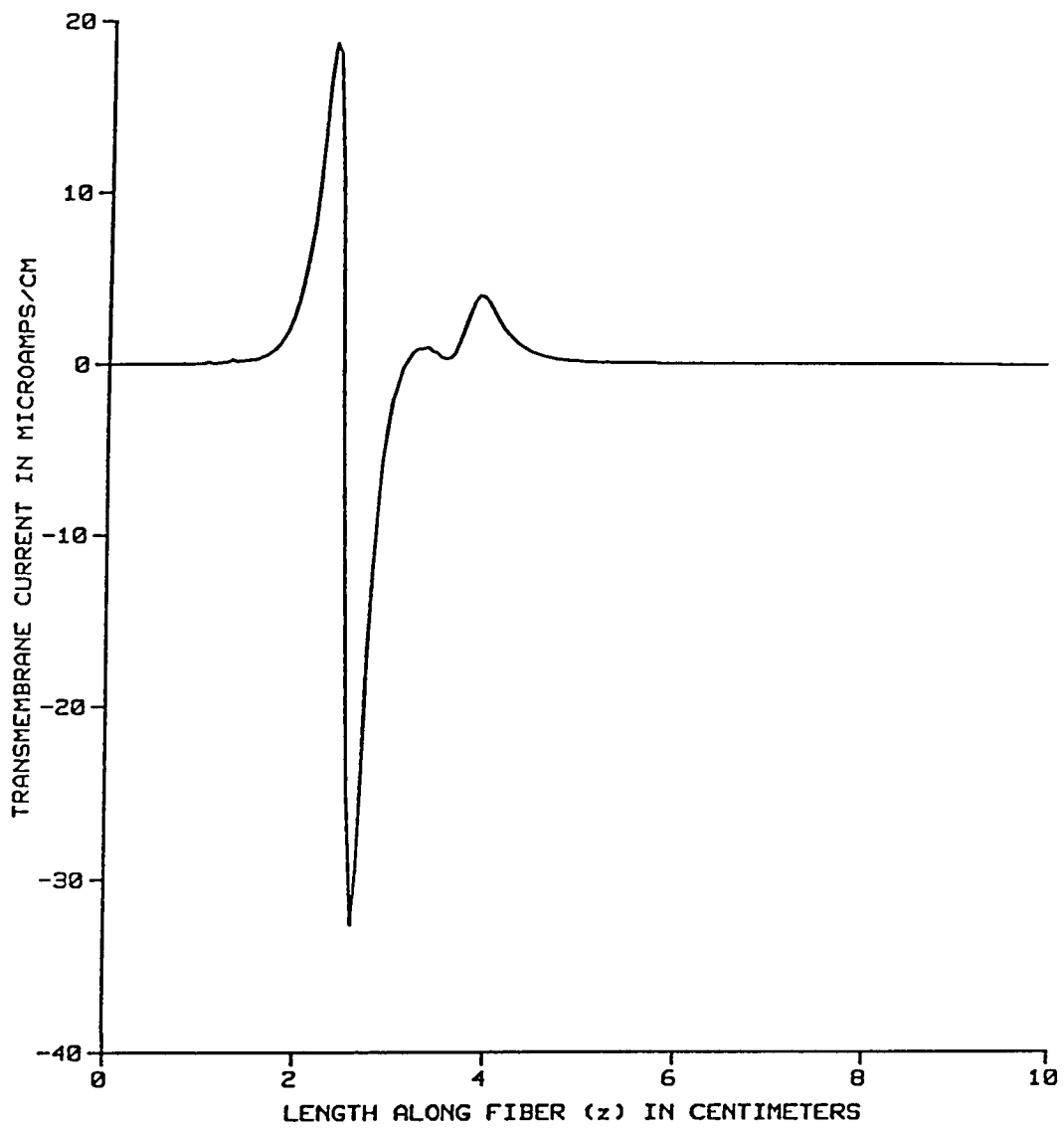


Figure 2.9 a Transmembrane current per unit length $i_m(z)$ for the unmyelinated fiber.

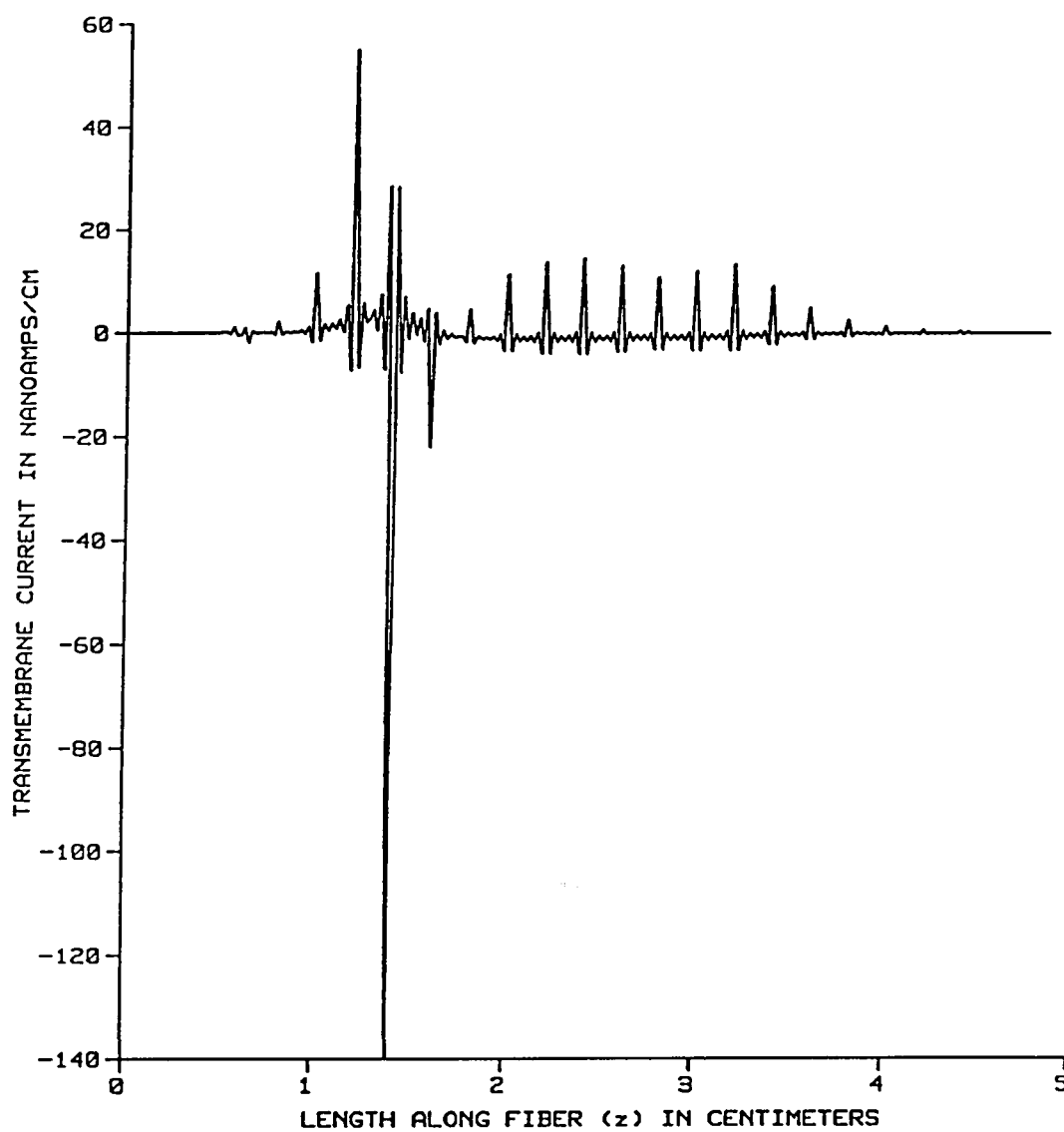


Figure 2.9 b Transmembrane current per unit length $i_m(z)$ for the myelinated fiber.

reflects the nature of that source in that, it peaks at spatial points corresponding to the location of the nodes of Ranvier in the myelinated fiber.

Figure 2.10 shows the total external longitudinal current $I_L^o(z)$ for the unmyelinated fiber in (a) and the myelinated fiber in (b). The total internal longitudinal current $I_L^i(z)$ is of the same shape and magnitude but of opposite sign for both cases. This result is consistent with the assumption of solenoidal current flow made in the core conductor model (equation (1.30)). For both the unmyelinated fiber and the myelinated fiber, the total external longitudinal currents are independent of the position of the outer boundary b , a result that is not surprising because of the integration that is performed over all values of ρ at each value of z in order to evaluate them. The integration is equivalent to an averaging process in a particular z -plane performed on the radial component of the current density $J_\rho(z)$ over the entire extent of the volume conductor which effectively removes any radial variations [see equation (1.41)].

A sensitive index of the changes that occur in the volume conductor as its is varied (i.e. as the position of the outer boundary b is changed) is the ratio of the radial and axial components of the current density, namely $J_\rho(z)/J_z(z)$. The ratio is a measure of the relative strength of the two components of the current density and indicates the orientation of the current density field. A large value of the ratio indicates a predominantly radial field while a small ratio indicates an axial field. This ratio is calculated at a fixed value of ρ for all values of z . Figure 2.11 shows this ratio as a function of z for different values of b , calculated at $\rho = 2a$ for the unmyelinated fiber in fig. 2.11 (a) and the myelinated fiber in fig. 2.11 (b). As is apparent from the figure, both the absolute magnitude and the shape of the ratio change with various values of b . When the extent of the volume conductor is very small ($b = 3a$ for the unmyelinated fiber and $b = 30a$ for the myelinated fiber) the ratio is almost zero for all values of z . This is the point at which the current density field is almost completely axial.

2.5 Discussion of results

The results in fig. 2.7, that show the extracellular potential increasing in both spatial extent and magnitude when the outer boundary of the volume conductor approaches the fiber surface, can be

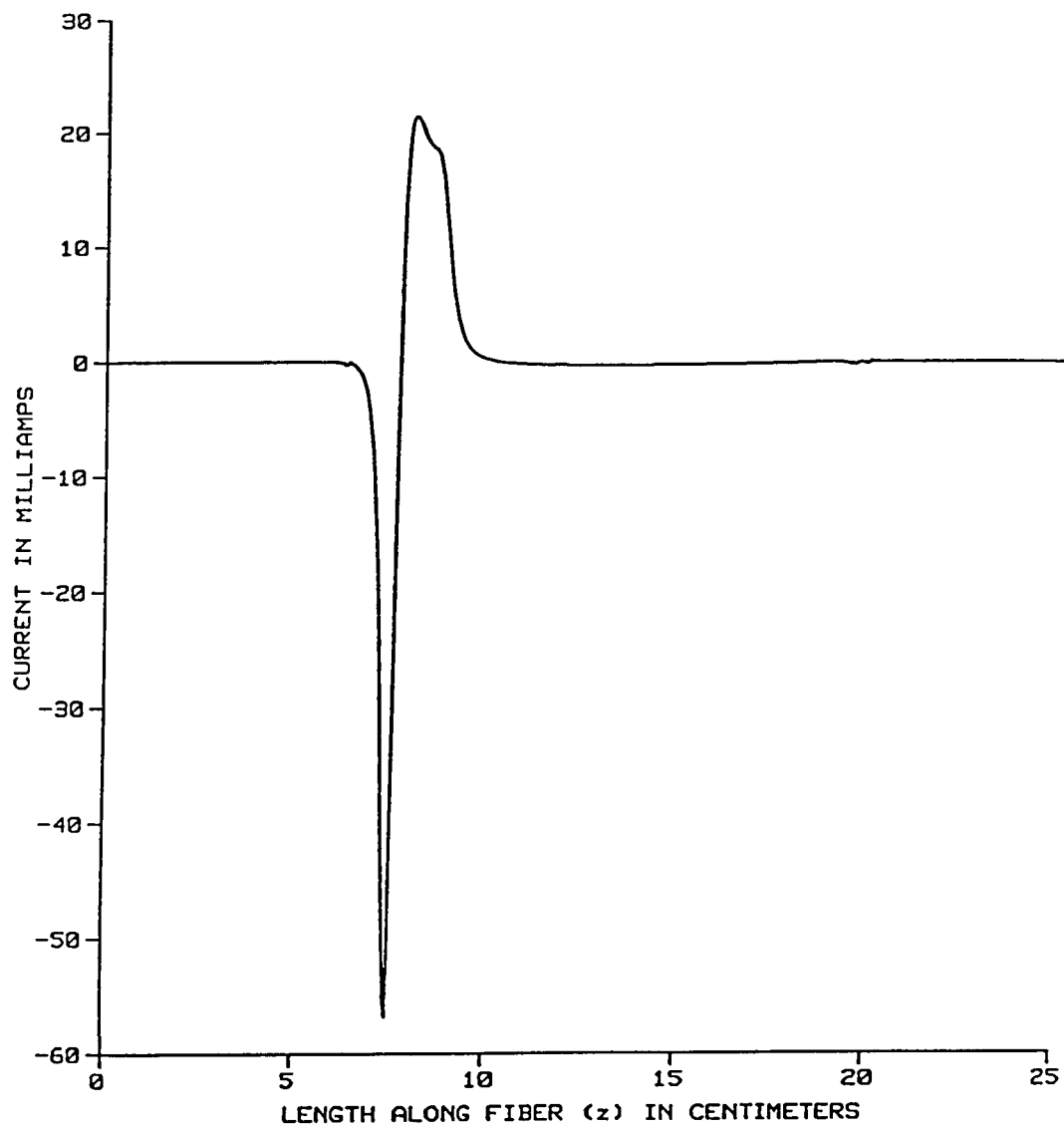


Figure 2.10 a Total external longitudinal current $I_L^o(z)$ for the unmyelinated fiber.

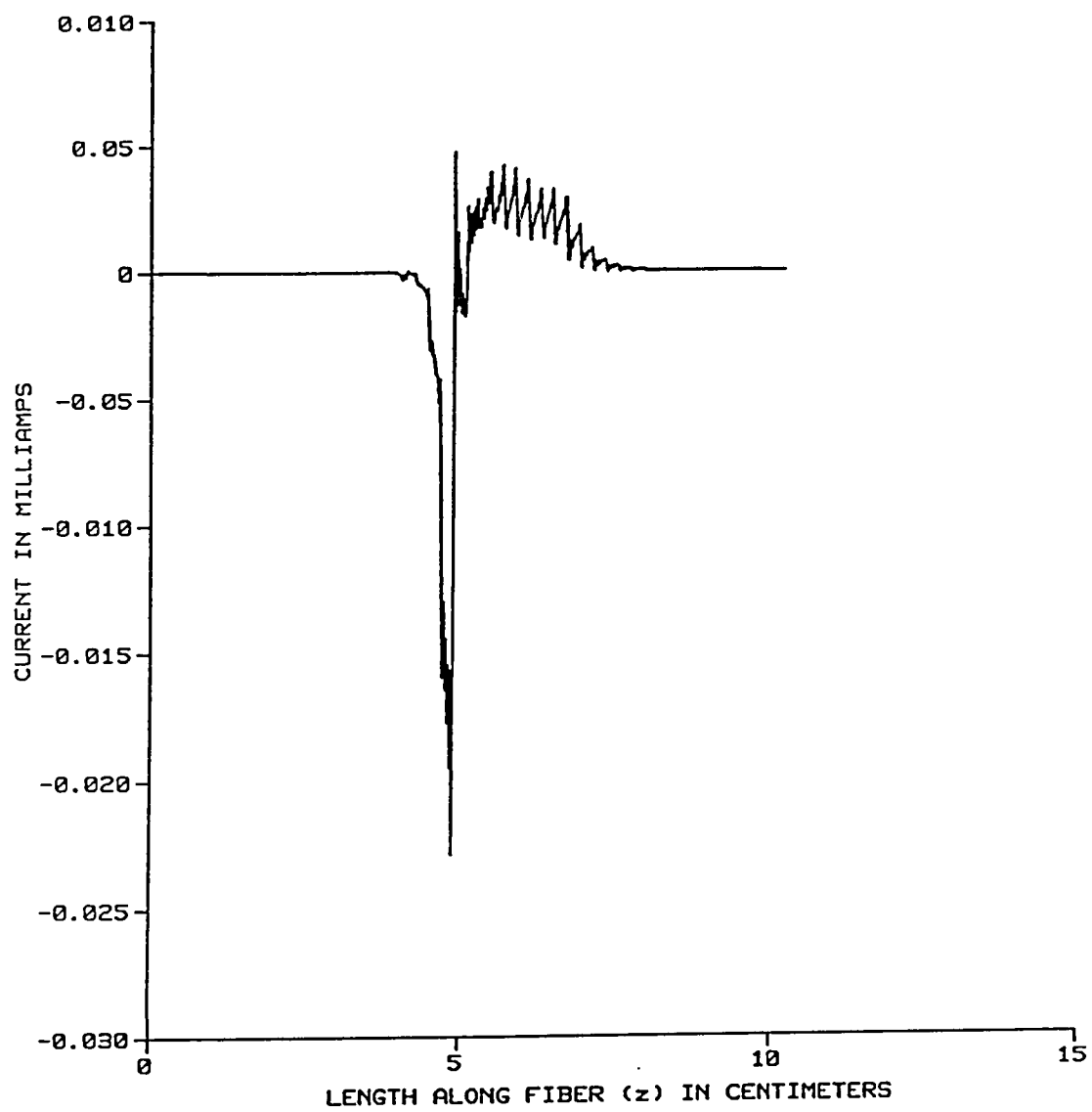


Figure 2.10 b Total external longitudinal current $I_L^0(z)$ for the myelinated fiber.

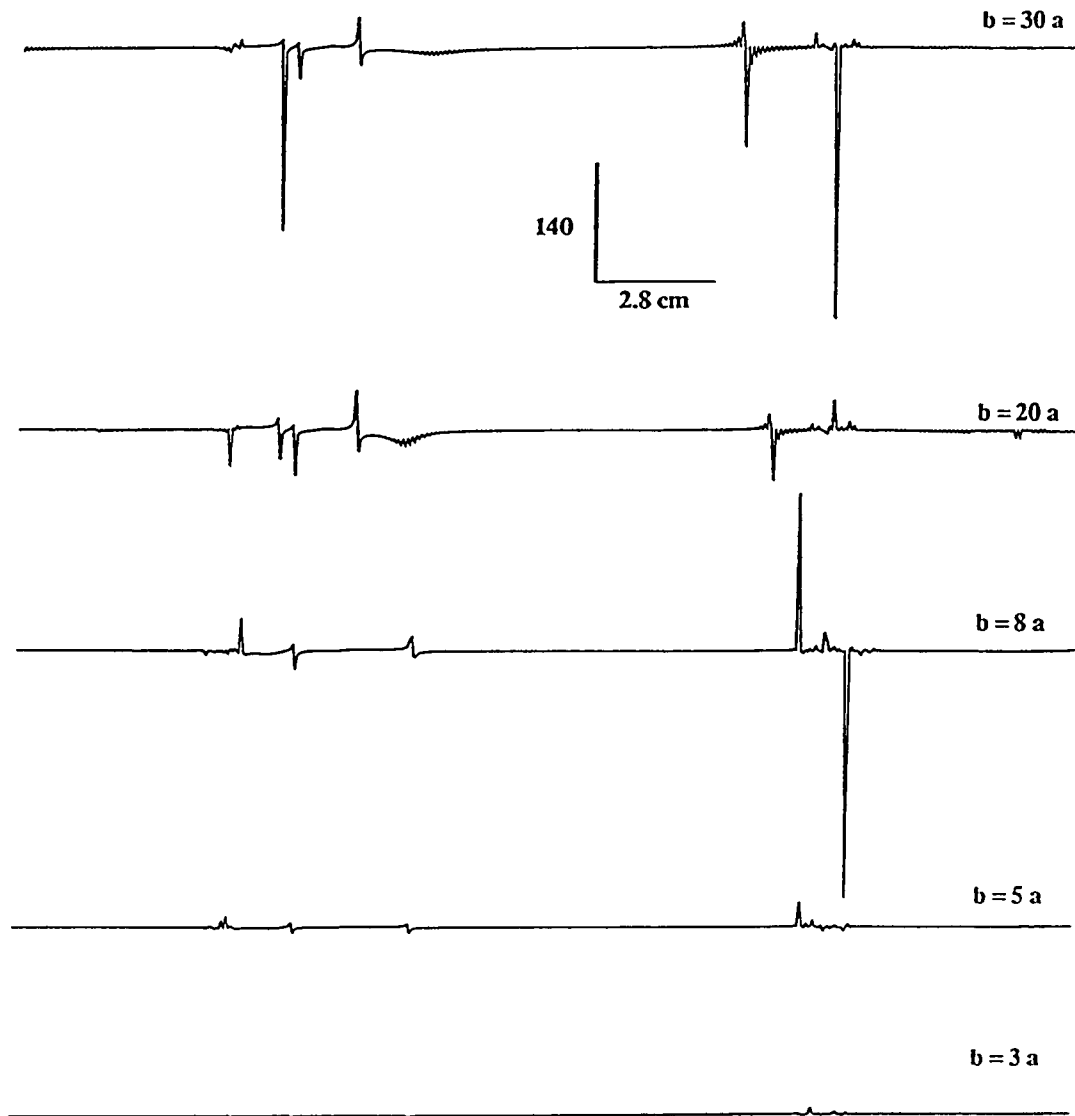


Figure 2.11 a The ratio of the radial component of the current density to the axial component of the current density $J_\rho(z)/J_z(z)$ for the unmyelinated fiber. The ratio is evaluated at $\rho = 2a$.

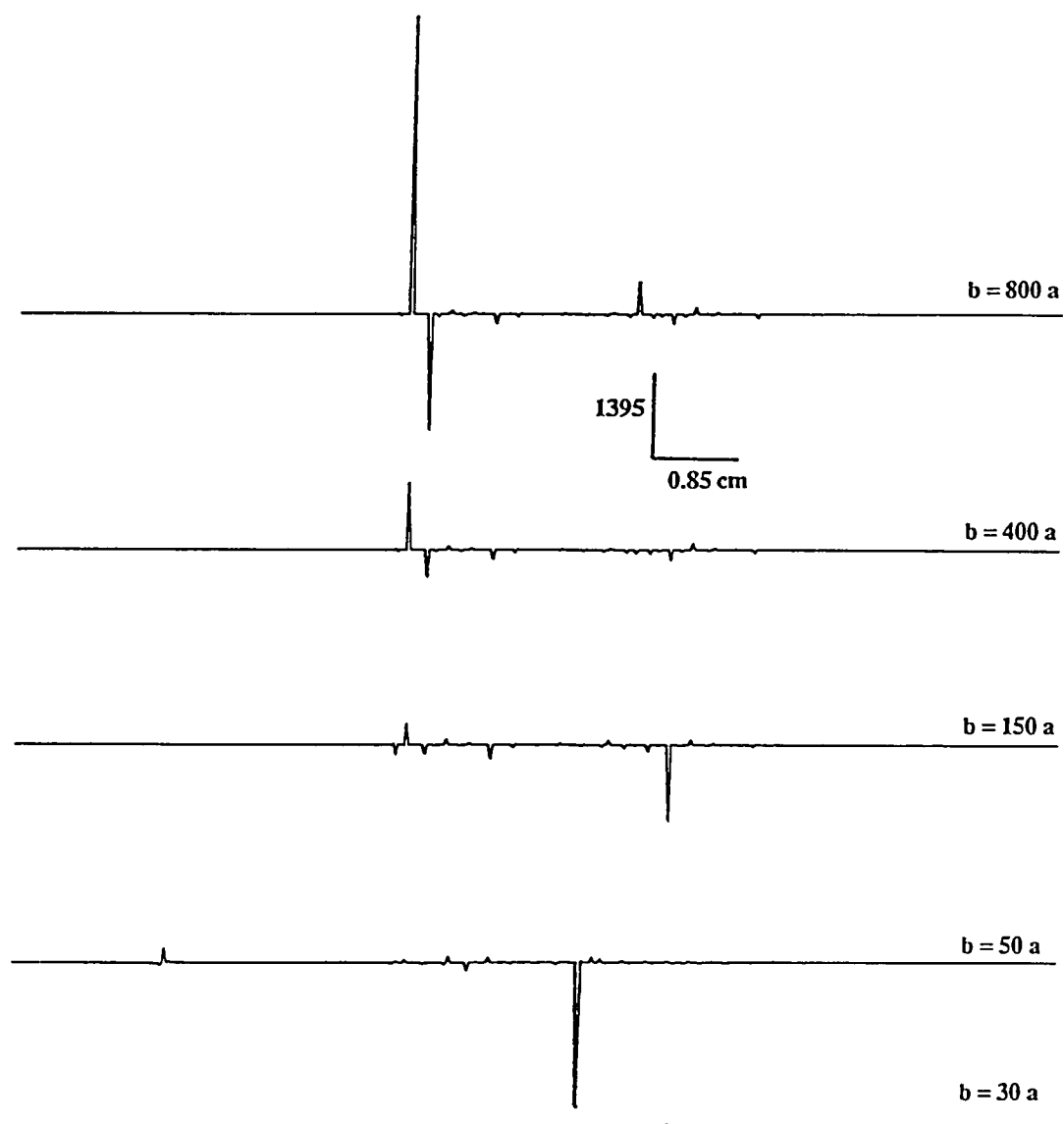


Figure 2.11 b The ratio of the radial component of the current density to the axial component of the current density $J_\rho(z)/J_z(z)$ for the myelinated fiber. The ratio is evaluated at $\rho = 2a$.

explained upon consideration of the characteristics of the membrane and medium filter functions. Referring back to fig. 2.5, the filter characteristics of both filters show an increase in lower spatial frequency gain as the outer boundary of the volume conductor is made smaller. This increase in lower spatial frequency gain results in a larger signal magnitude of relatively slow components of the signal, which is reflected in the fairly large slow triphasic component present in the calculated extracellular potential when the extent of the volume conductor is small.

In the core conductor model it is assumed that the extracellular medium may be characterized by a lumped resistance per unit length r_o . This assumption implies that the current in the extracellular medium is completely axial, a fact that is made apparent in the cable equations (1.29) through (1.32). The field theoretic technique employed here for the evaluation of the extra- and intracellular currents and potentials, does not make use of the assumption of a predominantly axial current flow in any region of the model. The results of the field evaluation are exact and can be used as a standard of measurement when evaluating the core conductor model. As is obvious from fig. 2.10 the current density in the extracellular medium can be considered to be axial only for relatively small values of the volume conductor radius b . For the most part the extracellular current density field consists of a fairly large radial component. It can therefore be stated that the core conductor model is a fairly inaccurate representation of events in the extracellular medium except in cases where the volume conductor is extremely small in extent, as in the case where a single nerve fiber is immersed in an oil bath, with only a thin adhering layer of conducting fluid serving as the extracellular medium. On the other hand, we have found the core conductor model to be a very good representation of electrical events occurring in the intracellular medium.

Besides evaluating the cable equations, the DFT technique employed here is a rapid, accurate and fairly powerful technique to calculate the complete current and potential fields in the region within and without the unmyelinated or myelinated nerve fiber. In the method used here the spatial distribution of the transmembrane potential distribution has been explicitly evaluated at each instant of time. As will be demonstrated in the next chapter, this fact can be made use of to rapidly calculate current and potential fields, at a specific point in the intra- or extracellular medium, as functions of time. This

is greatly facilitated because of the fact that the filter functions used in this technique are not functions of time, depending as they do only on geometric and electrical properties of the medium around the cell membrane.

CHAPTER 3

Currents and Potentials of the Active Myelinated Nerve Fiber

3.1 Introduction

The previous chapter was concerned in part with the evaluation of the Core Conductor Model for the active myelinated nerve fiber. This chapter is concerned with the accurate and rapid calculation of extracellular field potentials and currents from an active myelinated nerve fiber in a volume conductor, under conditions of normal and abnormal conduction. The neuroelectric source for the problem is characterized mathematically by using a modified version of the distributed parameter model of Goldman and Albus (1968) for the myelinated nerve fiber as described in the two previous chapters. Solution of the partial differential equation associated with the model, provides a waveform for the spatial distribution of the transmembrane potential $V(z)$. This model-generated waveform is then utilized as input to a second model that is based on the principles of electromagnetic field theory, and which allows one to easily calculate the spatial distribution for the potential everywhere in the surrounding volume conductor for the nerve fiber. In addition, the field theoretic model may be utilized to calculate the total longitudinal current in the extracellular medium ($I_L^o(z)$) and the transmembrane current per unit length ($i_m(z)$); both of these quantities being defined in connection with the well-known core conductor model and associated cable equations in electrophysiology. These potential and current quantities may also be calculated as functions of time and as such, are useful in interpreting measured $I_L^o(t)$ and $i_m(t)$ data waveforms. An analysis of the accuracy of conventionally employed measurement techniques to determine $I_L^o(t)$ and $i_m(t)$ is performed, particularly with regard to the effect of electrode separation distance and size of the volume conductor on these measurements. Also, a simulation of paranodal demyelination at a single node of Ranvier is made and its effects on potential and current waveforms as well as, on the conduction process are determined. The effects on the temporal waveshape of the field potentials as a result of non-uniform conduction are also demonstrated and dis-

cussed.

3.2 Modeling Aspects

An expression for the extracellular potential distribution $\Phi^o(\rho, z)$ from an active nerve fiber of radius a positioned at the center of a finite volume conductor of radius b (fig. 3.1) is given by equation (1.23) of chapter 1. This equation is obtained as a solution to Laplace's equation for the external volume conductor medium under quasistatic conditions, subject to appropriate boundary conditions at $\rho = a$ and $\rho = b$ (fig. 3.1). Here σ_o and σ_i are the specific conductivities (S/cm) of the extra- and intracellular media. The expressions are also given for the transmembrane current per unit length $i_m(z)$ in mA/cm and the total external longitudinal current $I_L^o(z)$ in mA, in equations (1.33) and (1.47) of chapter 1.

The problem of calculating currents and potential in terms of the integral equations is simplified via definition of the set of filter functions in equations (1.25), (1.26) for extracellular potential and in equations (1.49) and (1.51) for extracellular currents. Thus,

$$\Phi^o(\rho, z) = \frac{1}{2\pi} \int_{-\infty}^{\infty} W_o(|k|, \rho, b) F_m(k) e^{-jkz} dk \quad (3.1)$$

$$i_m(z) = -\sigma_o a \int_{-\infty}^{\infty} C_{mo}(|k|, a, b) F_m(k) e^{-jkz} dk \quad (3.2)$$

and

$$I_L^o(z) = -\sigma_o a \int_{-\infty}^{\infty} C_{Lo}(|k|, a, b) [jF_m(k)] e^{-jkz} dk \quad (3.3)$$

are the expressions for the potential and current in the region around the myelinated fiber.

The equivalent filtering approach is illustrated in fig. 3.1 for the case where extracellular potential is evaluated; the filters involved in the calculation are the membrane filter $M(|k|)$ and the medium filter $W_o(|k|, \rho, b)$ for a cylindrical volume conductor of radius b . The input to the membrane filter is the spatial distribution of the transmembrane potential along the nerve fiber $\Phi_m(z)$. This is the poten-

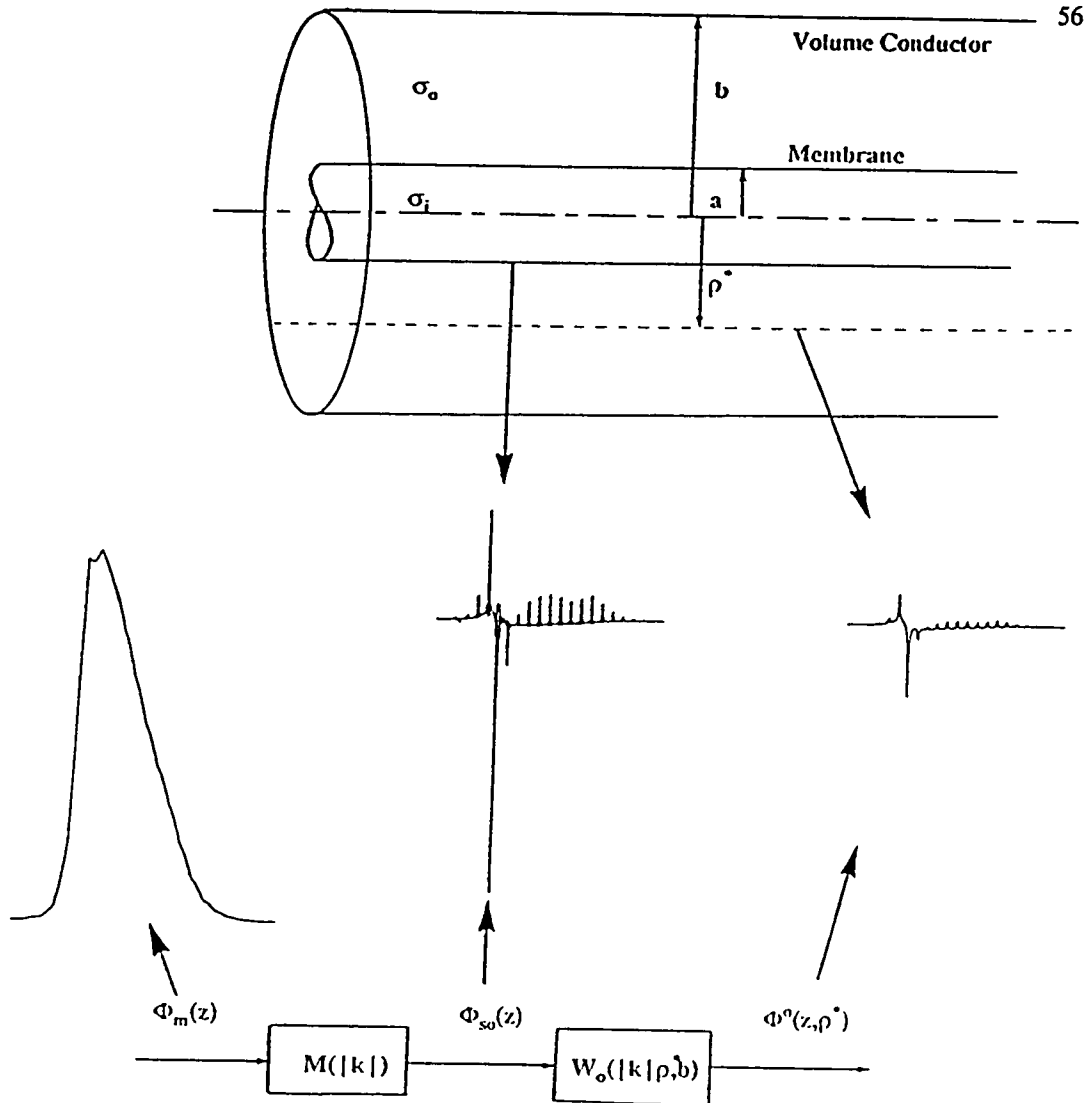


Figure 3.1 A stylized diagram of the equivalent filtering problem for the extracellular potential where $\Phi_m(z)$, $\Phi_{so}(z)$ and $\Phi^o(z, \rho^*)$ are the spatial transmembrane, outer membrane surface and field potential distributions, respectively. The membrane filter is $M(|k|)$ and $W_o(|k|, \rho, b)$ is the medium filter. Immediately above the block diagram are representative waveforms of the spatial transmembrane, outer membrane surface and field potential distributions. Fiber geometry is shown at the top of the figure.

tial distribution present across the equivalent cell membrane of the nerve fiber, along its entire length at an instant of time. The membrane filter transforms the spatial transmembrane potential distribution into the spatial potential distribution on the surface of the nerve fiber $\Phi_m(z)$, which in turn serves as input to the medium filter that produces the spatial potential distribution in the volume conductor medium at a particular radius ρ^* . Specifying a number of values of ρ^* , the potential distribution throughout the external volume conductor medium may be easily determined. The spatial current distributions $i_m(z)$ and $I_L^o(z)$ associated with the classical cable equations, may be evaluated in a similar fashion at any instant of time provided the transmembrane potential distribution is specified at that instant of time.

The filters used in this technique are time-invariant and depend on certain electrical and geometrical parameters. Only the model input, namely the spatial transmembrane potential $\Phi_m(z)$ changes with time; and it may be different at different instants of time. This fact may be exploited when the extracellular currents and potentials are reconstructed as functions of time in that, the filter functions need only be calculated once in the entire process for any given geometric and electrical configuration. Therefore, the particular spatial transmembrane potential distribution at each instant of time is presented as input to the field theoretic model and output is returned consisting of the desired current or potential distribution at that particular time instant.

In order to obtain the spatial transmembrane potential distribution along the fiber at each instant of time a distributed parameter model characterizing the myelinated nerve fiber is evaluated. This simulation of the myelinated nerve fiber is run for a predetermined length of time for a given length of the nerve fiber, which implies that a certain fixed number of "time portraits" of the electrical activity along the fiber can be generated. Each one of these time portraits is a spatial transmembrane potential distribution. In order to reconstruct the extracellular currents and potentials, each of these time portraits is presented to the field theoretic model and the corresponding extracellular current or potential distribution is returned. Given an adequate (Nyquist) sampling rate in time, the resulting set of time portraits of the extracellular currents and potentials completely define the extracellular currents and potentials as functions of time.

The process of reconstruction of the time waveform is further simplified by the fact that there exists a basic set of spatial transmembrane potential distributions that repeat with time. The number of members in this set depends on the velocity of propagation of the electrical activity along the nerve fiber, the spatial sampling interval Δz , and the sampling interval in time Δt . Under conditions of uniform conduction, this set consists of very few members that are needed to completely specify the extracellular potentials and currents at any given spatial point along the nerve, for any instant of time. All the time portraits of the transmembrane potential, that are generated by the distributed parameter model simulation of the myelinated nerve fiber, are therefore not required as input to the field theory model. During abnormal conduction however, the number of spatial transmembrane potential distributions required increases several fold, depending upon the extent of the region of abnormality. A large region of abnormality results in the distortion of several representative spatial waveforms through the region and most of these need to be included in the basic set for a successful reconstruction.

3.3 Computational Aspects

As discussed in section 2.2 of the previous chapter, the propagation of electrical activity along the myelinated nerve fiber is simulated using the distributed parameter model based on the work done by Goldman and Albus (1968). As detailed there, the Frankenhaeuser-Huxley model is employed to model both the nodal and the paranodal regions of the myelinated fiber. Slowed conduction can then be introduced by simulating paranodal demyelination which not only changes the myelin specific capacitance and conductance on either side of the node, but also strengthens the potassium and non-specific currents from the exposed area of the paranodal region. Complete conduction block may also be induced in this manner. The various values of the parameters used in the simulation are given in table 3.1 which lists the standard set for both electrical and geometric parameters. The radius of the volume conductor b is specified as a multiple of the fiber radius a . The partial differential equation that describes the propagation of the electrical activity along the nerve is numerically integrated using a stable, implicit finite difference scheme called the Crank-Nicholson method (Crank, 1947).

Table 3.1 : Electrical & Geometric Model Parameters

Parameter	Value Used
Fiber radius (a)	0.0005 cm
Myelin thickness (at)	0.0002 cm
Length of a node of Ranvier (NL)	0.0004 cm
Internodal distance (INL)	0.2 cm
Radius of the volume conductor (b)	$n \cdot a$
External resistivity (R_o)	70 Ω cm
Internal resistivity (R_i)	100 Ω cm
External resistance per unit length (r_o)	$R_o/\{\pi a^2(n^2-1)\}$
Internal resistance per unit length (r_i)	$R_i/\pi a^2$
Membrane Capacitance (C_m)	2 $\mu\text{F}/\text{cm}^2$
Myelin Capacitance (C_{my})	0.00387 $\mu\text{F}/\text{cm}^2$
Myelin Conductance (g_{my})	0.083308 $\mu\text{mho}/\text{cm}^2$
Leak Potential (E_l)	0.026 mV
Leak conductance (g_l)	30.3 m mho/cm^2
Sodium permeability constant (P_{Na})	0.008 cm/sec
Potassium permeability constant (P_K)	0.0012 cm/sec
Non-specific permeability constant (P_p)	0.00054 cm/sec
External Sodium concentration ($[Na^+]_o$)	114.5 mM
Internal Sodium concentration ($[Na^+]_i$)	13.74 mM
External Potassium concentration ($[K^+]_o$)	2.5 mM
Internal Potassium concentration ($[K^+]_i$)	120.0 mM

3.4 Results

With the parameter values specified in Table 3.1, the distributed parameter network for the myelinated nerve fiber can be solved to obtain the transmembrane potential difference at every point along the fiber for any time instant desired. The solution is shown as a three dimensional view in fig. 3.2 where the transmembrane potential is shown along a small length of the fiber, covering five nodes of Ranvier. The spatial transmembrane potential can be seen along the isochronal lines in the figure; electrical activity is shown here as propagating in the negative z direction. The familiar action potential is seen in the transmembrane potential as a function of time, at a fixed point in space. The discontinuous nature of the propagation velocity along the nerve fiber manifests itself as discontinuities in the spatial waveform which can be traced along each isochronal line.

The extracellular potential calculated at the fiber surface as a function of time, at different points along the nerve fiber is shown in fig. 3.3. The magnitude of the calculated potential at the nodes of Ranvier is ten times its value at the internodes (note scale changes in fig. 3.3). The discontinuous nature of the propagation is illustrated more clearly in this figure where the activity is proceeding from bottom to top along the fiber.

Fig. 3.4 is a three dimensional view of the transmembrane current per unit length i_m . Upward currents in the figure are inward membrane currents, therefore the current spikes seen pushing out of the plane are inward currents. The troughs seen in the figure represent outward current. It can be seen that there is a strong inward current at the nodes of Ranvier followed by a prolonged outward current. At the internodal points along the fiber the current is completely outward and is ten times smaller in magnitude than the peak to peak current at the nodes. Once again the propagation is in the negative z direction which means that the activity is traveling from right to left along the fiber.

A three dimensional view of the total longitudinal current outside the fiber I_L^o is presented in fig. 3.5. The longitudinal current has also been reversed in polarity for clarity of view. The total longitudinal current outside the fiber is mostly an inward current both at the nodes and the internodes, however the strength of the current drops slightly at the nodes of Ranvier where the transmembrane current per unit length is strongest. This effect is illustrated better in fig. 3.6. Propagation in fig. 3.5 is in the

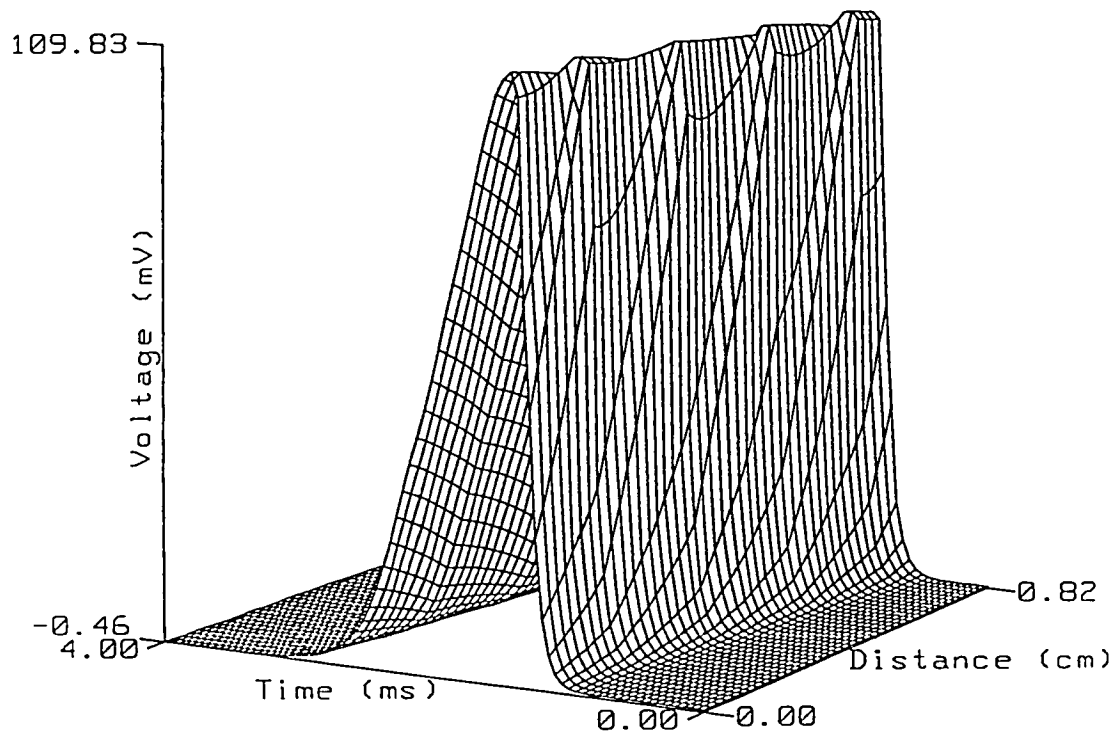


Figure 3.2 A three dimensional view of the propagating action potential, propagating from right to left along the spatial axis (negative z direction). The activity is shown over a time period of 4 milliseconds and a spatial distance of 0.82 centimeters which includes five nodes of Ranvier.

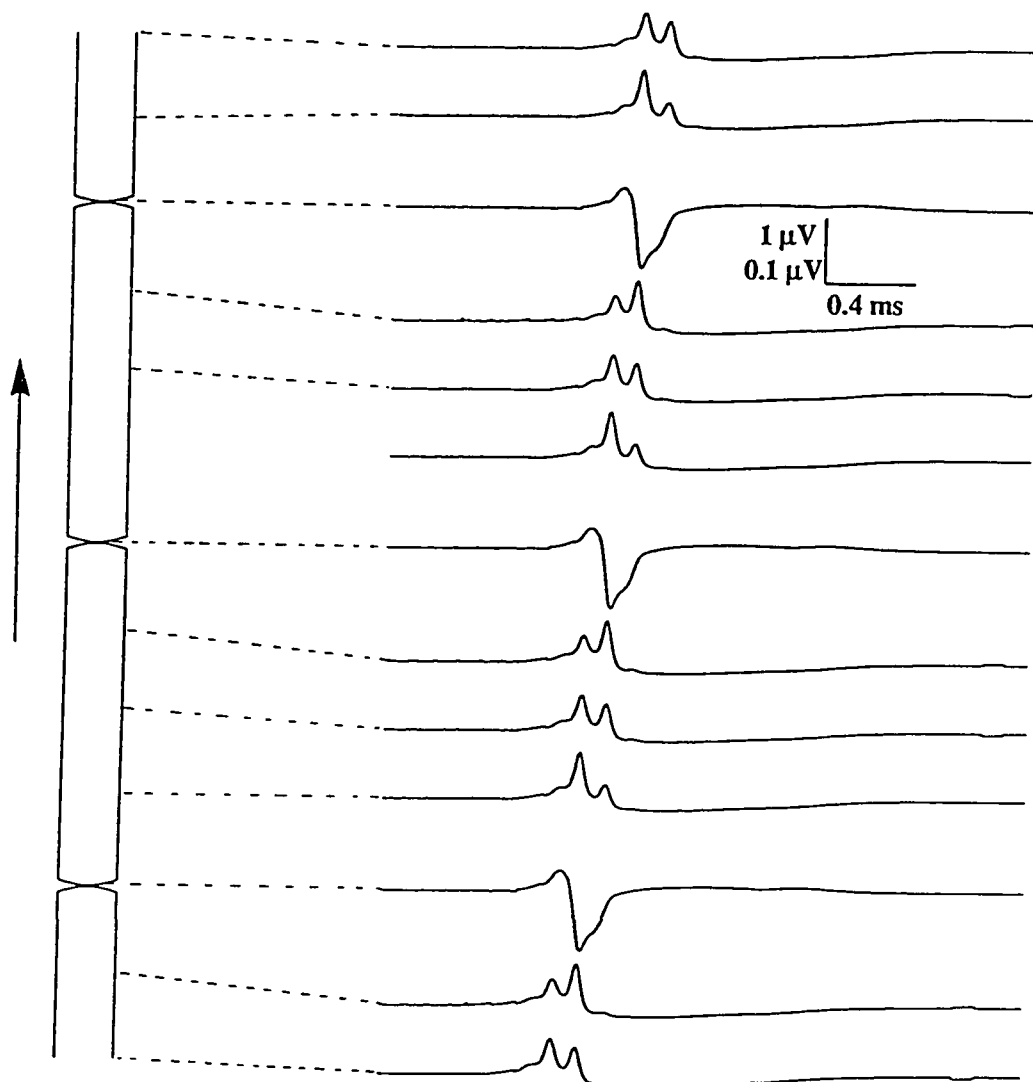


Figure 3.3 The values of extracellular potential as a function of time at several points on the surface of the nerve fiber. The potentials at the nodes of Ranvier are plotted on a scale ten times the scale at which the potentials in the internodal region are drawn. The arrow indicates the direction of propagation of the electrical activity along the fiber.

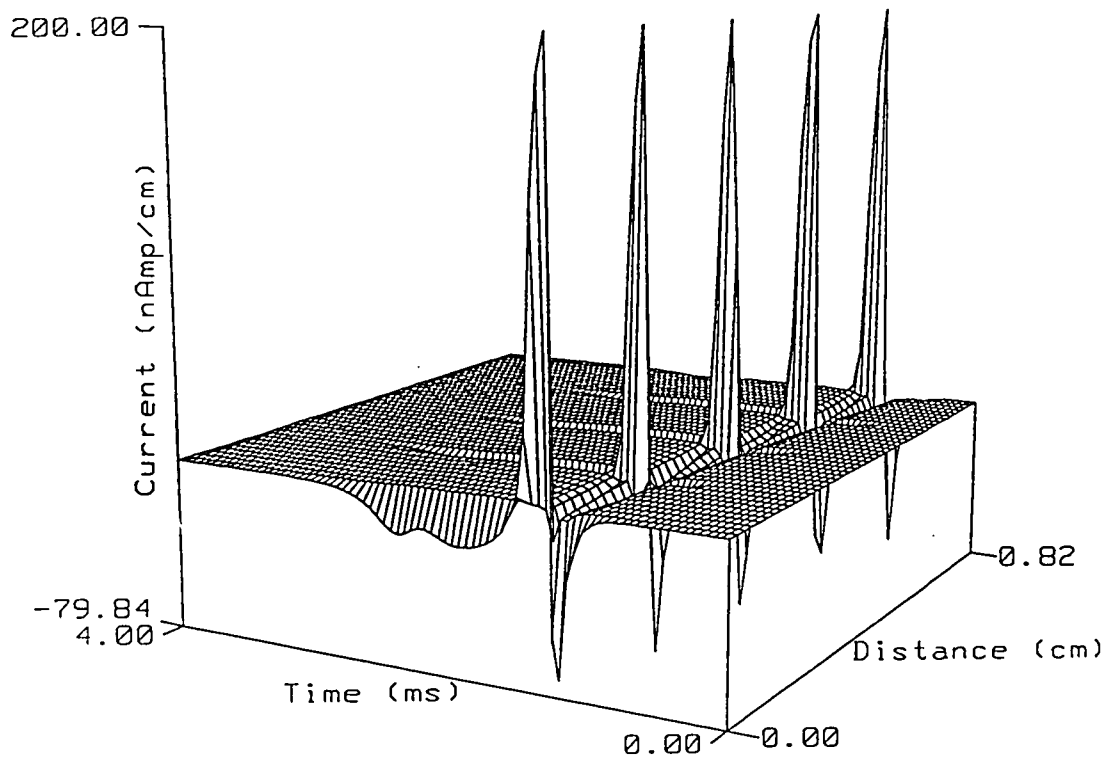


Figure 3.4 A three dimensional view of the transmembrane current per unit length across the equivalent cell membrane of the fiber. The polarity of the current has been reversed so that troughs represent outward currents and spikes inward currents. Propagation is from right to left along the spatial axis and the activity is shown for a time period of 4 milliseconds over five nodes of Ranvier.

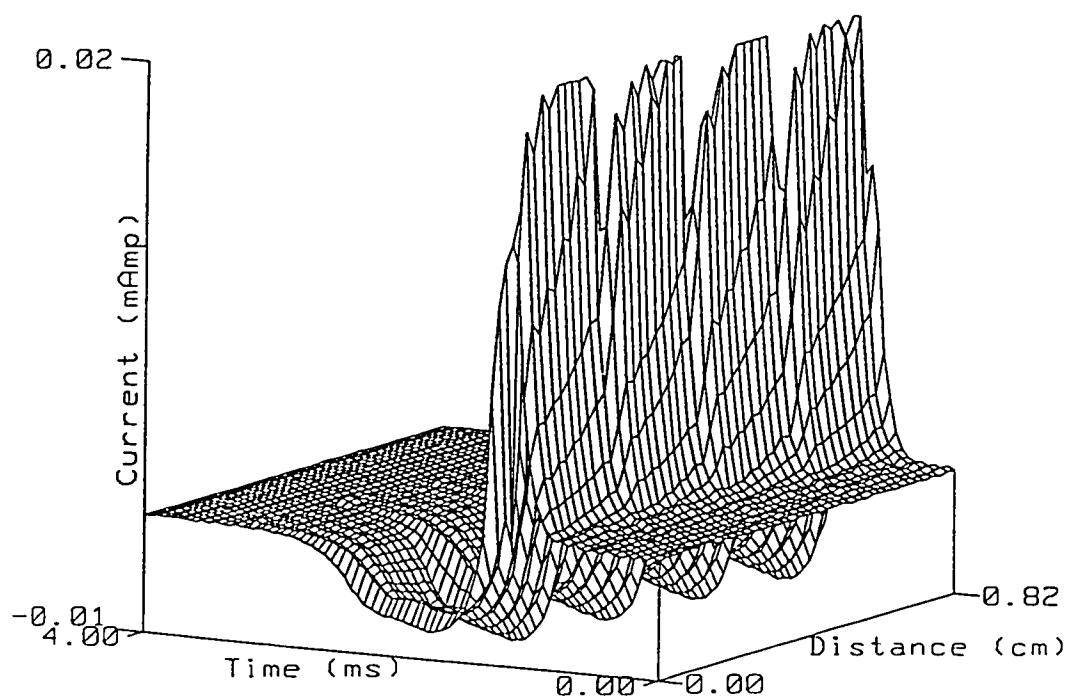


Figure 3.5 A three dimensional view of the total longitudinal current outside the nerve fiber. The polarity of the current is such that troughs represent outward currents and spikes inward currents. Propagation is from right to left along the spatial axis (negative z direction).

same direction as in figures 3.2 and 3.4 i.e. in the negative z direction.

Fig. 3.6a shows the transmembrane current per unit length as a function of time, at several points along the fiber. These spatial points correspond to those that were considered when the extracellular potential on the outer surface of the fiber was shown in fig. 3.3. The current waveforms at the nodes are plotted on a scale ten times the magnitude of the scale used to plot the currents at the internodes. As can be easily seen on comparing figures 3.3 and 3.6a, the extracellular potential on the outer surface of the fiber follows the transmembrane current per unit length very closely, which is not surprising when it is recalled that the extracellular medium is treated in this model as a simple resistive medium.

The total longitudinal current outside the fiber is shown as a function of time at the same spatial points as those used in figures 3.3 and 3.6a, in fig. 3.6b. As stated before, it can be seen here that the longitudinal current decreases in magnitude at the nodes; however the difference in magnitude is not as significant as in the case of the transmembrane current or the extracellular potential. For example, the total longitudinal current in the internodal region is only twice as much as its value at the nodes. The discontinuous nature of the propagation of the electrical activity along the myelinated fiber is very prominent in fig. 3.6 where the electrical activity is shown moving from bottom to top along the fiber.

When experimental measurements of current are made, the procedure is to record the voltage at two points along the fiber and from this differential voltage measurement, first the total longitudinal current and then the transmembrane current per unit length are estimated (Paintal (1965), Paintal (1966), Rasminsky & Sears (1972), Bostock & Sears (1978)). In order to study the effects of this technique on the current finally evaluated, we simulated the same approximation scheme in our model. Fig. 3.7 is an illustration of the total longitudinal current obtained by using the extracellular potential difference between two points that were 120 microns apart, and dividing the difference by the resistance per unit length of the volume conductor medium (r_o). This approximates the well-known cable equation formula $I_L^o(z) = \frac{1}{r_o} \frac{\partial V^o(z)}{\partial z}$. By taking the difference of two values of the longitudinal current obtained at points 120 microns apart and dividing the result by the distance between the two points, an

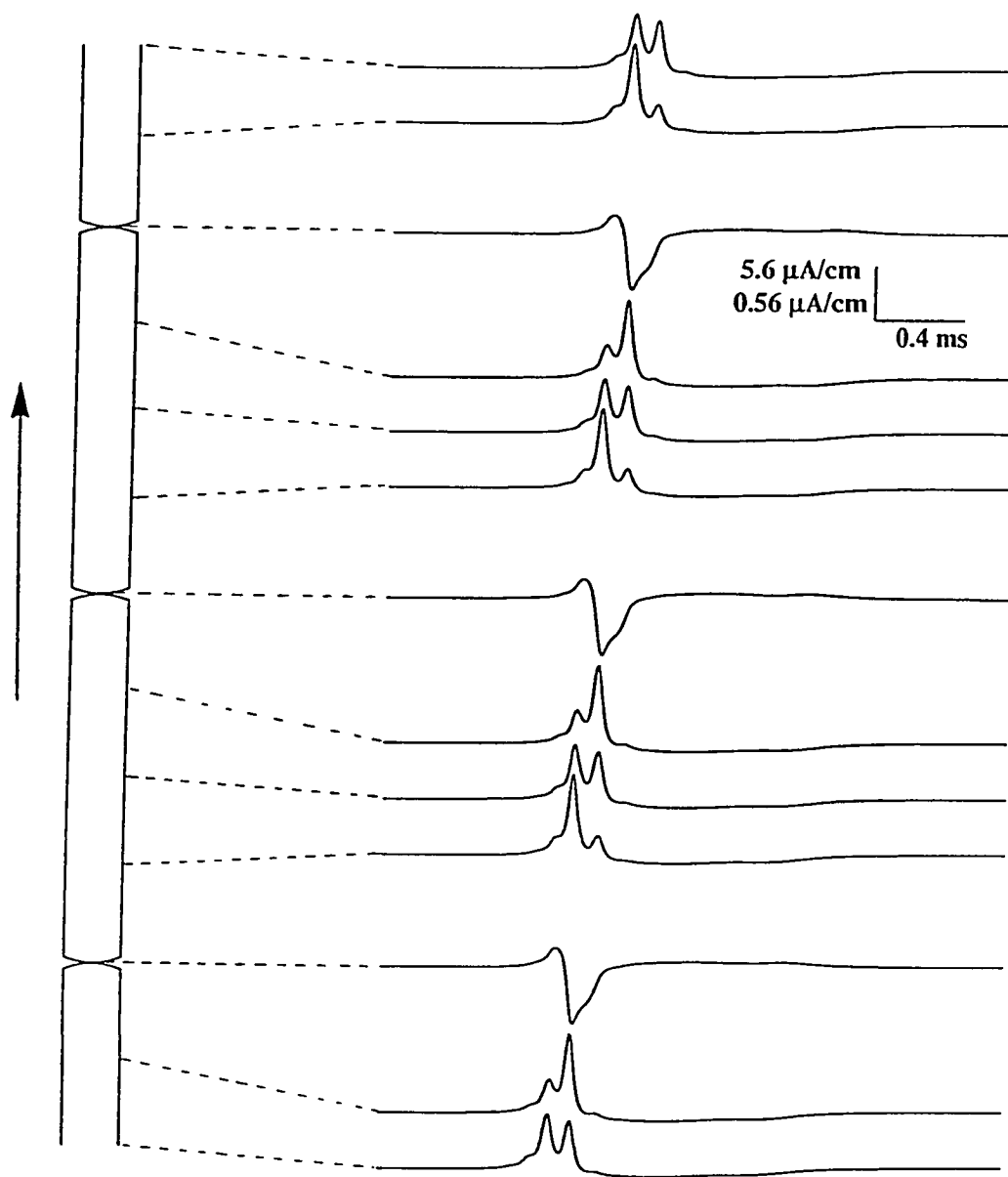


Figure 3.6 a The calculated current waveforms for the transmembrane current per unit length as functions of time at several points on the surface of the fiber. The current values at the nodes are on a scale ten times that used for the waveforms at the internodal points. The propagation of electrical activity is from bottom to top along the fiber as indicated by the arrows.

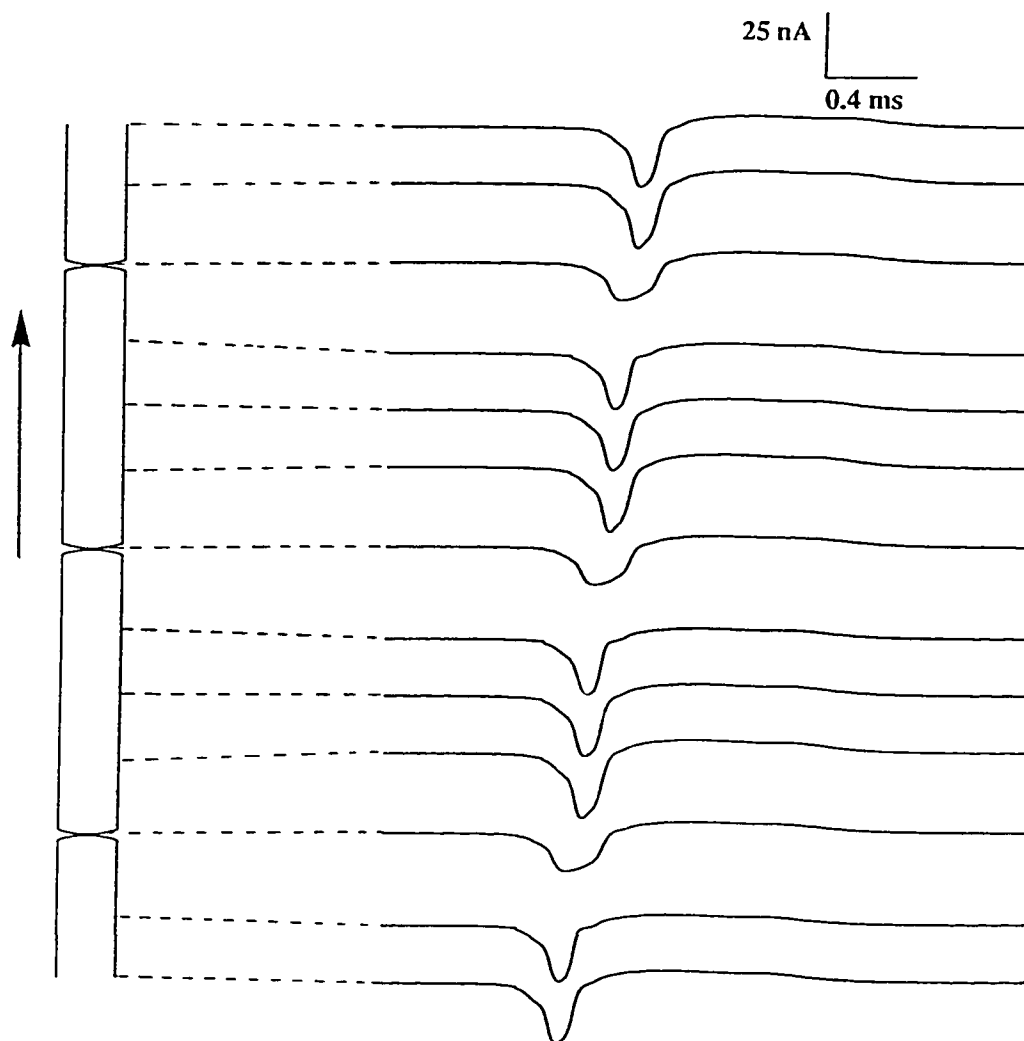


Figure 3.6 b The calculated current waveforms for the total longitudinal current outside the fiber as functions of time at several points on the surface of the fiber. The propagation of electrical activity is from bottom to top along the fiber as indicated by the arrows.

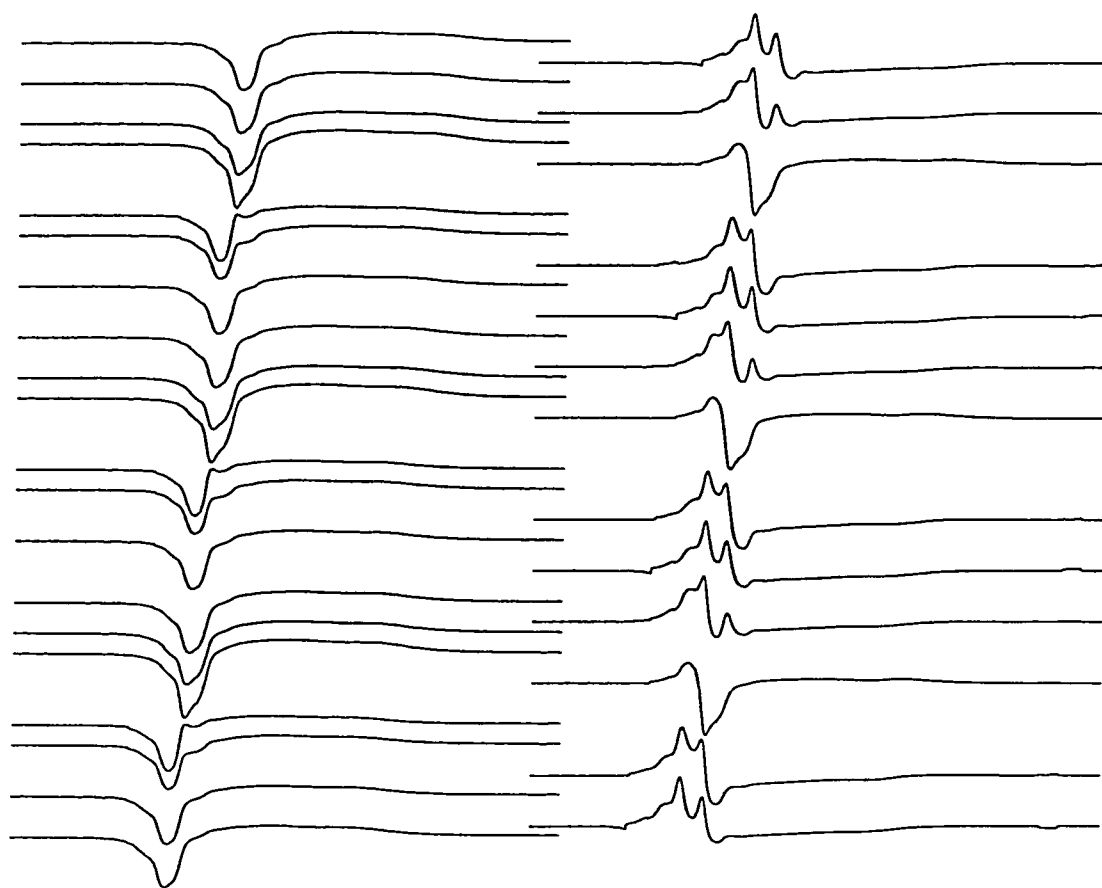


Figure 3.7 Estimates of total longitudinal current and transmembrane current per unit length as functions of time at several points along the fiber. These estimates were made with an electrode separation of 120 microns. See text for details.

estimate of the transmembrane current per unit length is found. On the left hand side of fig. 3.7 several longitudinal current waveforms are plotted in this fashion. To the right of these waveforms is an estimate of the transmembrane current per unit length found using the same differencing technique on the longitudinal current waveforms at the left. The results obtained in this fashion agree very well with the results predicted by our model. All the calculations seen in fig. 3.7 were performed for a volume conductor radius $b = 30 a$.

When the external volume conductor is reduced in extent i.e. when the value of b is made to approach that of the fiber radius a , the calculated extracellular potential waveforms are considerably larger in peak to peak magnitude. The same differencing scheme that was used in obtaining the results in fig. 3.7 may be repeated for different values of the volume conductor radius as well as for different values of separation distance between the values used to estimate the current waveforms. Changing the separation distance between the values used to estimate the currents is equivalent to changing the separation distance of the electrodes used to make the differential recording experimentally. The results of this simulation are shown in fig. 3.8a for the longitudinal current and fig. 3.8b for the transmembrane current per unit length. In both fig. 3.8a and fig. 3.8b, the first column corresponds to an electrode separation of 200 microns, the center column to a separation distance of 400 microns and the third column to a separation distance of 600 microns. In all cases we found that the estimate made with an electrode separation of 200 microns agreed very well with the calculated value at that point, both for the total longitudinal current and the transmembrane current per unit length. When the volume conductor radius was reduced both the total longitudinal current and the transmembrane current per unit length increased in magnitude. The estimates made for the current waveforms using an electrode separation larger than 200 microns resulted in an under-determination of the current magnitude. The extent by which the total longitudinal current was underestimated reduced when the volume conductor boundary approached the fiber surface. This effect was apparent to a much smaller extent in the case where the transmembrane current per unit length was estimated. All these estimates were made with the electrodes centered about the node.

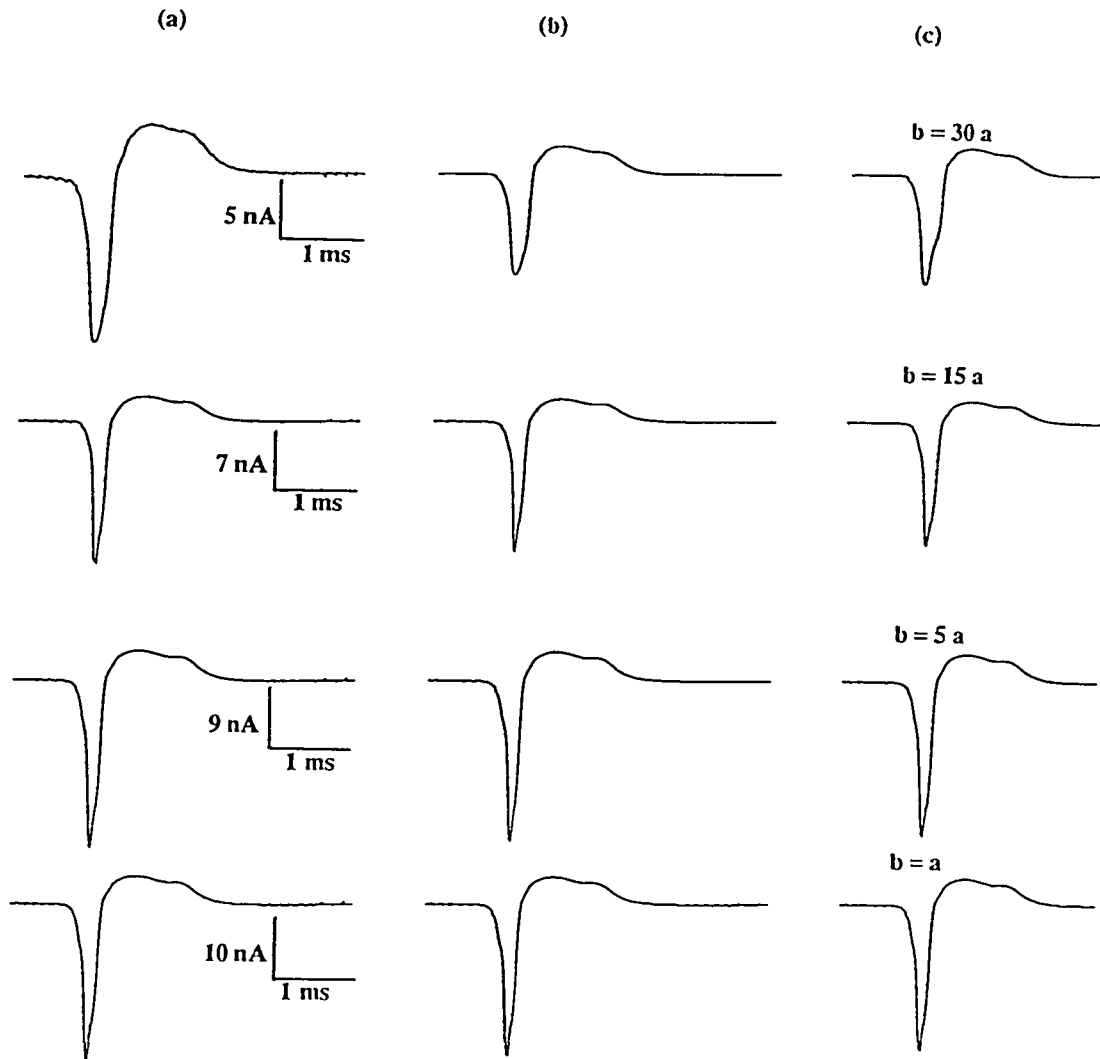


Figure 3.8 a Estimates of total longitudinal current outside the fiber as functions of time; for different electrode separations and various volume conductor extents. Column (a) corresponds to an electrode separation of 200 microns, column (b) to an electrode separation of 400 microns and column (c) to an electrode separation of 600 microns. The various rows correspond to the different values of volume conductor radius b .

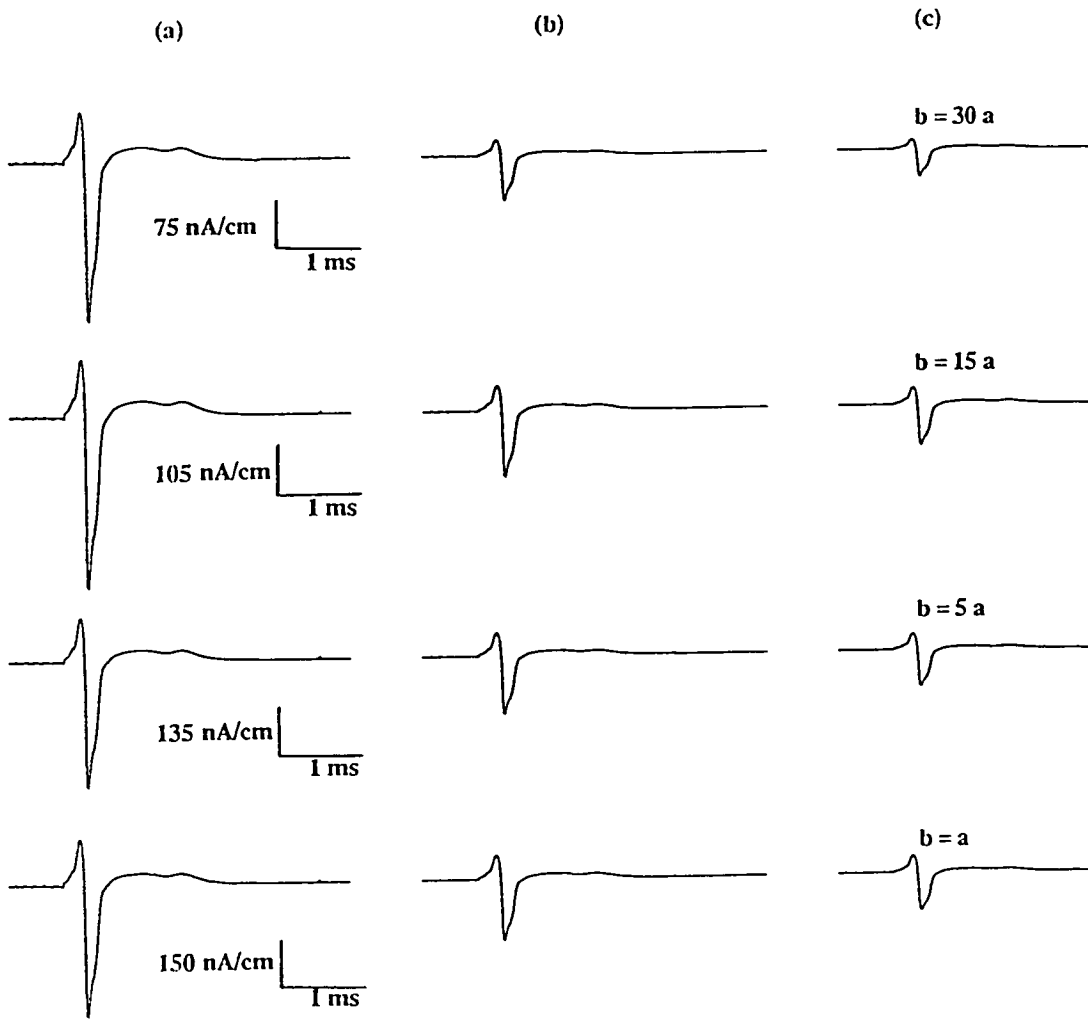


Figure 3.8 b Estimates of the transmembrane current per unit length as functions of time; for different electrode separations and various volume conductor extents. Column (a) corresponds to an electrode separation of 200 microns, column (b) to an electrode separation of 400 microns and column (c) to an electrode separation of 600 microns. The various rows correspond to the different values of volume conductor radius b .

When the node was not centered between the electrodes the estimate was found to be underdetermined even when the electrode separation was 200 microns. Fig. 3.9 shows the results of a simulation where the pair of measurement electrodes was swept across the node of Ranvier from left to right, starting with the node centered between the pair of measurement electrodes up to a point when the left hand side electrode is on the node. The estimated current waveforms are smaller in duration and amplitude when the node is no longer centered between the electrodes. As the position of the node moves closer to the electrode on the left the waveform also shifts toward the left leading to an error in the estimated time of occurrence of the waveform. All three errors, namely the amplitude error, the duration error and the time of occurrence error decrease with a reduction in the volume conductor extent. In the case of the estimated transmembrane current per unit length waveform, when the volume conductor extent is made zero, corresponding to the case where a thin adhering layer of conducting fluid is present around the fiber, the estimated current waveform is error-free even when the node is off-center by as much as 50 microns. The estimated longitudinal current is more sensitive to electrode positioning and under the same conditions it can be estimated correctly only when the node is off-center by less than 25 microns. The estimated transmembrane current per unit length can be correctly found for a volume conductor of radius $b = 30 a$ even when the node is off-center by 25 microns, which is certainly not the case for the estimated total longitudinal current, as is clearly seen from fig. 3.9a. Under all circumstances we found that the estimated transmembrane current per unit length was less sensitive to electrode positioning than the estimated total longitudinal current waveform.

The effects of slowed conduction, simulated by inducing paranodal demyelination at one node in the cable, are shown in fig. 3.10a for the transmembrane potential distribution and in fig. 3.10b for the calculated transmembrane current per unit length; once again the spikes represent inward current, troughs represent outward current and conduction is in the negative z direction. As expected, the transmembrane potential drops in magnitude as it reaches the abnormal region. The transmembrane current at the abnormal node has a very strong component of outward current as can be seen from the fairly well pronounced trough at that point (fig. 3.10b). There is also a prolongation of the inward

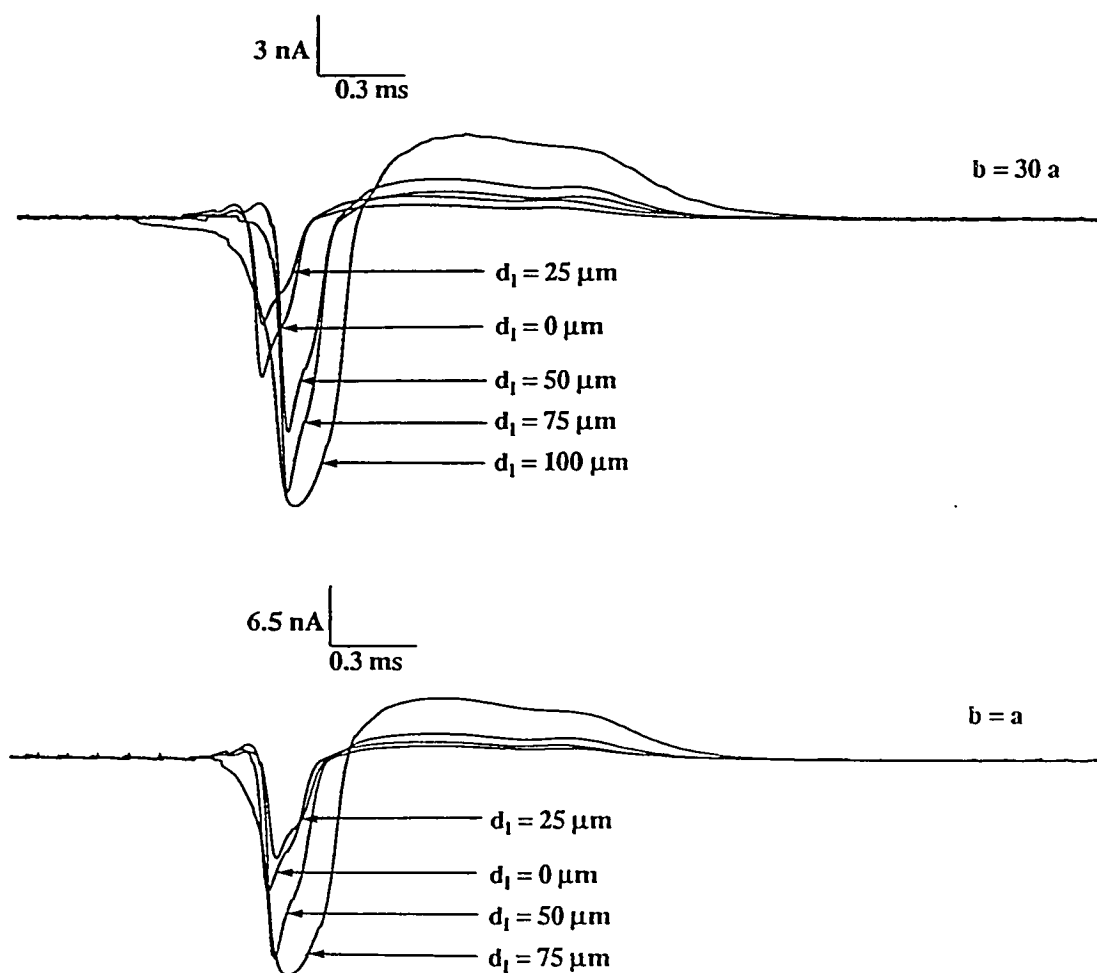


Figure 3.9 a Estimates of total longitudinal current outside the fiber as functions of time; for two volume conductor extents when the pair of measurement electrodes is moved from left to right across a node of Ranvier. The distance d_l is the separation distance between the node and the electrode on the left of the electrode pair. The electrode separation is 200 microns.

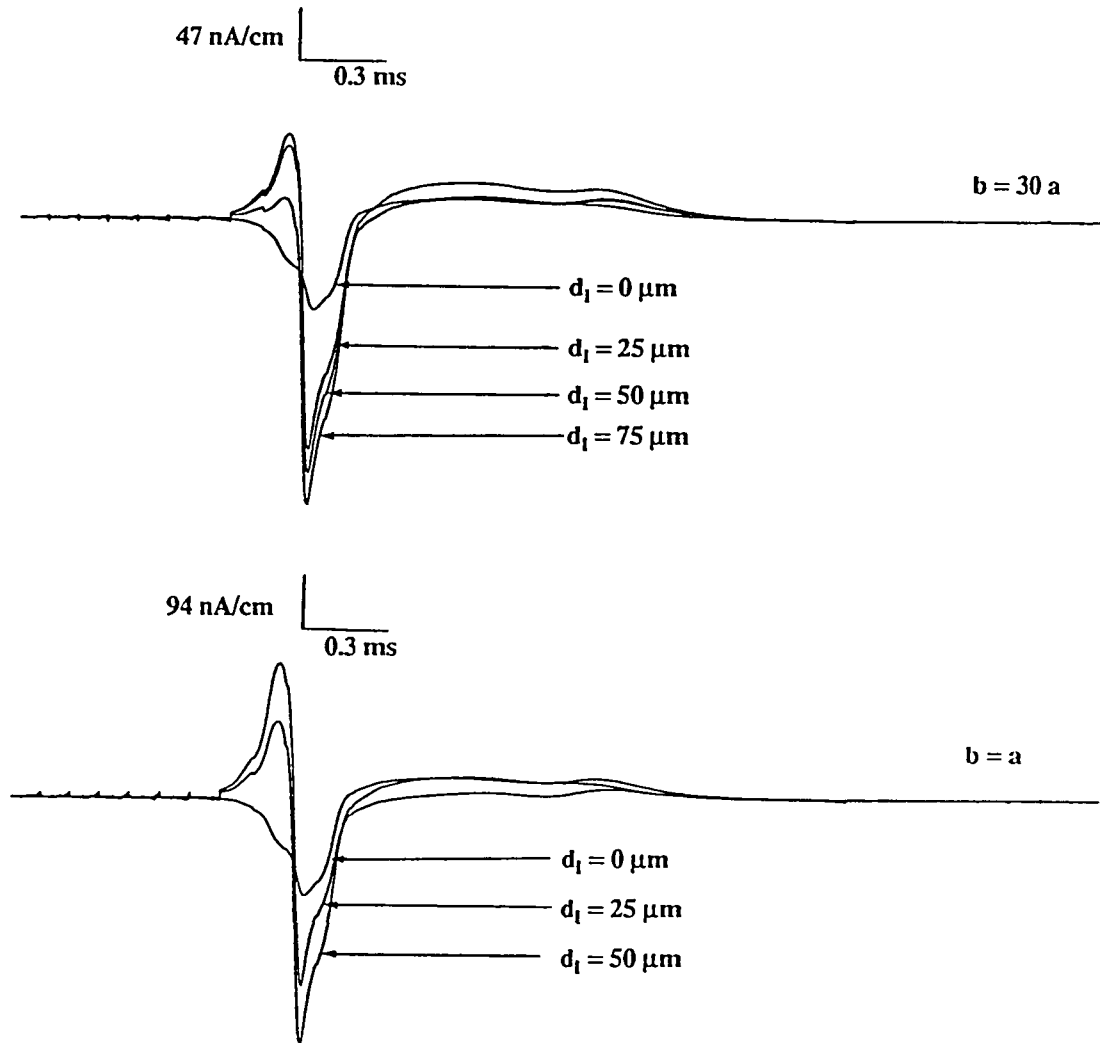


Figure 3.9 b Estimates of the transmembrane current per unit length as functions of time; for two volume conductor extents when the pair of measurement electrodes is moved from left to right across a node of Ranvier. The distance d_l is the separation distance between the node and the electrode on the left of the electrode pair. The electrode separation is 200 microns.

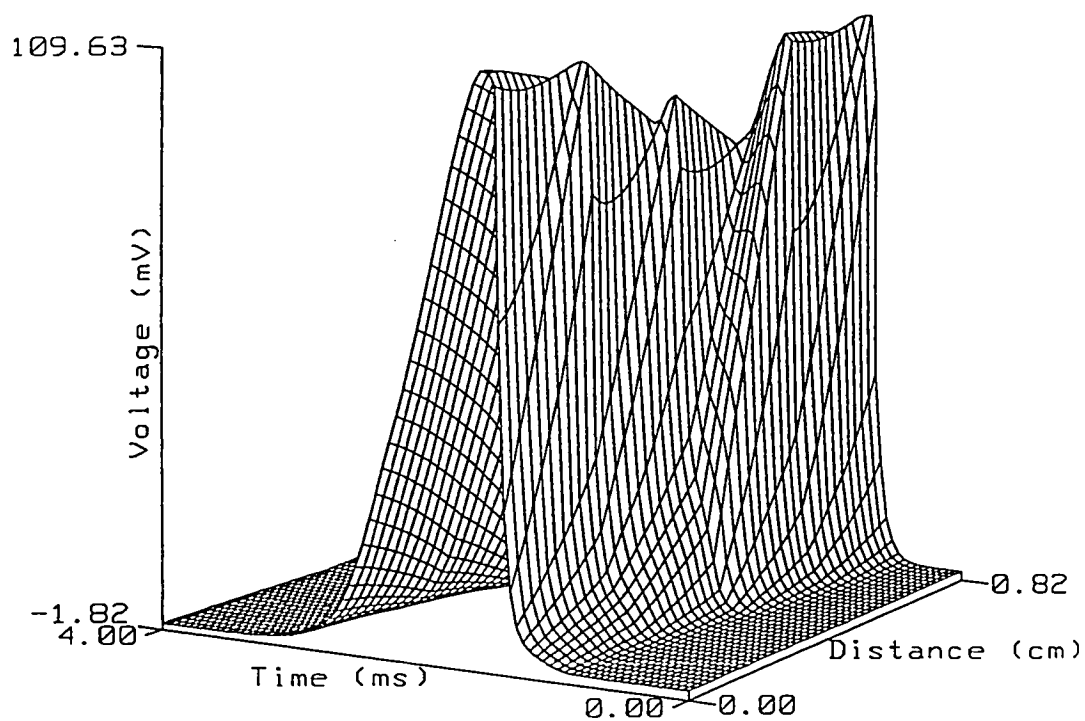


Figure 3.10 a A three dimensional view of transmembrane potential for slowed conduction induced by simulating paranodal demyelination at one node. The electrical activity is shown as propagating from right to left along the spatial axis.

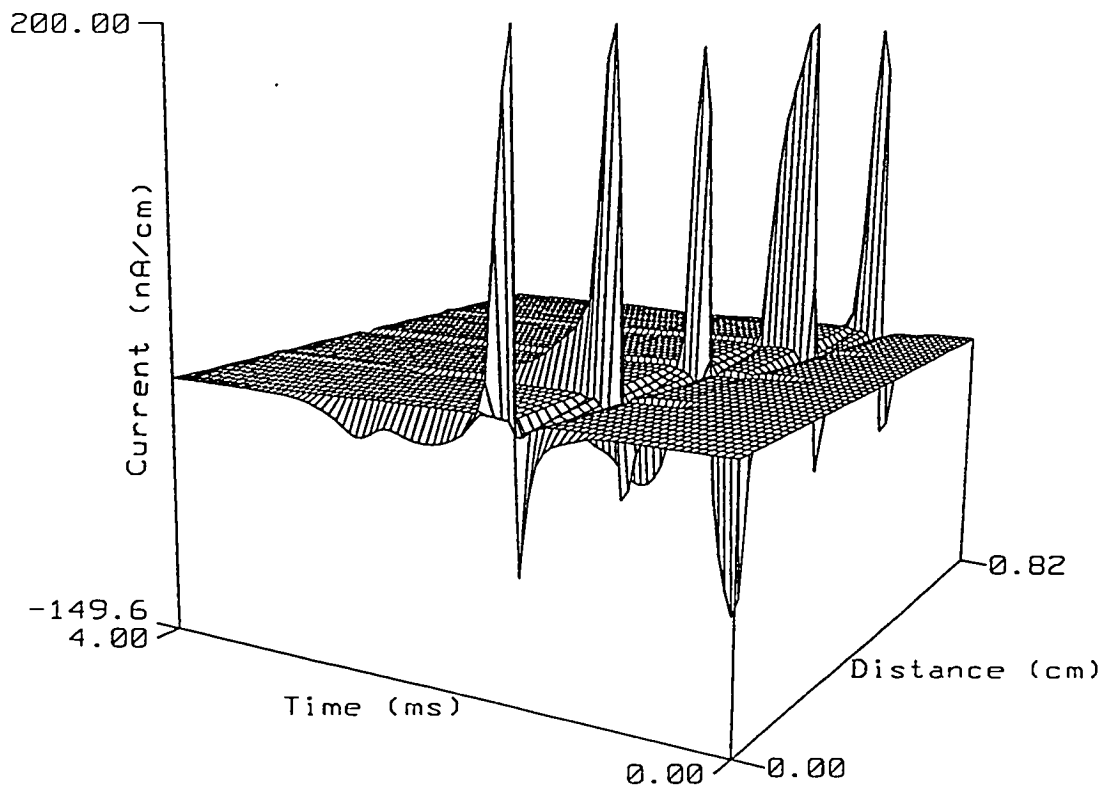


Figure 3.10 b A three dimensional view of calculated transmembrane current per unit length for slowed conduction induced by simulating paranodal demyelination at one node. The electrical activity is shown as propagating from right to left along the spatial axis. The current polarity is such that the upward spikes are inward membrane currents and the troughs are outward membrane currents.

current just before and just after the abnormal region. This is not a surprising result if it is recalled that one of the effects of slowed conduction is the prolongation of the action potential through the abnormal region. One of the consequences of the broadening of the action potential is to prolong the voltage drive on the sodium channel, thereby prolonging the inward current. Also as the electrical activity crosses the abnormal region, there is an abrupt slope change in the spatial waveform through that region as a consequence of the change in conduction velocity. The resulting strong discontinuity in the transmembrane potential waveform is emphasised in the transmembrane current record.

The effects of slowed conduction on the transmembrane current per unit length and the total longitudinal current outside the fiber are seen very distinctly in fig. 3.11a and b. The electrical activity is shown as propagating from bottom to the top of the fiber. Fig. 3.11 shows that both the transmembrane current per unit length and the total longitudinal current waveforms are distorted as the activity propagates into the abnormal region. The decrease in the velocity of propagation is very prominent in both figures, and both waveforms are smeared in time as they pass through the abnormal region. The waveform shapes are restored to normal by the time the activity reaches the node that is distant one node beyond the abnormal node. The records shown in fig. 3.11 are in general agreement with the experimental findings of Bostock and Sears (1978). The extracellular potential waveforms faithfully follow the transmembrane current per unit length waveforms, which is as it should be for a passive, resistive external medium.

Fig. 3.12 shows the calculated extracellular field potential as a function of time at a point directly above a node of Ranvier for normal conduction in (a) and for slowed conduction in (b). With increasing distance from the fiber surface the extracellular potential falls in magnitude and frequency content for both normal and abnormal conduction. In the case of abnormal conduction the calculated extracellular potential has a strong positive peak reflecting the presence of the strong outward current. The extracellular potential also has a second positive peak that corresponds to the hyperpolarization seen in the transmembrane potential at the end of the action potential.

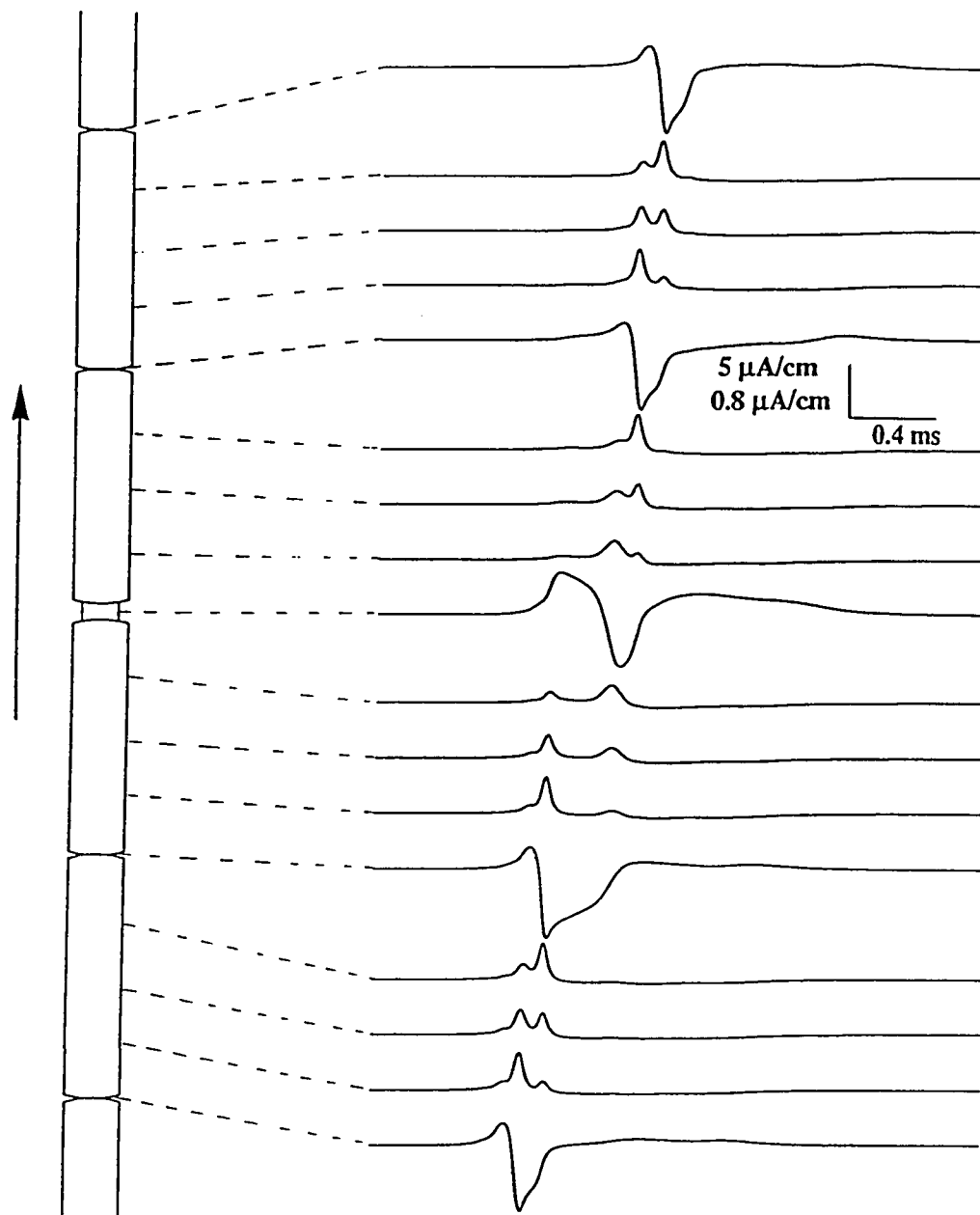


Figure 3.11 a The calculated current waveforms for the transmembrane current per unit length as functions of time at several points on the surface of the fiber for the case of slowed conduction.

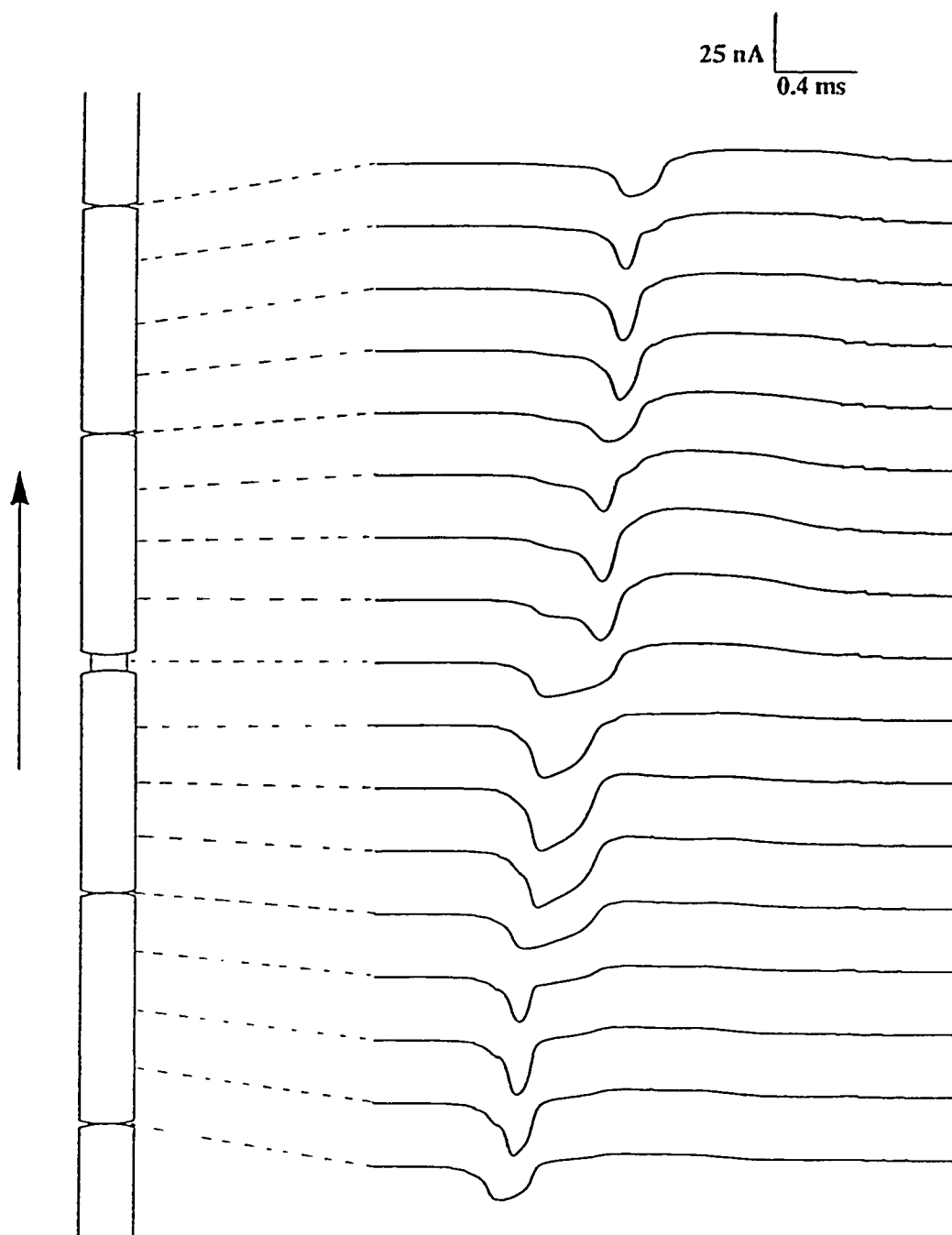


Figure 3.11 b The calculated current waveforms for the total longitudinal current outside the fiber as functions of time at several points on the surface of the fiber for the case of slowed conduction.

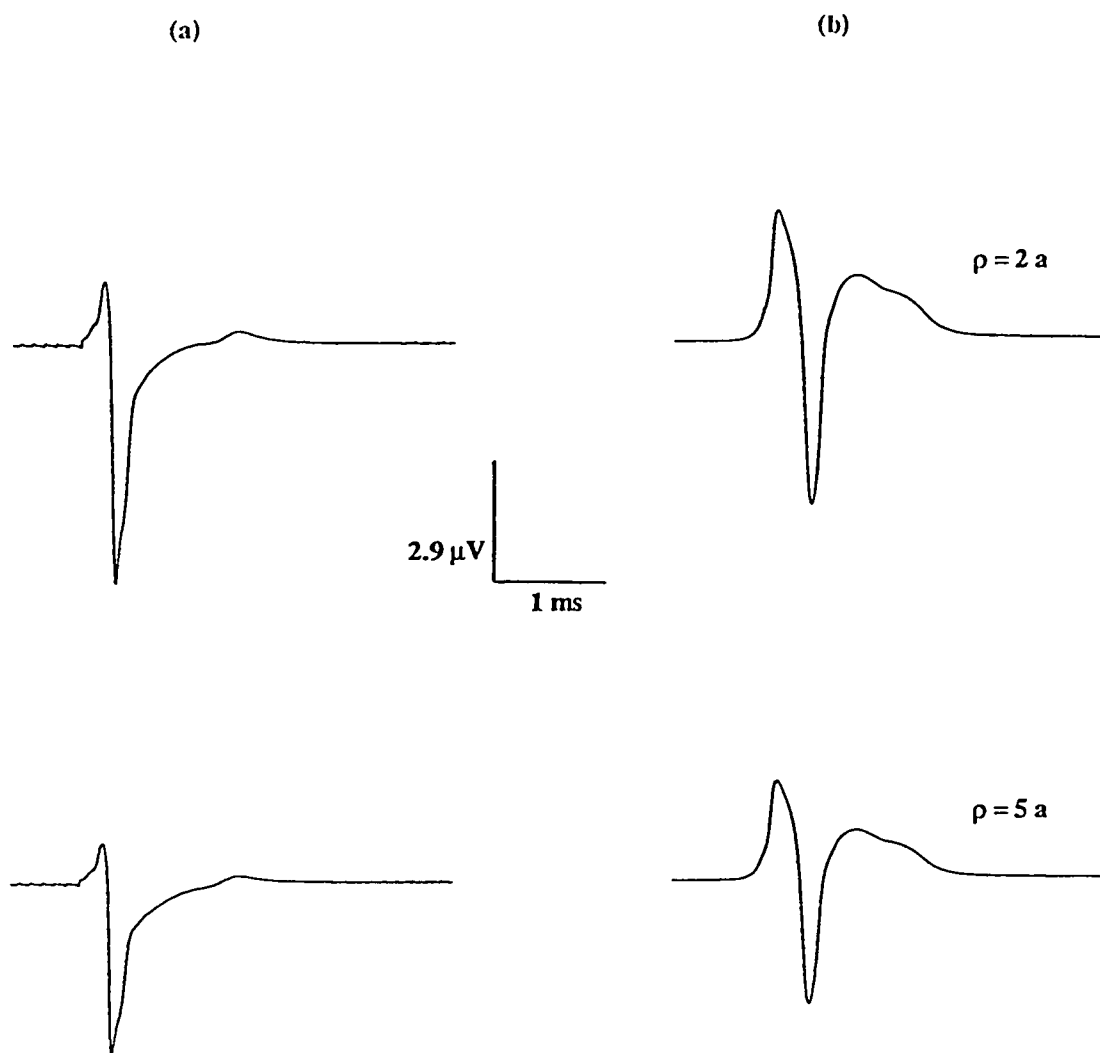


Figure 3.12 The extracellular potential as a function of time at a distance equal to twice the fiber radius and five times the fiber radius from the fiber surface, directly above a node of Ranvier. The node considered is the central node in the simulation when the propagation of electrical activity is (a) normal and (b) slowed. In the case of slowed conduction the node considered here, is the single node at which paranodal demyelination has been induced.

3.5 Discussion of results

In this chapter it is shown that it is possible to reconstruct the extracellular currents and potentials as functions of time using a simple and efficient filter theory approach. The resulting currents and potential waveform correspond well with experimental values in literature. Also simulated is the experimental technique that is used to measure currents in practice. The results of the simulation indicate that electrode separation and placement are critical factors when such measurements are made. The node of Ranvier must be centered between the electrodes for the estimate of current magnitudes to be correct. Decreasing the extent of volume conductor (fig. 3.8) makes electrode separation a less critical factor for the estimation of the total longitudinal current, but this improvement is not as apparent for the case of the transmembrane current per unit length.

Electrode positioning (fig. 3.9) was found to be a critical factor for obtaining error free estimates when relatively large volume conductors were considered. With a decreasing volume conductor extent, the position of the node relative to the two measuring electrodes was found to be less critical. This can be explained if it is recalled that with a decreasing volume conductor extent the extracellular potentials tend to be larger in magnitude and spatial duration (chapter 2, fig. 2.7) The difference between the potentials at two closely spaced points along the fiber is therefore less significant under these circumstances, making the effects of slight shifts in electrode positioning negligible.

The effects of slowed conduction are seen in the transmembrane potential, the transmembrane current, the external longitudinal current and the calculated extracellular potential waveforms (figures 3.10 through 3.12). The method by which paranodal demyelination was simulated results in the strengthening of the outward potassium currents from the paranodal regions of the abnormal node. This is reflected in the prolonged trough seen in the transmembrane current per unit length waveform of fig. 3.10b and 3.12a and also in the strong second positive peak of the extracellular potential waveform of fig. 3.12 column (b). The calculated extracellular potential waveforms are in general of the same shape as the transmembrane current per unit length, which is as it should be for a passive, resistive extracellular medium, and hence both reflect the prolonged outward current that exists at the abnormal node. The upstroke velocity of the action potential in the abnormal region decreases and this

is reflected in the extracellular potential and the transmembrane current per unit length waveforms as a broadening of the first positive and negative peaks.

As stated before, the calculation technique described in this chapter is quite rapid involving a small fraction of the computational time required by a comparable finite difference or finite element characterization of the myelinated nerve fiber's immediate surroundings. The field theory model can be easily modified to include one or more regions around the nerve fiber, each with varying degrees of anisotropy. This technique which combines a distributed parameter model of the nerve fiber with a field theory model of its environment, can therefore be extended to the quantitative study of a number of intriguing problems in nerve electrophysiology including: (a) the electric field stimulation of myelinated nerve and the subsequent determination of excitability thresholds; and (b) a more detailed study of nerve conduction in demyelination disease.

CHAPTER 4

Extracellular Potentials from Skeletal Muscle

4.1 Introduction

This chapter is devoted to the study of extracellular potentials from an active muscle fiber in a muscle bundle. Just as in the case of the nerve fiber, the skeletal muscle fiber is modeled as a distributed parameter model of resistive and capacitive elements as shown in fig. 1.3, and a numerical solution for the transmembrane potential distribution across of the fiber is obtained. The extracellular potentials are evaluated using a field theory model developed for an eccentric source in a finite volume conductor.

The potential due to the presence of more than one active fiber in the muscle is evaluated using principles of superposition. Compound action potentials are generated allowing for a desynchronization in the time of activation of the various muscle fibers active in the muscle. The effects of multiple fibers being active at slightly different times are studied using a motor unit consisting of nine individual muscle fibers. The muscle fibers considered are all assumed to have identical geometrical and electrical parameters.

4.2 Modeling Aspects

4.2.1 Potential in a finite volume conductor

The fundamental problem considers a circular cylindrical muscle fiber of radius a (cm) and specific sarcoplasmic conductivity σ_i (S/cm), to be located eccentrically in a finite, homogeneous, anisotropic volume conductor of radius b and specific conductivity $\sigma_{o,r}$ and $\sigma_{o,z}$ in the transverse and longitudinal directions respectively, as illustrated in fig. 4.1. Under conditions of quasistationarity the general solution to Laplace's equation within the cylindrical volume conductor $0 \leq \rho \leq b$, a region that excludes the volume occupied by the source fiber is given as :

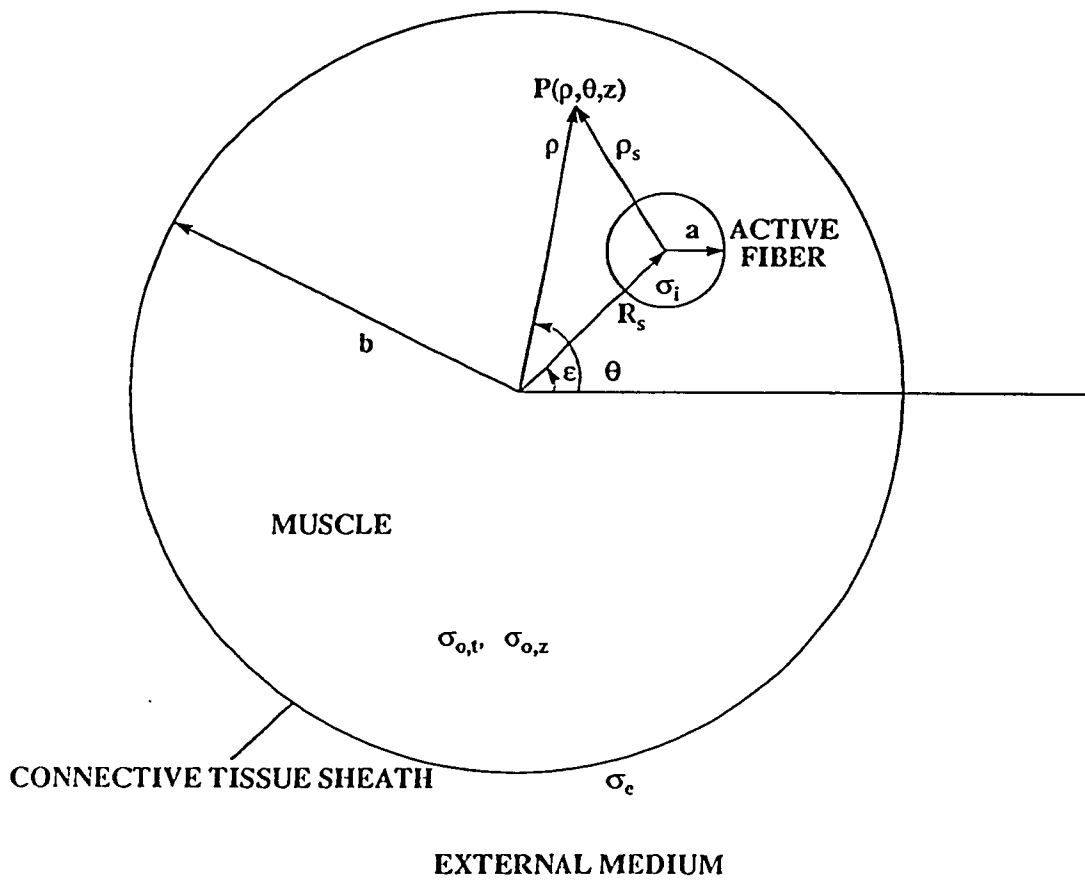


Figure 4.1 Fiber geometry. The fiber radius is denoted by a and the muscle radius is b and $P(\rho, \theta, z)$ is the field point at which the potentials are to be calculated.

$$\Phi^o(\rho, \theta, z) = \Phi_s(\rho, \theta, z) + \sum_{n=-\infty}^{\infty} e^{-jn(\theta-\epsilon)} \int_{-\infty}^{\infty} A_n(k) I_n(\lambda | k | \rho) e^{-jkz} dk \quad (4.1)$$

where ϵ is the angle that the radius vector R_s from the origin to the center of the source fiber makes with the horizontal; I_n is the modified Bessel function of the first kind, order n ; and λ is the anisotropy ratio that represents the anisotropic nature of the medium inside the volume conductor, and is defined as :

$$\lambda \equiv \left(\frac{\sigma_{ox}}{\sigma_{of}} \right)^{1/2} \quad (4.2)$$

Here the term Φ_s represents the potential distribution outside the source fiber, when it is positioned in an infinite, homogeneous, anisotropic volume conductor with the specified properties. A suitable expression for the potential distribution Φ_s , modified for the particular case of an anisotropic external medium, is given by :

$$\Phi_s(\rho, \theta, z) = \Phi_s(\rho_s, z) = \frac{1}{2\pi} \int_{-\infty}^{\infty} \frac{F_m(k) K_0(\lambda | k | \rho_s)}{\alpha_m(\lambda | k | a) K_0(\lambda | k | a)} e^{-jkz} dk \quad (4.3)$$

where the relationship between ρ and ρ_s is given by the law of cosines as :

$$\rho_s^2 = \rho^2 + R_s^2 - 2\rho R_s \cos(\theta - \epsilon) \quad (4.4)$$

and λ is given by (4.2). In equation (4.3) a is the fiber radius, K_n is the modified Bessel function of the second kind, order n ; and F_m is the Fourier transform of the transmembrane potential distribution of the source fiber when it is located in an infinite volume conductor medium. The term $\alpha_m(\lambda | k | a)$ is called the membrane filter function and is defined as :

$$\alpha_m(\lambda | k | a) \equiv - \left[1 + \delta \frac{K_1(\lambda | k | a) I_0(|k| a)}{K_0(\lambda | k | a) I_1(|k| a)} \right] \quad (4.5)$$

where

$$\delta = \frac{\lambda \sigma_{of}}{\sigma_i} \quad (4.6)$$

Using the relationship in (4.4) and the Bessel function addition theorem (Abramowitz and Stegun,

1965), the modified Bessel function $K_0(\lambda|k|\rho_s)$ may be written as :

$$K_0(\lambda|k|\rho_s) = \sum_{n=-\infty}^{\infty} \cos n(\theta-\epsilon) K_n(\lambda|k|R_s) I_n(\lambda|k|\rho) \quad \rho < R_s \quad (4.7)$$

and

$$K_0(\lambda|k|\rho_s) = \sum_{n=-\infty}^{\infty} \cos n(\theta-\epsilon) I_n(\lambda|k|R_s) K_n(\lambda|k|\rho) \quad \rho < R_s \quad (4.8)$$

Therefore the general form of the solutions to Laplace's equation in the cylindrical volume conductor region $0 \leq \rho \leq b$, under conditions of quasistationarity are :

$$\Phi^o(\rho, \theta, z) = \sum_{n=-\infty}^{\infty} e^{-jn(\theta-\epsilon)} \int_{-\infty}^{\infty} [A_n(k) + P_n(k)] I_n(\lambda|k|\rho) e^{-jkz} dk \quad 0 \leq \rho < R_s \quad (4.9)$$

$$\Phi^o(\rho, \theta, z) = \sum_{n=-\infty}^{\infty} e^{-jn(\theta-\epsilon)} \int_{-\infty}^{\infty} [A_n(k) I_n(\lambda|k|\rho) + Q_n(k) K_n(\lambda|k|\rho)] e^{-jkz} dk \quad R_s \leq \rho < b \quad (4.10)$$

where the terms $P_n(k)$ and $Q_n(k)$ are defined as :

$$P_n(k) = \frac{F_m(k) K_n(\lambda|k|R_s)}{\alpha_m(\lambda|k|a) K_0(\lambda|k|a)} \quad (4.11)$$

and

$$Q_n(k) = \frac{F_m(k) I_n(\lambda|k|R_s)}{\alpha_m(\lambda|k|a) K_0(\lambda|k|a)} \quad (4.12)$$

The general form for the potential in the external region ($\rho < b$) characterized by a specific conductivity σ_e (S/cm), is given by :

$$\Phi^e(\rho, \theta, z) = \sum_{n=-\infty}^{\infty} e^{-jn(\theta-\epsilon)} \int_{-\infty}^{\infty} B_n(k) K_n(\lambda|k|\rho) e^{-jkz} dk \quad b \leq \rho \quad (4.13)$$

The coefficients $A_n(k)$ and $B_n(k)$ can be solved for by applying the following boundary conditions at $\rho = b$.

At $\rho = b$ we have a resistive capacitive sheath and the current crossing the connective tissue sheath is assumed to be continuous. Hence :

$$-\sigma_{o,e} \frac{\partial \Phi^o}{\partial \rho} \bigg|_b = -\sigma_e \frac{\partial \Phi^e}{\partial \rho} \bigg|_b = J_{sh}(\theta, z) \quad (4.14)$$

where σ_e is the specific conductivity of the medium outside the volume conductor and J_{sh} is the trans-sheath current density given as :

$$J_{sh}(\theta, z) = \bar{\sigma}_{sh} \Phi_{sh}(\theta, z) + \bar{C}_{sh} \frac{\partial \Phi_{sh}(\theta, z)}{\partial t} \quad (4.15)$$

where $\bar{\sigma}_{sh}$ is the specific conductivity of the sheath (S/cm²) and \bar{C}_{sh} is the specific capacity of the sheath ($\mu\text{F}/\text{cm}^2$). The trans-sheath potential $\Phi_{sh}(\theta, z)$ is defined as :

$$\Phi_{sh}(\theta, z) \equiv \Phi^o(b, \theta, z) - \Phi^e(b, \theta, z) \quad (4.16)$$

If v is the velocity of propagation of the electrical activity along the fiber in the negative z direction, all field properties vary as $(z + vt)$ and so for any field quantity $\Psi(\rho, \theta, z)$ we have :

$$\Psi(\rho, \theta, z) = \Psi[\rho, \theta, (z + vt)] \quad (4.17)$$

Consequently,

$$\frac{\partial \Psi}{\partial t} = v \frac{\partial \Psi}{\partial z} \quad (4.18)$$

Thus, equation (4.15) may be rewritten as :

$$J_{sh}(\theta, z) = \bar{\sigma}_{sh} \Phi_{sh}(\theta, z) + v \bar{C}_{sh} \frac{\partial \Phi_{sh}(\theta, z)}{\partial z} \quad (4.19)$$

Upon considering the form of the expressions for potentials Φ^o and Φ^e in equations (4.10) and (4.13) and their dependence on axial distance z , the derivative of the trans-sheath potential with respect to z , is given as :

$$\frac{\partial \Phi_{sh}(\theta, z)}{\partial z} = -jk \Phi_{sh}(\theta, z) \quad (4.20)$$

Using the above expression equation (4.19) may be rewritten as :

$$J_{sh}(\theta, z) = (\bar{\sigma}_{sh} - jk\nu\bar{C}_{sh})\Phi_{sh}(\theta, z) \quad (4.21)$$

Defining the complex admittance $\sigma^*(k)$ as :

$$\sigma^*(k) \equiv \bar{\sigma}_{sh} - jk\nu\bar{C}_{sh} \quad (4.22)$$

and employing equation (4.21), the two equations that specify the boundary condition at $\rho = b$ are :

$$\sigma_{o,r} \left. \frac{\partial \Phi^o}{\partial \rho} \right|_b + \sigma^*(k)\Phi_{sh} = 0 \quad (4.23)$$

and

$$\sigma_e \left. \frac{\partial \Phi^e}{\partial \rho} \right|_b + \sigma^*(k)\Phi_{sh} = 0 \quad (4.24)$$

Applying the mixed boundary condition specified by (4.23) one obtains :

$$\begin{aligned} \sum_{n=-\infty}^{\infty} e^{-jn(\theta-\epsilon)} \int_{-\infty}^{\infty} \{ \sigma_{o,r} [A_n(k)I'_n(\lambda|k|b) + Q_n(k)K'_n(\lambda|k|b)] \\ + \sigma^*(k)[A_n(k)I_n(\lambda|k|b) + Q_n(k)K_n(\lambda|k|b) - B_n(k)K_n(|k|b)] \} e^{-jkz} dk = 0 \end{aligned} \quad (4.25)$$

Here I' and K' are the first derivatives of the modified Bessel functions I_n and K_n , respectively. For the integral to equal zero, the terms within parenthesis must be equal to zero, which, after rearrangement of terms, may be written as :

$$\begin{aligned} A_n(k)\{\sigma_{o,r}I'_n(\lambda|k|b) + \sigma^*(k)I_n(\lambda|k|b)\} - B_n(k)\{\sigma^*(k)K_n(|k|b)\} \\ + Q_n(k)\{\sigma_{o,r}K'_n(\lambda|k|b) + \sigma^*(k)K_n(\lambda|k|b)\} = 0 \end{aligned} \quad (4.26)$$

Similarly, applying the boundary condition expressed in equation (4.24) results in the following :

$$\begin{aligned} \sum_{n=-\infty}^{\infty} e^{-jn(\theta-\epsilon)} \int_{-\infty}^{\infty} \{ \sigma_e B_n(k)K'_n(|k|b) \\ + \sigma^*(k)[A_n(k)I_n(\lambda|k|b) + Q_n(k)K_n(\lambda|k|b) - B_n(k)K_n(|k|b)] \} e^{-jkz} dk = 0 \end{aligned} \quad (4.27)$$

Once again the term within parenthesis must equal zero for the equation to hold. After rearrangement

of terms, and this results in the expression :

$$A_n(k)\{\sigma^*(k)I_n(\lambda|k|b)\} + B_n(k)\{\sigma_e K'_n(|k|b) - \sigma^*(k)K_n(|k|b)\} + Q_n(k)\{\sigma^*(k)K_n(\lambda|k|b)\} = 0 \quad (4.28)$$

Eliminating $B_n(k)$ between equations (4.26) and (4.28) the coefficient $A_n(k)$ may be obtained in terms of $Q_n(k)$ as :

$$A_n(k) = Q_n(k)X_n(k) \quad (4.29)$$

where

$$X_n(k) \equiv \frac{b_n(k)}{c_n(k)} \quad (4.30)$$

and the terms $b_n(k)$ and $c_n(k)$ are given as follows.

$$\begin{aligned} b_n(k) = & -\sigma_e \sigma_{o,r} K'_n(\lambda|k|b) K'_n(|k|b) + \sigma_{o,r} \sigma^*(k) K'_n(\lambda|k|b) K_n(|k|b) \\ & - \sigma_e \sigma^*(k) K_n(\lambda|k|b) K'_n(|k|b) \end{aligned} \quad (4.31)$$

$$\begin{aligned} c_n(k) = & \sigma_e \sigma_{o,r} I'_n(\lambda|k|b) K'_n(|k|b) - \sigma_{o,r} \sigma^*(k) I'_n(\lambda|k|b) K_n(|k|b) \\ & + \sigma_e \sigma^*(k) I_n(\lambda|k|b) K'_n(|k|b) \end{aligned} \quad (4.32)$$

Eliminating $A_n(k)$ between equations (4.26) and (4.28) results in the solution of $B_n(k)$ in terms of $Q_n(k)$ as :

$$B_n(k) = Q_n(k)Y_n(k) \quad (4.33)$$

where

$$Y_n(k) \equiv \frac{d_n(k)}{c_n(k)} \quad (4.34)$$

the term $d_n(k)$ being defined as :

$$d_n(k) = \sigma_{o,r} \sigma^*(k) [I_n(\lambda|k|b) K'_n(\lambda|k|b) - I'_n(\lambda|k|b) K_n(\lambda|k|b)] \quad (4.35)$$

The final expressions for potential are given as :

$$\Phi^o(\rho, \theta, z) = \sum_{n=-\infty}^{\infty} e^{-jn(\theta-\epsilon)} \int_{-\infty}^{\infty} W_n^1(\rho, \theta, k) F_m(k) e^{-jkz} dk \quad 0 \leq \rho < R_s \quad (4.36)$$

$$\Phi^o(\rho, \theta, z) = \sum_{n=-\infty}^{\infty} e^{-jn(\theta-\epsilon)} \int_{-\infty}^{\infty} W_n^2(\rho, \theta, k) F_m(k) e^{-jkz} dk \quad R_s \leq \rho < b \quad (4.37)$$

$$\Phi^e(\rho, \theta, z) = \sum_{n=-\infty}^{\infty} e^{-jn(\theta-\epsilon)} \int_{-\infty}^{\infty} W_n^e(\rho, \theta, k) F_m(k) e^{-jkz} dk \quad b \leq \rho \quad (4.38)$$

where the terms denoted by W_n are filter functions defined as :

$$W_n^1(\rho, \theta, k) \equiv \left[X_n(k) I_n(\lambda | k | R_s) + K_n(\lambda | k | R_s) \right] \frac{I_n(\lambda | k | \rho)}{\alpha_m(\lambda | k | a) K_0(\lambda | k | a)} \quad 0 \leq \rho < R_s \quad (4.39)$$

$$W_n^2(\rho, \theta, k) \equiv \left[X_n(k) I_n(\lambda | k | \rho) + K_n(\lambda | k | \rho) \right] \frac{I_n(\lambda | k | R_s)}{\alpha_m(\lambda | k | a) K_0(\lambda | k | a)} \quad R_s \leq \rho < b \quad (4.40)$$

$$W_n^e(\rho, \theta, k) \equiv \frac{I_n(\lambda | k | R_s)}{\alpha_m(\lambda | k | a) K_0(\lambda | k | a)} Y_n(k) K_n(\lambda | k | \rho) \quad b \leq \rho \quad (4.41)$$

We now define the two dimensional Fourier transform pairs for the potentials Φ^o and Φ^e for a specified value of radial distance ρ^* as :

$$F^o(n, k) \equiv \sum_{n=-\infty}^{\infty} e^{-jn\epsilon} \int_{-\infty}^{\infty} \Phi^o(\rho^*, \theta, z) e^{jkz} dz \quad (4.42)$$

$$\Phi^o(\rho^*, \theta, z) \equiv \sum_{n=-\infty}^{\infty} e^{jn\epsilon} \int_{-\infty}^{\infty} F^o(n, k) e^{-jkz} dz \quad 0 \leq \rho^* \leq b \quad (4.43)$$

and

$$F^e(n, k) \equiv \sum_{n=-\infty}^{\infty} e^{-jn\epsilon} \int_{-\infty}^{\infty} \Phi^e(\rho^*, \theta, z) e^{jkz} dz \quad (4.44)$$

$$\Phi^e(\rho^*, \theta, z) \equiv \sum_{n=-\infty}^{\infty} e^{jn\epsilon} \int_{-\infty}^{\infty} F^e(n, k) e^{-jkz} dz \quad \rho^* > b \quad (4.45)$$

which are discrete in n , the θ direction spatial frequency and continuous in k , the z direction spatial frequency.

4.22 Discrete Fourier Methods of Solution

In the preceding sections, Fourier integral expressions have been developed for the extracellular potentials inside and outside the volume conductor namely $\Phi^o(\rho, \theta, z)$ and $\Phi^e(\rho, \theta, z)$. Computation of these quantities is greatly facilitated by reformulation of these integral expressions in terms of the methodology of the two dimensional discrete Fourier Transform (2DFT) technique (Oppenheim and Schaeffer, 1975). Reformulation of these equations for representation in the discrete spatial (θ, z) and spatial frequency (n, k) domains will be illustrated using the potential outside the volume conductor $\Phi^e(\rho, \theta, z)$ as an example. Following the development in previous work (Wilson et al, 1985), the discretization proceeds as follows :

$$F^e(\rho, Ru, Pq) = \sum_{m=-M}^{M-1} \sum_{n=-N}^{N-1} e^{jn\pi} \Phi^e e^{j\pi m q / M} e^{j\pi n u / N} = 2DFT [\Phi^e(\rho, Sn, Zm)] \quad (4.46)$$

and

$$\Phi^e(\rho, Sn, Zm) = \sum_{q=-M}^{M-1} \sum_{u=-N}^{N-1} F^e(\rho, Ru, Pq) e^{-j\pi m q / N} e^{-j\pi n u / N} = 2IDFT [F^e(\rho, Ru, Pq)] \quad (4.47)$$

where

$$P \equiv \frac{\pi}{MZ} \quad (4.48)$$

and

$$R \equiv \frac{\pi}{NS} \quad (4.49)$$

Here Z and P are the sampling intervals in the z - and k -domains, respectively, S and R are the sampling intervals in the θ - and the θ -spatial domains, respectively, m , n , u and q are integers. The function $\Phi^e(\rho, \theta, z)$ is normally limited in both the z - and θ -domains, meaning that $\Phi^e(\rho, \theta, z)$ is nonzero for a small finite range of z values ($-Z_1 < z < Z_2$) and a finite range of θ values ($\Theta_1 < \theta < \Theta_2$), and is

essentially zero outside this range. Similarly, $\Phi^e(\rho, \theta, z)$ is limited with respect to frequency content; therefore $F^e(\rho, n, k)$ is nonzero only within a small range $|k| < K$ and $|n| < N$ (K and N being constants). Thus, the discrete functions $\Phi^e(\rho, S_n, Z_m)$ and $F^e(\rho, Ru, Pq)$ approach zero as S_n and Z_m and Ru and Pq , respectively, become large. The sampling intervals S and Z are chosen to be small enough so that no aliasing occurs in the frequency domain, and the number of samples or sampling duration, NS and MZ , are chosen to include the entire signal. Relationships similar in form to the 2DFT pair of equations (i.e., (4.46) and (4.47)) exist for $\Phi^o(\rho, \theta, z)$ and $F^o(\rho, n, k)$ as well.

Thus the various integral equations can be evaluated as products of 2DFTs (equivalent to a two dimensional linear convolution). Once again the potential outside the muscle is given as an example.

$$F^e(\rho, Ru, Pq) = e^{jn\pi} F_m(Pq) W_n^e(\rho, Ru, Pq, a, b) \quad (4.50)$$

where $q = 1, \dots, M$ and $r = 1, \dots, N$.

The external potential itself is given by

$$\Phi^e(\rho, S_n, Z_m) = 2IDFT [\Phi^e(\rho, Ru, Pq)] \quad (4.51)$$

The other integral equations are also evaluated in a similar fashion using two dimensional FFTs.

4.3 Computational Aspects

The type of active fiber considered in this study is the skeletal muscle fiber, that uses the model due to Adrian and Peachey (1973) as the membrane model. The values of the model parameters in used in the cable-like simulation and in the electromagnetic field theoretic model (fig. 4.1) are listed in table 4.1. The resistivity of the sarcoplasm (R_i) is assumed to be 125 Ω -cm, a value obtained from the measurements of Elmqvist et al (1960) and Lipicky et al (1971). The nominal value of the anisotropy ratio λ used in the model model is taken from the compendium of data compiled by Geddes and Baker (1967), specifically it corresponds to a value of 2.78 for λ^2 found by Burger and van Dongen (1960-61). A typical transmembrane potential spatial distribution $\Phi_m(z)$ for a skeletal muscle fiber described in terms of the parameters given in table 4.1 is shown in figure 4.2. This transmembrane potential distribution $\Phi_m(z)$ then serves as input to the volume conductor model for determination of the extracellu-

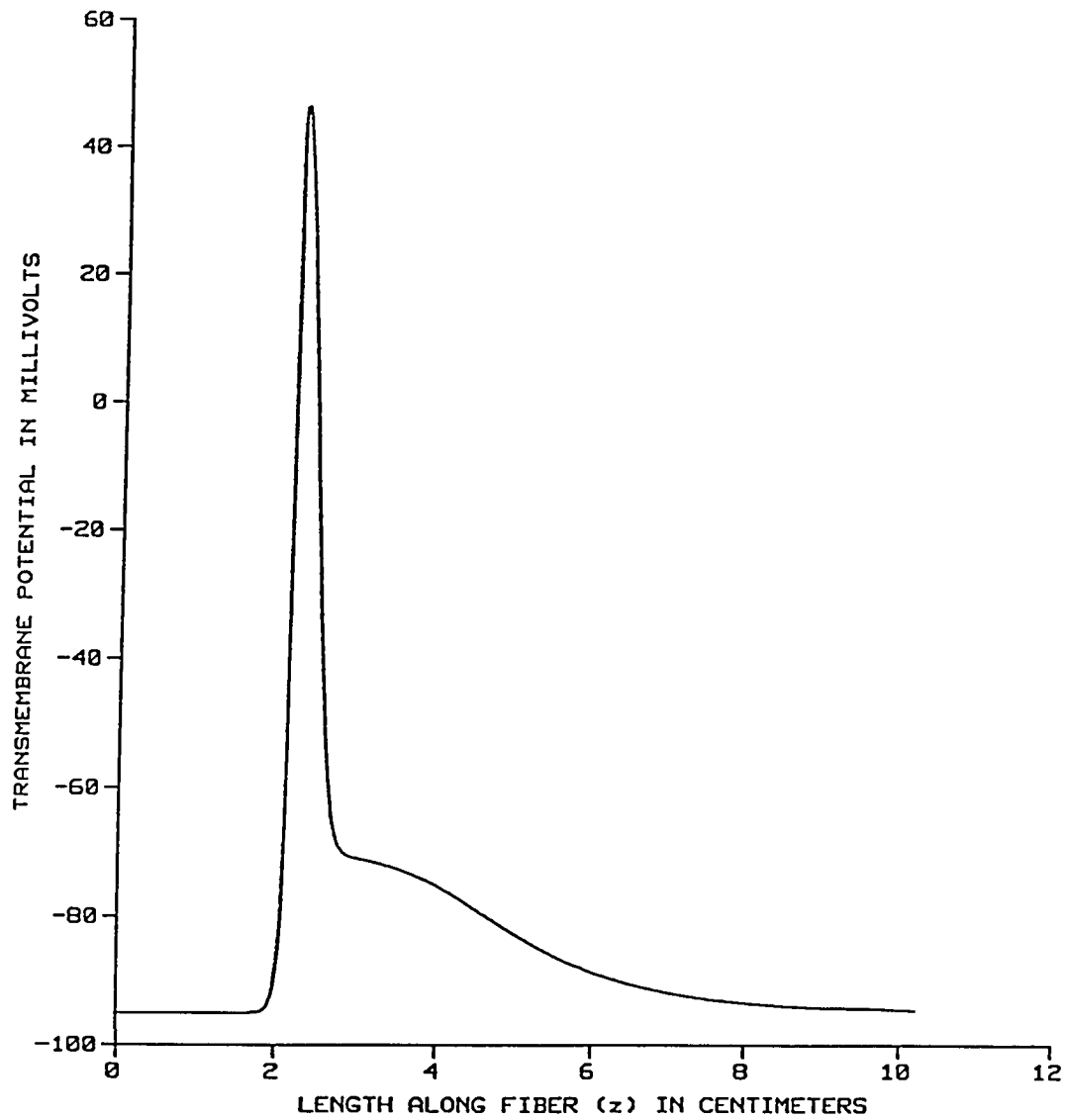


Figure 4.2 Typical action potential distribution $\Phi_m(z)$ for the active skeletal muscle fiber generated by the distributed model of the fiber.

lar field potential.

Table 4.1 : Model Parameters

Parameter	Value Used
Fiber radius (a)	0.005
Source radius (R_s)	0.0125
Muscle radius (b)	na
Muscle medium anisotropy ratio (λ)	1.67
Step size in time (Δt)	0.01 msec
Step size in space (Δz)	0.05 cm
Extracellular resistivity (R_o)	70 Ω cm
Intracellular resistivity (R_i)	125 Ω cm
Extracellular resistance per unit length (r_o)	$R_o / \{\pi a^2 (n^2 - 1)\}$
Intracellular resistance per unit length (r_i)	$R_i / \pi a^2$
External medium conductivity (σ_e)	0.05 S/cm
Sheath specific conductance (σ_{sh})	0.001 S/cm ²
Sheath specific capacitance (C_{sh})	0.02 μ F/cm ²
Membrane Capacitance (C_m)	1 μ F/cm ²
Sodium Nernst Potential (E_{Na})	145 mV
Potassium Nernst Potential (E_K)	25 mV
Leak Potential (E_l)	-5 mV
Sodium conductance constant (\bar{g}_{Na})	180 m mho/cm ²
Potassium conductance constant (\bar{g}_K)	41.5 m mho/cm ²
Leak conductance (g_l)	0.24 m mho/cm ²

Using the potential filter functions defined in equations (4.39) through (4.41) the volume conductor problem may be viewed as an equivalent filter problem as shown in figure 4.3. The input to the filter is $F_m(n,k)$ the Fourier transform of the transmembrane potential distribution and the particular value of ρ where the field distribution is to be evaluated (i.e. $\rho = \rho^*$). The output of the filter is $F^o(n,k)$ the Fourier transform of the potential distribution in the muscle medium when either filter W_π^1 or W_π^2 is used. These filters are defined in equations (4.39) and (4.40) and the value of ρ^* determines which filter is employed. If the value of $\rho^* \geq b$ the filter W_π^* defined in (4.41) is utilized. In this case the output is $F^e(n,k)$ the Fourier transform of the field potential distribution in the external medium.

Figure 4.4 shows the characteristics of the various filter functions used in this process. These filters are "almost real" meaning that the imaginary part of the expressions in equations (4.39) through (4.41) is very small compared to the real part. This is true for a range of values of the sheath capacitance C_{sh} from ten times smaller to ten times larger than typical physiological values. Also, all the filter functions are plotted after the exclusion of the membrane filter from the filter function expressions. The membrane filter is a second derivative filter that serves to convert the monophasic transmembrane potential into the familiar triphasic extracellular potential waveform (Ganapathy et al, 1985) and its properties depend only on the fiber radius and the ratio of specific conductivities inside and outside the fiber. The filter function defined in equation (4.39) for the region of the muscle $\rho \leq R_s$ is illustrated in fig. 4.4a after excluding the membrane filter term from the expression. Figures 4.4b and c show the filter function used inside the muscle in the region $\rho > R_s$ and in the external medium, respectively. All the filter functions have the general characteristics of a low-pass filter; and the further away from the source the field point moves, the lower the cut off frequency and gain of the filter. This implies that the potentials decrease both in amplitude and frequency the further away from the active source fiber they are measured. In all cases the zeroth order filter function, corresponding to an angular position of $\theta = 0$, is several orders of magnitude higher than the filter functions of all other orders. This means that there is almost no change in the calculated field potential as the field point is moved around the muscle at a fixed value of ρ .

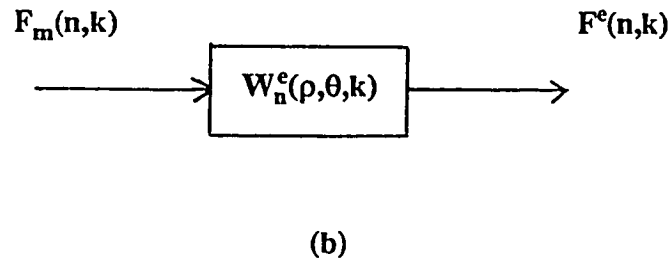
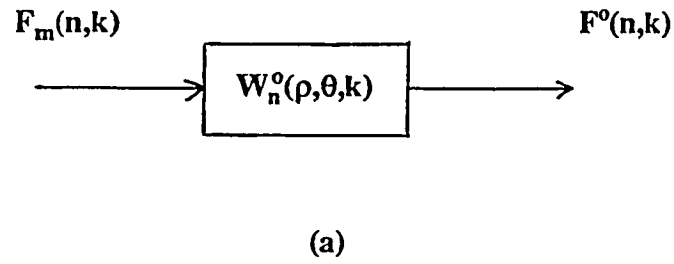


Figure 4.3 Representation of the volume conductor problem as an equivalent filtering problem for the (a) muscle medium potential and the (b) potential in the external medium. Here F_m , F^o , and F^e are the two dimensional Fourier transforms of the transmembrane, muscle medium and external medium field potential distributions respectively, $W_n^o(\rho, \theta, k)$ is the muscle medium filter and $W_n^e(\rho, \theta, k)$ is the external medium filter--see text.

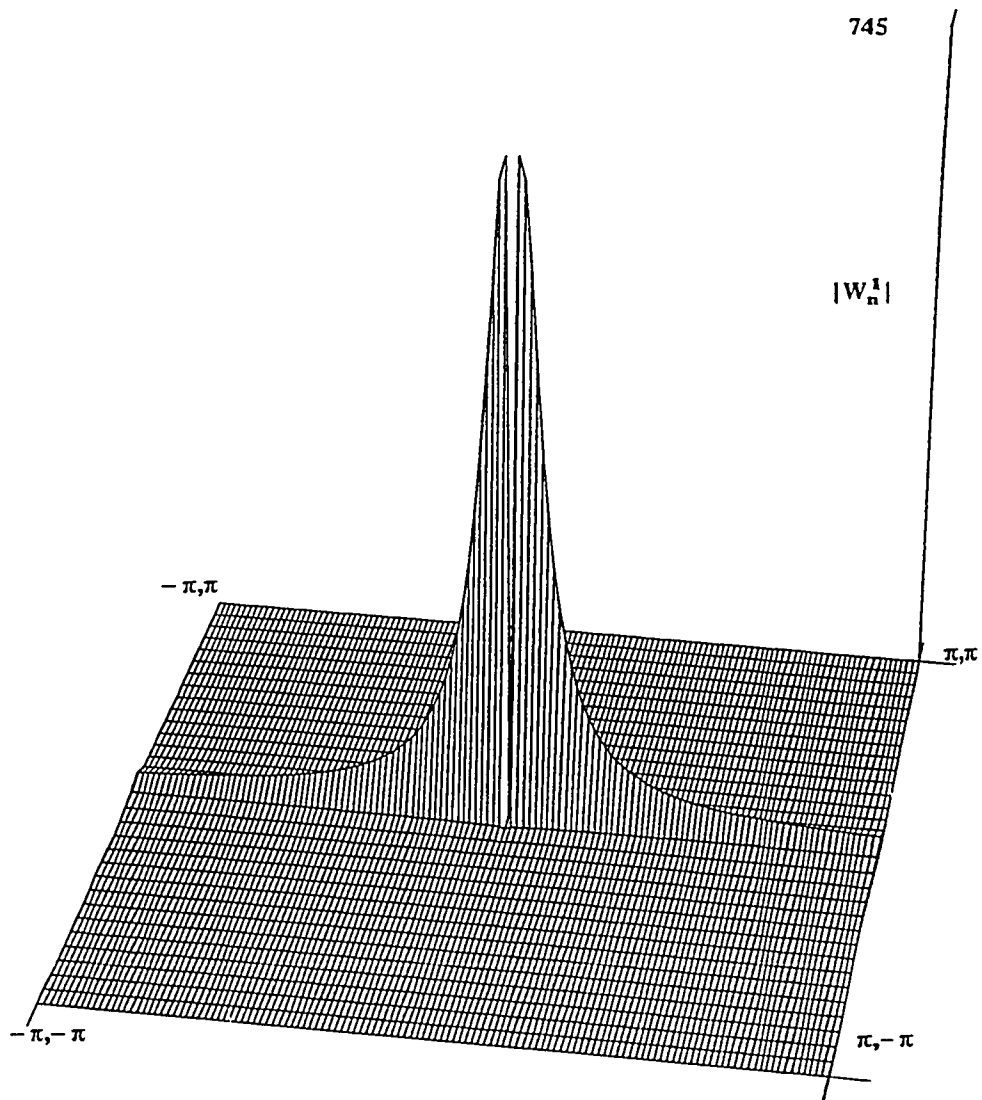


Figure 4.4 a The characteristics of the muscle medium filter function within the source radius W_n^1 vs. k for $\lambda = 1.67$ and $b = 250$ microns.

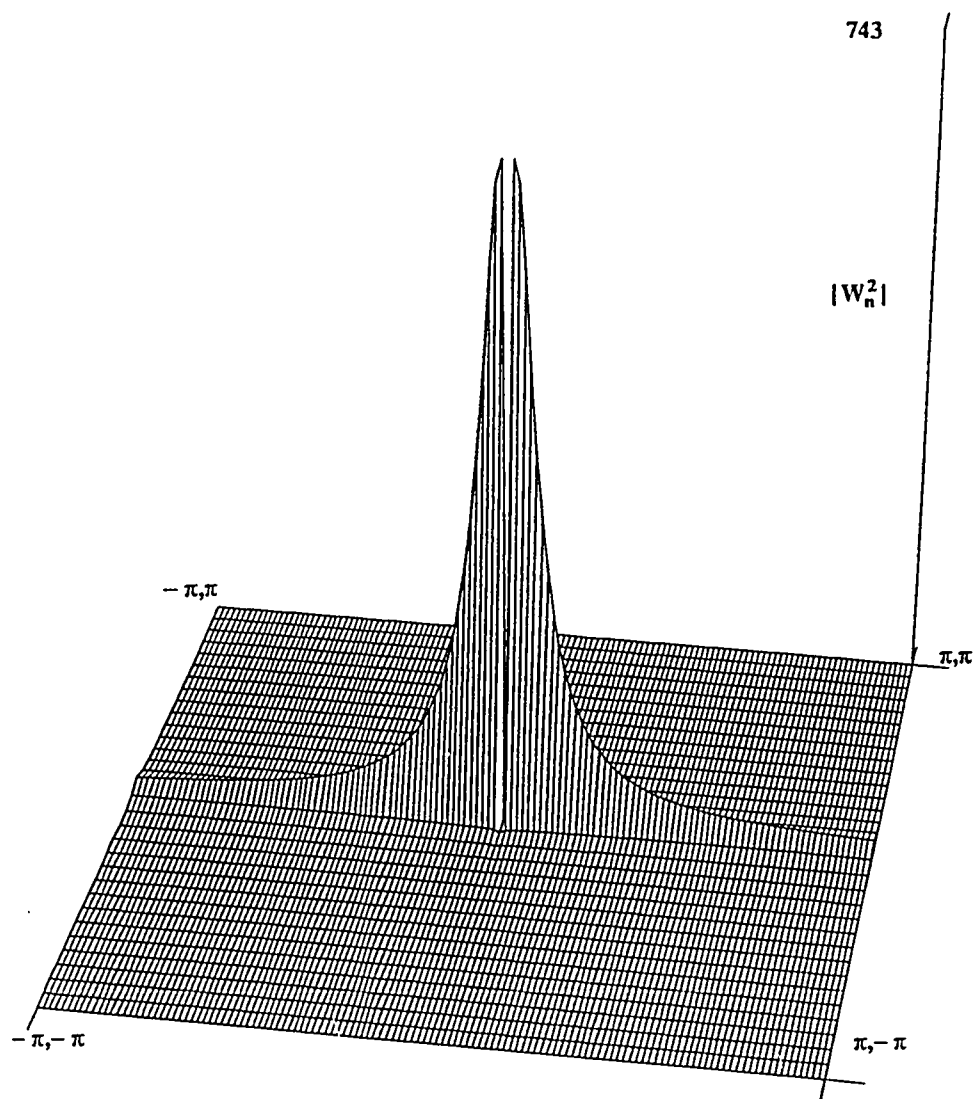


Figure 4.4 b The characteristics of the muscle medium filter function in the region outside the source radius W_n^2 vs. k for $\lambda = 1.67$ and $b = 250$ microns.

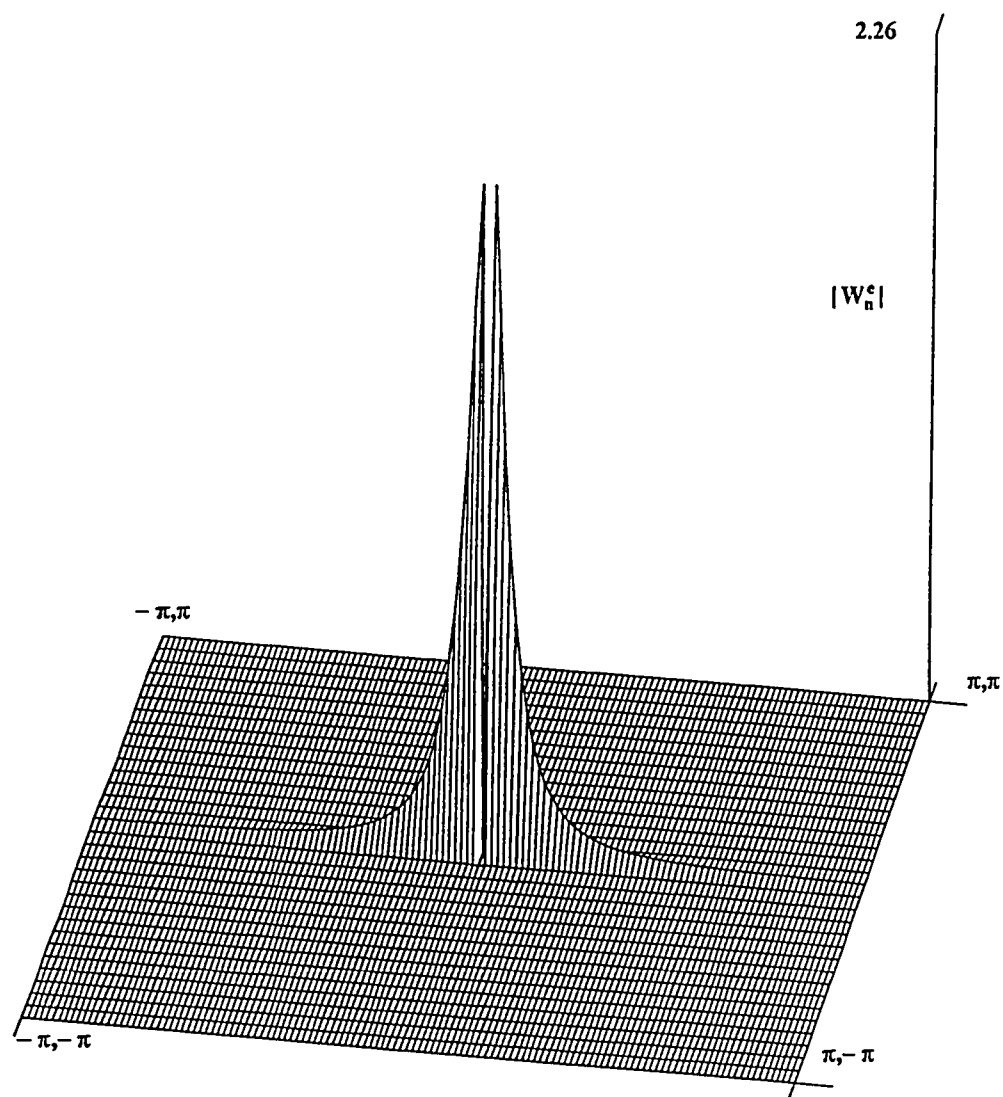


Figure 4.4 c The characteristics of the external medium filter function W_n^e vs. k for $\lambda = 1.67$ and $b = 250$ microns.

4.4 Results

4.41 Single Fiber Studies

The transmembrane potential distribution shown in fig. 4.2 is converted to a two dimensional signal by multiplication by the term e^{inc} which is present in all the equations (4.9) through (4.13) that describe the potential everywhere in the media surrounding the active fiber. This two dimensional signal is then utilized as input to the field theoretic model; consequently the potential everywhere at a given radius from the center of the muscle may be determined. The results of one such simulation is shown in fig. 4.5. The potential fall-off as the field point is moved around the muscle is almost negligible, a result that was predicted by the filter function characteristics of fig. 4.4. The results shown here are for the general muscle medium ($0 \leq \rho \leq b$) but outside the volume occupied by the source fiber for a muscle radius $b = 250$ microns.

When the volume conductor extent is fairly large compared with the fiber radius (i.e. when $b = 2000$ microns), there is a noticeable variation in potential in the θ direction. These results are shown in fig. 4.6a and b when the potential is evaluated on the surface of the muscle. The potential waveform loses both magnitude and frequency content as the field point moves away from the source in an angular direction. The change in the shape and amplitude of the waveform is most obvious between the points $\theta = 0^\circ$ and $\theta = 45^\circ$ as shown in fig 4.6b.

This variation in potential with the angular position θ is predicted by the filter function evaluated for $b = 2000$ microns, shown here in fig. 4.7. The shape of the filter function differs from that in fig. 4.4c in that the filter now has a small but significant gain for its first and second order terms. The zeroth order term still has a maximum gain which implies that the variation in potential with the angular position θ is not very significant, a fact that is verified by the results in fig. 4.6.

The magnitude of the calculated potential is dependent on several factors, the anisotropy ratio and the radius of the muscle being two rather influential parameters. Fig. 4.8 is a calculation of the potential around the muscle at the same field radius used in fig. 4.5 but for different anisotropy ratios. The value of b used here is 250 microns. As the muscle medium becomes increasingly anisotropic,

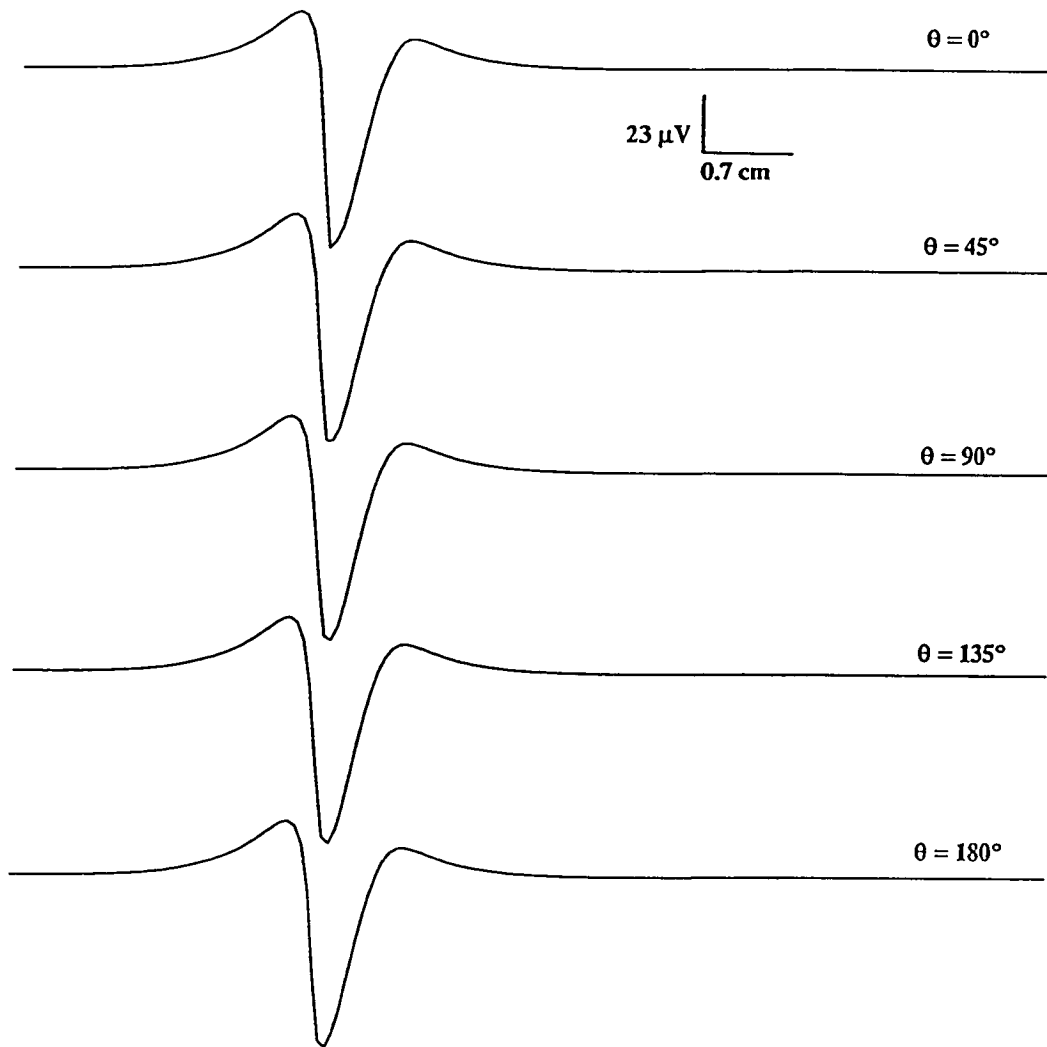


Figure 4.5 Computed extracellular potential waveforms at a point inside the muscle distant $\rho = 160$ microns from the center of the muscle, and for different angular positions around the muscle. All waveforms are computed for a value of $\lambda = 1.67$ and $b = 250$ microns.

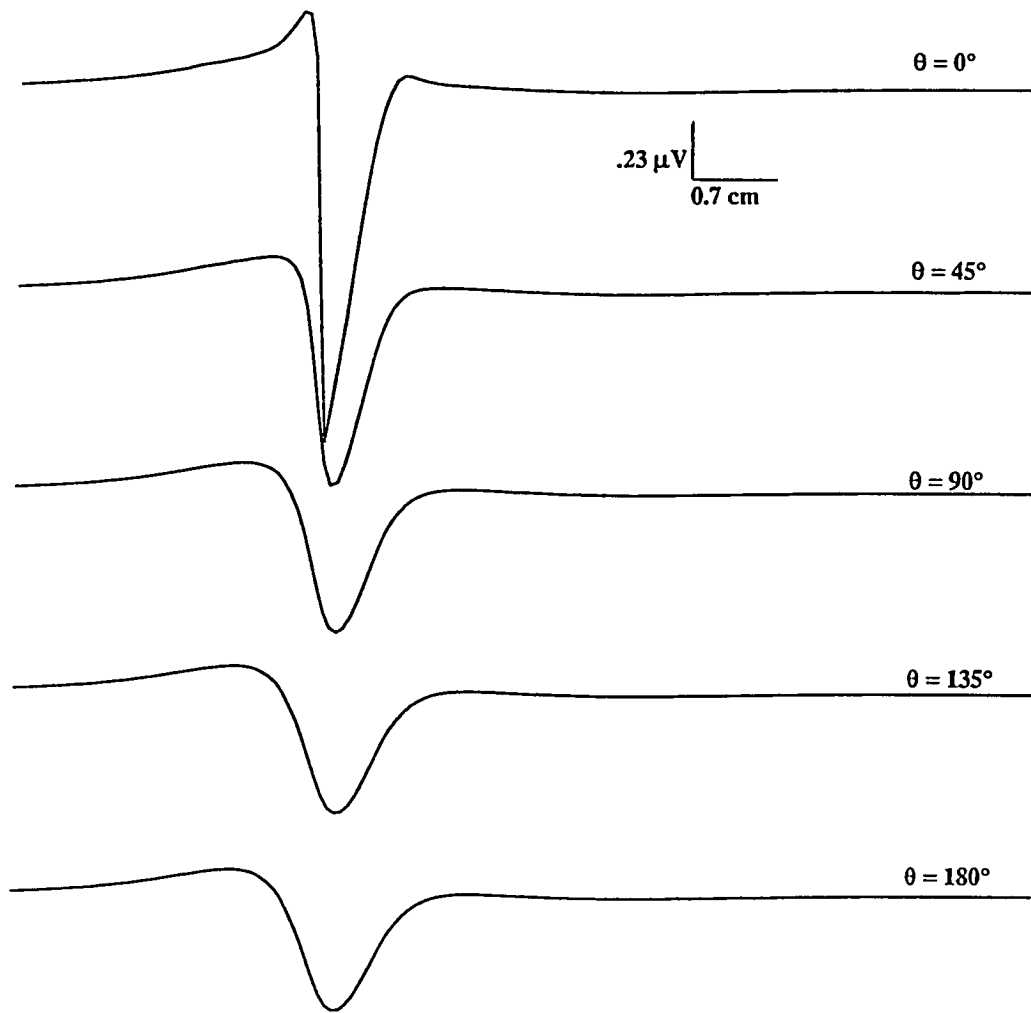


Figure 4.6 a Computed extracellular potential waveforms at the muscle surface i.e. for $\rho = b$, and for different angular positions around the muscle. All waveforms are computed for a value of $\lambda = 1.67$ and $b = 2000$ microns.

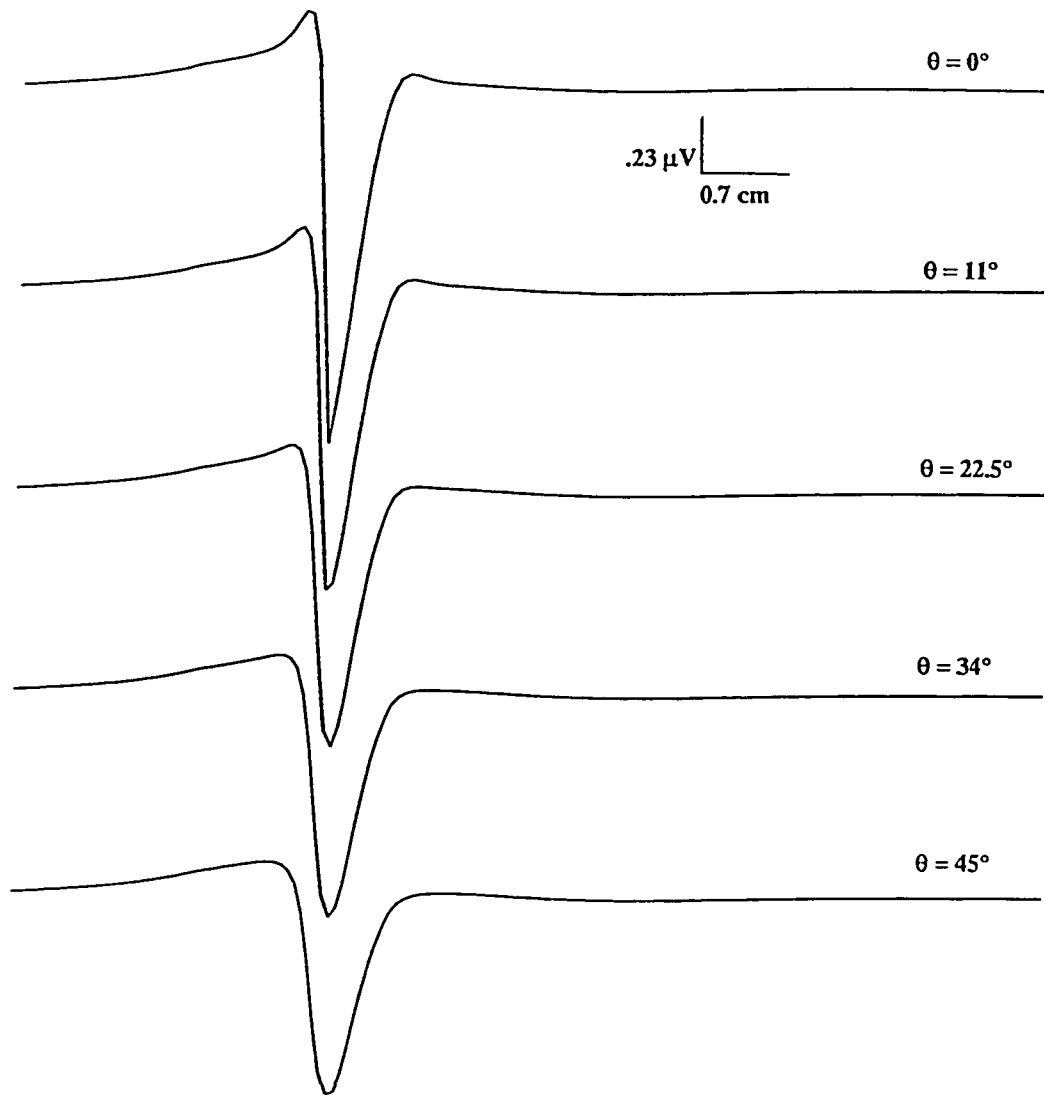


Figure 4.6 b Computed extracellular potential waveforms at the muscle surface i.e. for $p = b$, and for different angular positions around the muscle. All waveforms are computed for a value of $\lambda = 1.67$ and $b = 2000$ microns.

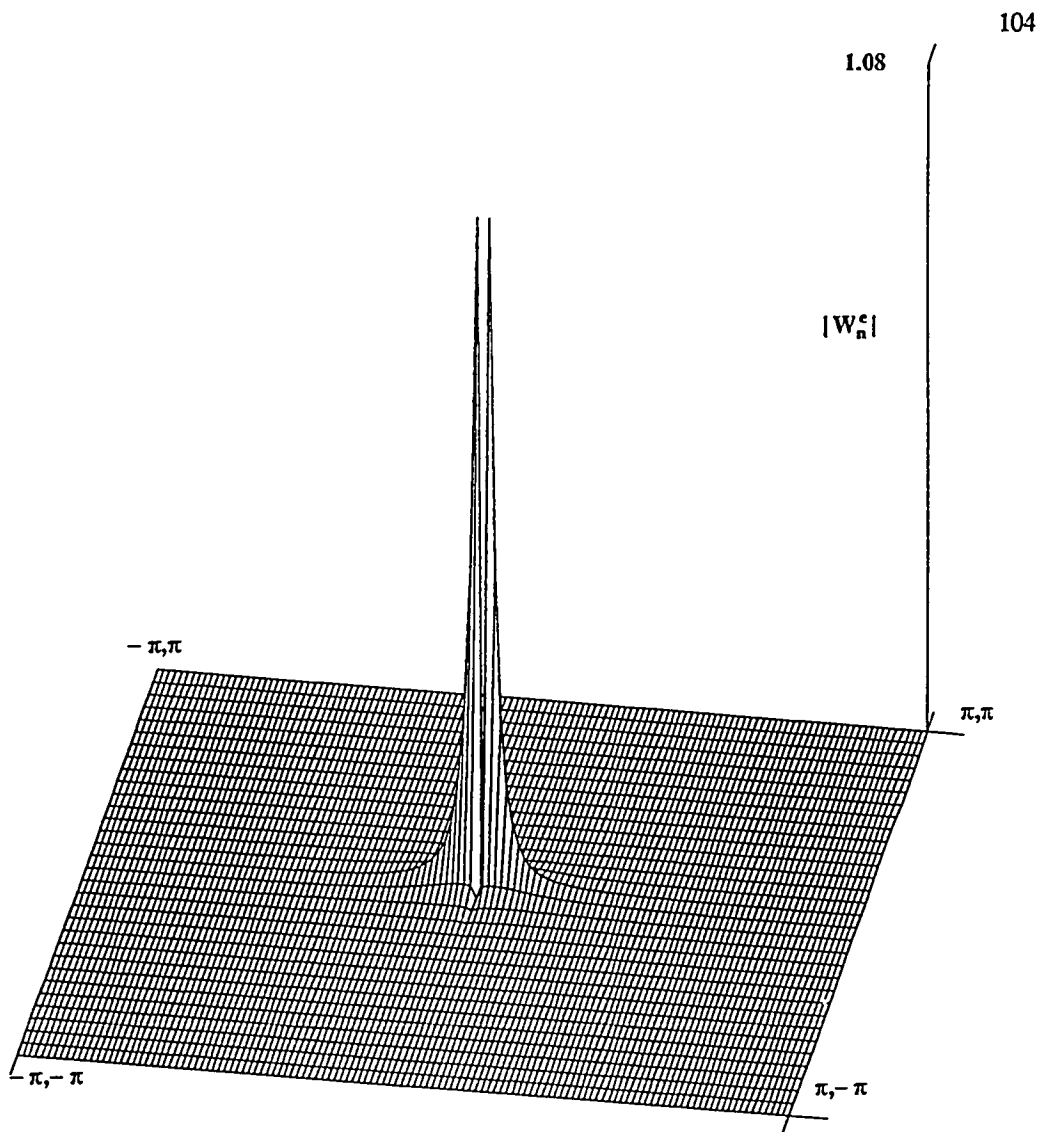


Figure 4.7 The characteristics of the external medium filter function W_n^e vs. k for $\lambda = 1.67$ and $b = 2000$ microns.

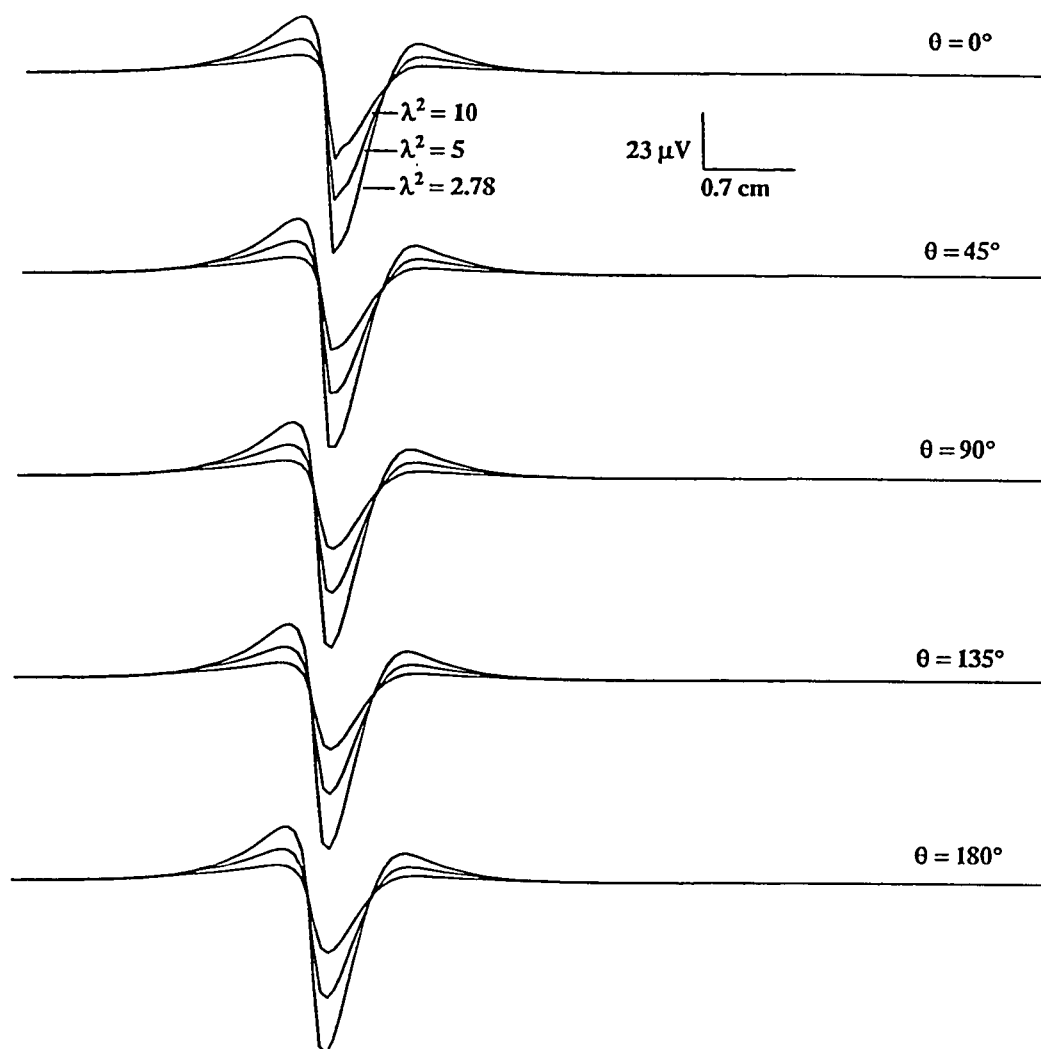


Figure 4.8 Computed extracellular potential waveforms at same points as in fig. 4.5 for different values of the anisotropy ratio λ .

the amplitude of the calculated potential decreases; this is not an unusual result if it is recalled that the anisotropy ratio is a measure of the medium conductivities in the longitudinal and transverse directions. An increasing value of this ratio implies a preferential increase in the longitudinal conductivity which in turn results in a corresponding increase in the longitudinal component of the current density fields. The effect is to confine the field to regions close to the source and thereby increase the rate of potential fall-off in the volume conductor medium.

The magnitude of the calculated potential in the muscle medium is also profoundly influenced by the extent of the medium. As can be seen in fig. 4.9, with a decreasing value of the muscle medium radius b , the magnitude of the calculated potential in the muscle medium increases. The magnitude of the potential nearly doubles when the value of b is decreased from 250 microns, a value corresponding to $5a$, to 175 microns, a number equal to $3.5a$. This increase is true for all values of calculated potential regardless of their position in θ .

4.42 Multiple Fiber Studies

Electromyograms (EMG's) recorded on the surface of a muscle are generally the result of multiple fiber activity within the muscle. Since the basic fundamental element of skeletal muscle is the motor unit, the fundamental component of the EMG is the combined field potential activity of the muscle fibers comprising a given motor unit; i.e. the motor unit action potential or MUAP. In order to simulate the contribution of a single motor unit to a surface recorded EMG, we use an arrangement of nine individual fibers arranged as shown in fig. 4.10. Linear superposition is assumed to apply. The fibers are considered to be identical as regards the geometric and electric parameters characterizing them. As a consequence the same distributed parameter model may be used to simulate the individual fibers and the fibers may be fired synchronously, or in any desired firing pattern. The effects of allowing all nine fibers to fire simultaneously are shown in fig. 4.11. This model would seem to be a good approximation for surface EMG recordings where the recording point lies in the far field of the active motor unit. As the recording point is brought closer to the motor unit, the interference pattern produced by the geometrical distribution of the individual active fibers would become progressively more important. Consequently, other mathematical approaches would have to be taken.

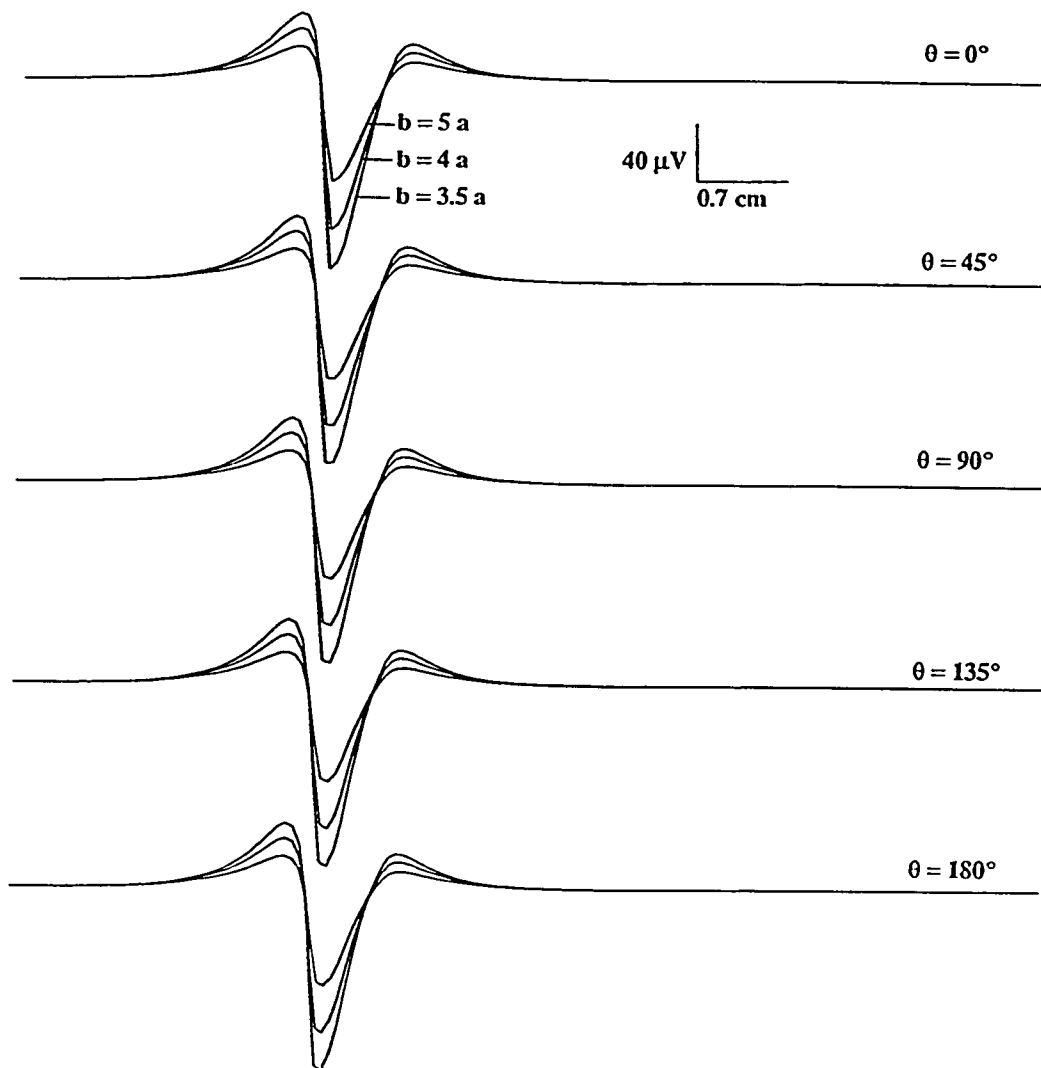


Figure 4.9 Computed extracellular waveforms at a point within the muscle distant $p = 160$ microns from the center for various values of the muscle medium radius b .

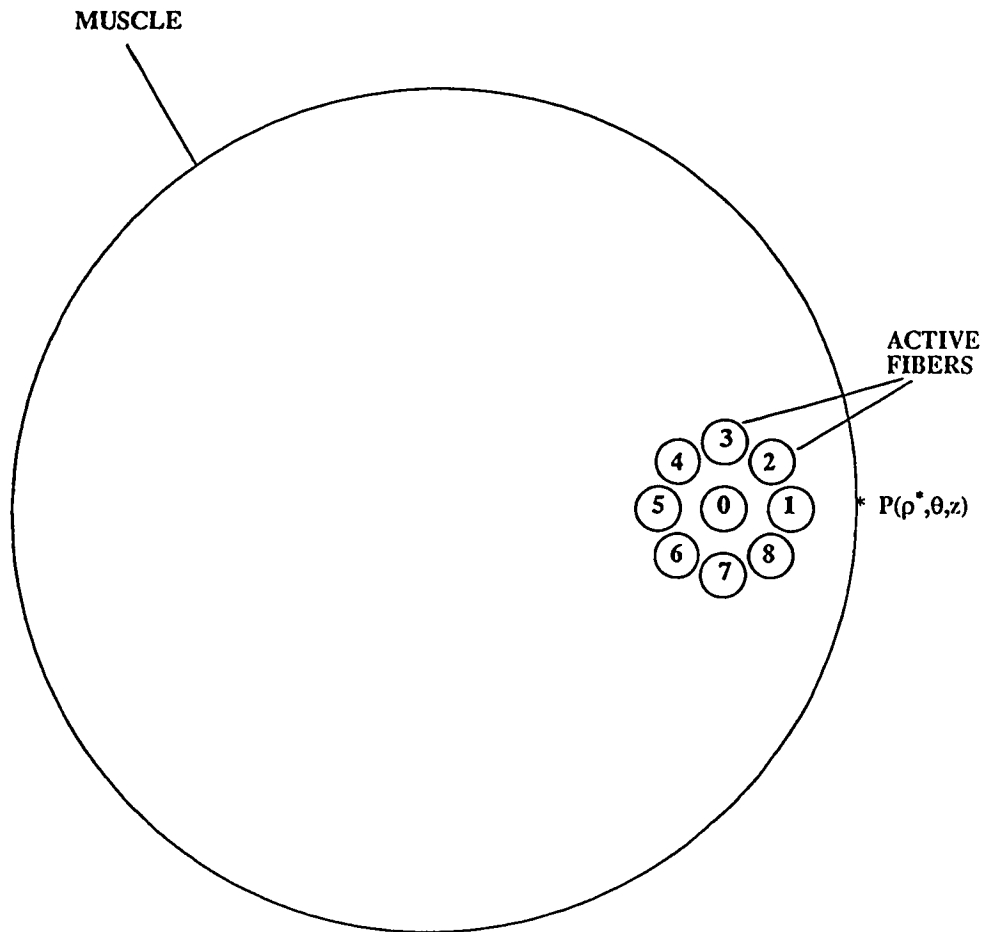


Figure 4.10 An arrangement of nine active fibers numbered 0 through 8 within the muscle, any or all of which may be active at a given time instant. The point $P(\rho, \theta, z)$ is the field point in the external medium at which the composite potential waveform is evaluated.

The potential in fig. 4.11 is calculated on the muscle surface at $\rho = b$ and the nine fibers are labeled as shown in fig. 4.10. Fig. 4.11a shows the calculated potential when the fiber numbered 0 is the only fiber that is active. Fig. 4.11b is the calculated potential when all nine fibers are simultaneously active and are stimulated at the same instant. As is obvious on comparing the two figures the shape of the calculated potential remains unchanged but there is a nine fold increase in magnitude. Once again there is a change in potential amplitude and frequency content with angular position θ as the results shown are for a value of $b = 2000$ microns.

There is a marked change in the waveshape of the calculated potential when the fibers are stimulated at different instants of time. Fig. 4.12 illustrates the effects of stimulating the nine individual fibers within the muscle at slightly different instants of time. These results are displayed as functions of time and not as functions of the spatial distance z like all the preceding results. The electrical activity propagates along the fiber with a constant velocity of propagation and therefore the spatial variable is directly proportional to time, the constant of proportionality being the velocity. To convert a potential that is a function of the spatial variable z into a potential that is a function of time all that is required is that the independent variable z be scaled by the constant velocity. All three sets of waveforms in the figure are calculated at the surface of the muscle i.e. at $\rho = b$. The complex waveforms shown in fig. 4.12a result when the fibers are stimulated in the order 0, 1, 2, 3, 4, 5, 6, 7, 8 with a 0.5 ms interval between successive stimuli. The same stimulus sequence is repeated with a time interval of 0.75 ms between successive stimuli, and the result is shown in the waveforms in fig. 4.12b. The two sets of complex waveforms differ in both shape and duration. Maintaining the same stimulus sequence but with an interval of 1.5 ms between the individual stimuli, results in the waveform set shown in fig. 4.12c. This set of waveforms is considerably different both in shape and duration from the sets shown in figures 4.12a and b. All three sets were calculated for $b = 2000$ microns, and hence there is a marked loss in frequency content and amplitude with angular position θ . As is apparent from the figure the shape, amplitude and duration of the composite waveform is dependent on the stimulus pattern and the time allowed to elapse between successive stimuli.

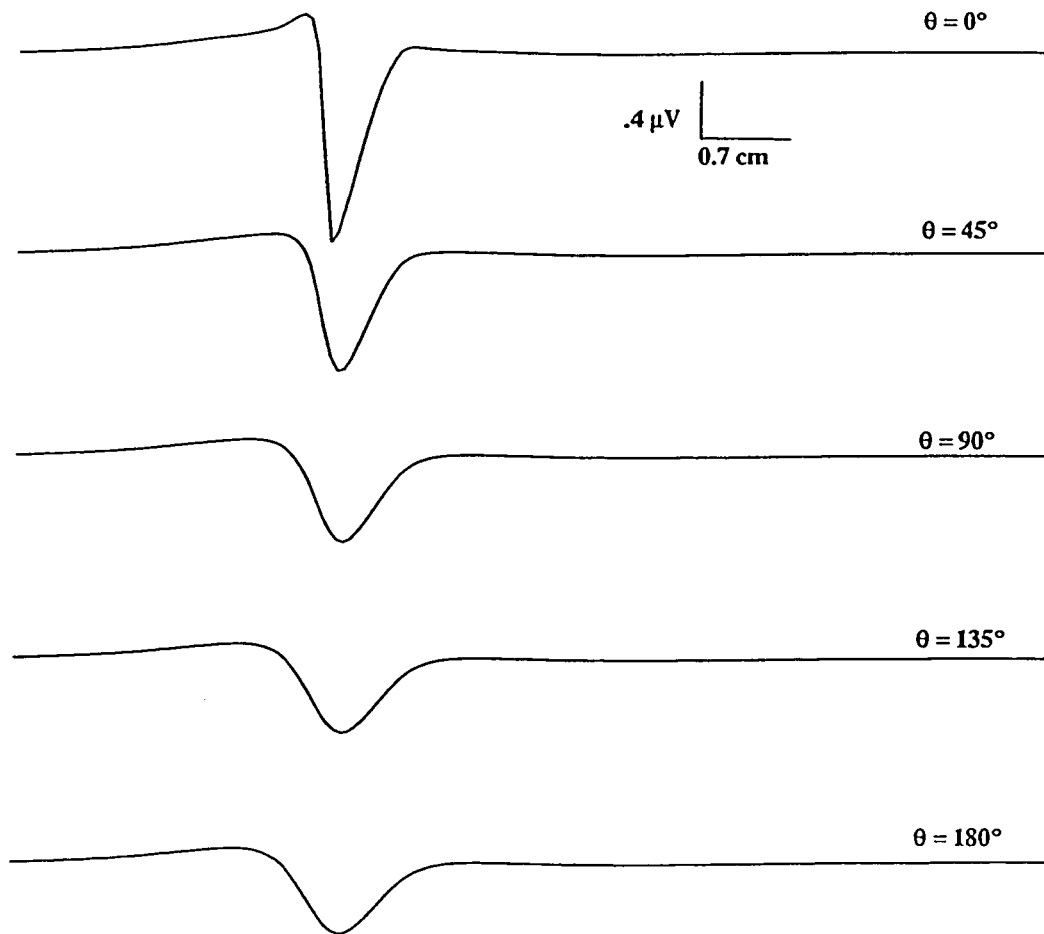


Figure 4.11 a The calculated composite potential at the point P of fig. 3.10 when only fiber 0 is active.

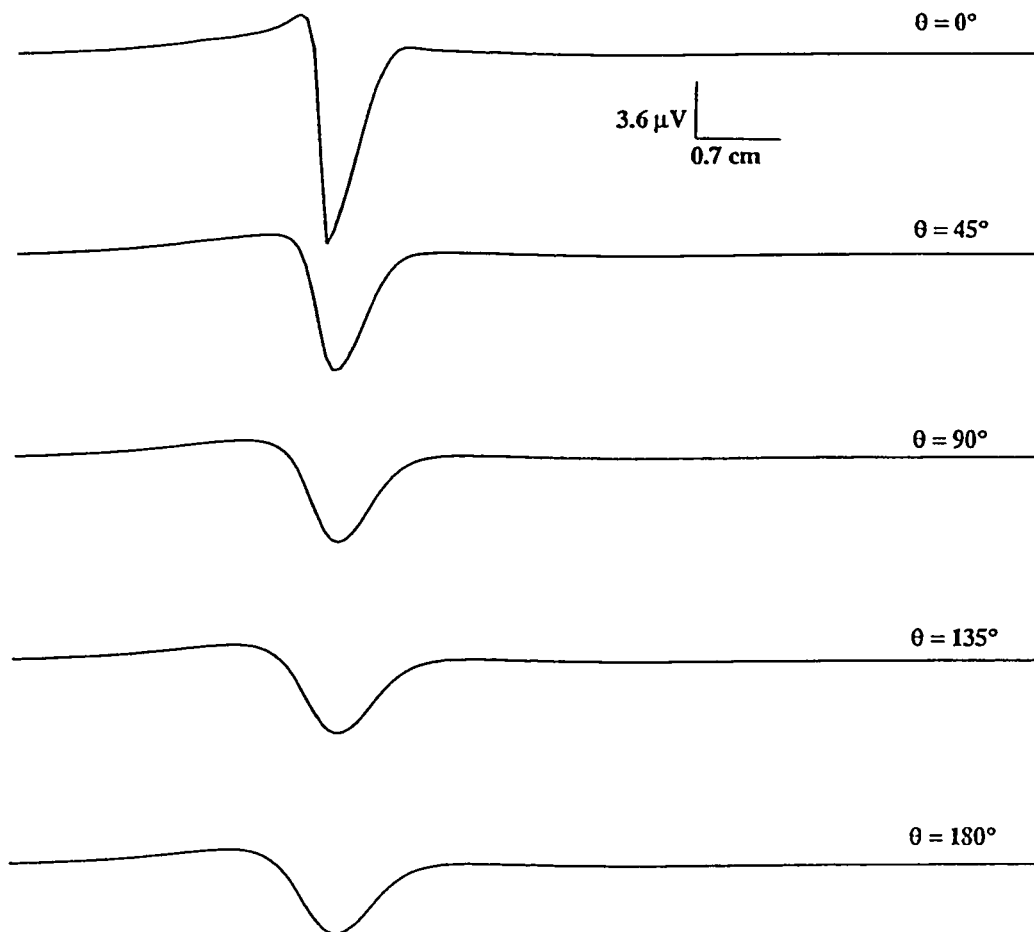


Figure 4.11 b The calculated composite potential at the point P of fig. 3.10 when all the nine fibers are synchronously active.

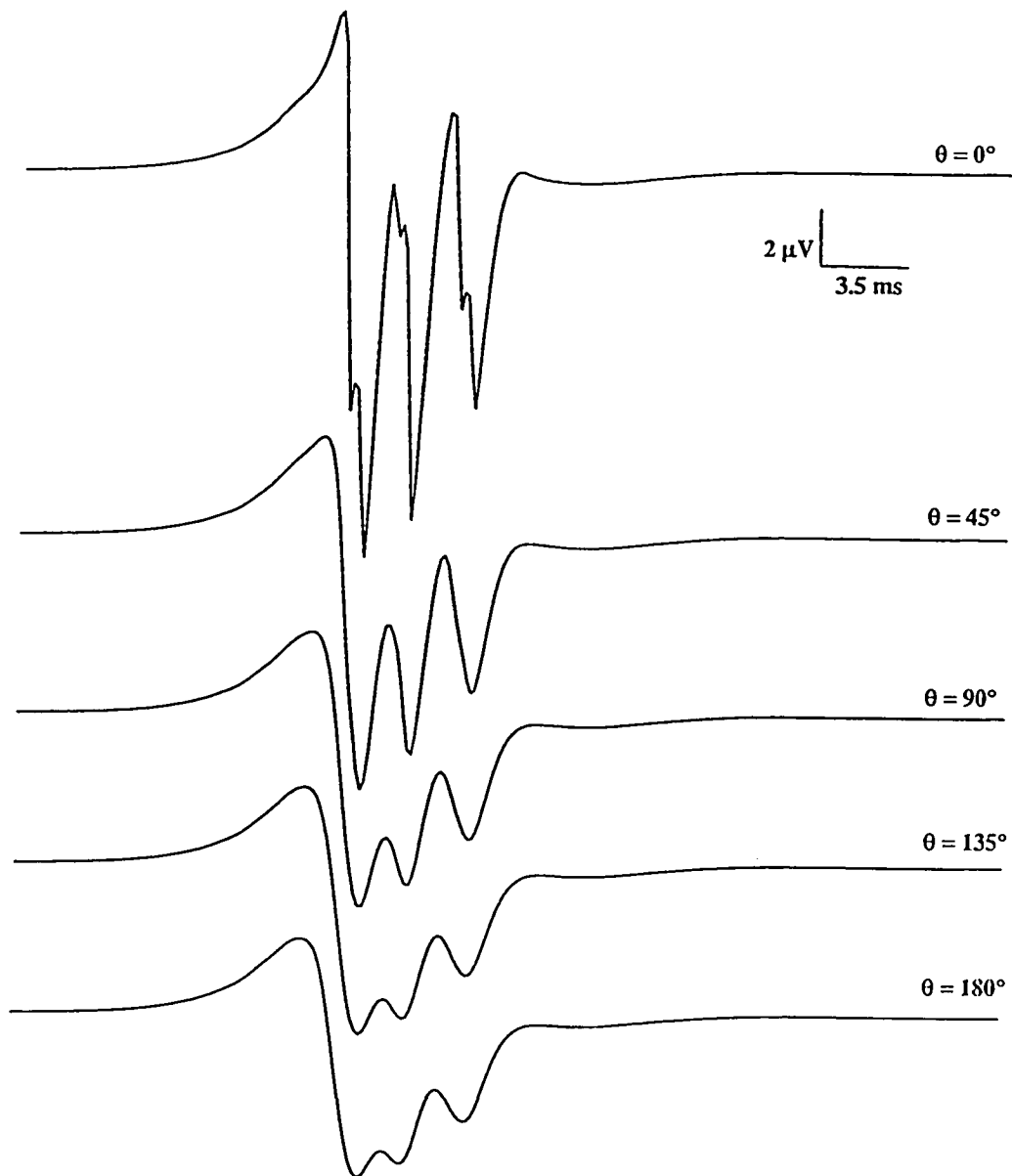


Figure 4.12 a The calculated composite potential waveform at the point P of fig. 3.10 when the stimulus is applied in succession to fiber 0, 1, 2, 3, 4, 5, 6, 7, 8 at 0.5 ms intervals. The muscle is considered to have a radius $b = 2000$ microns and $\lambda = 1.67$.

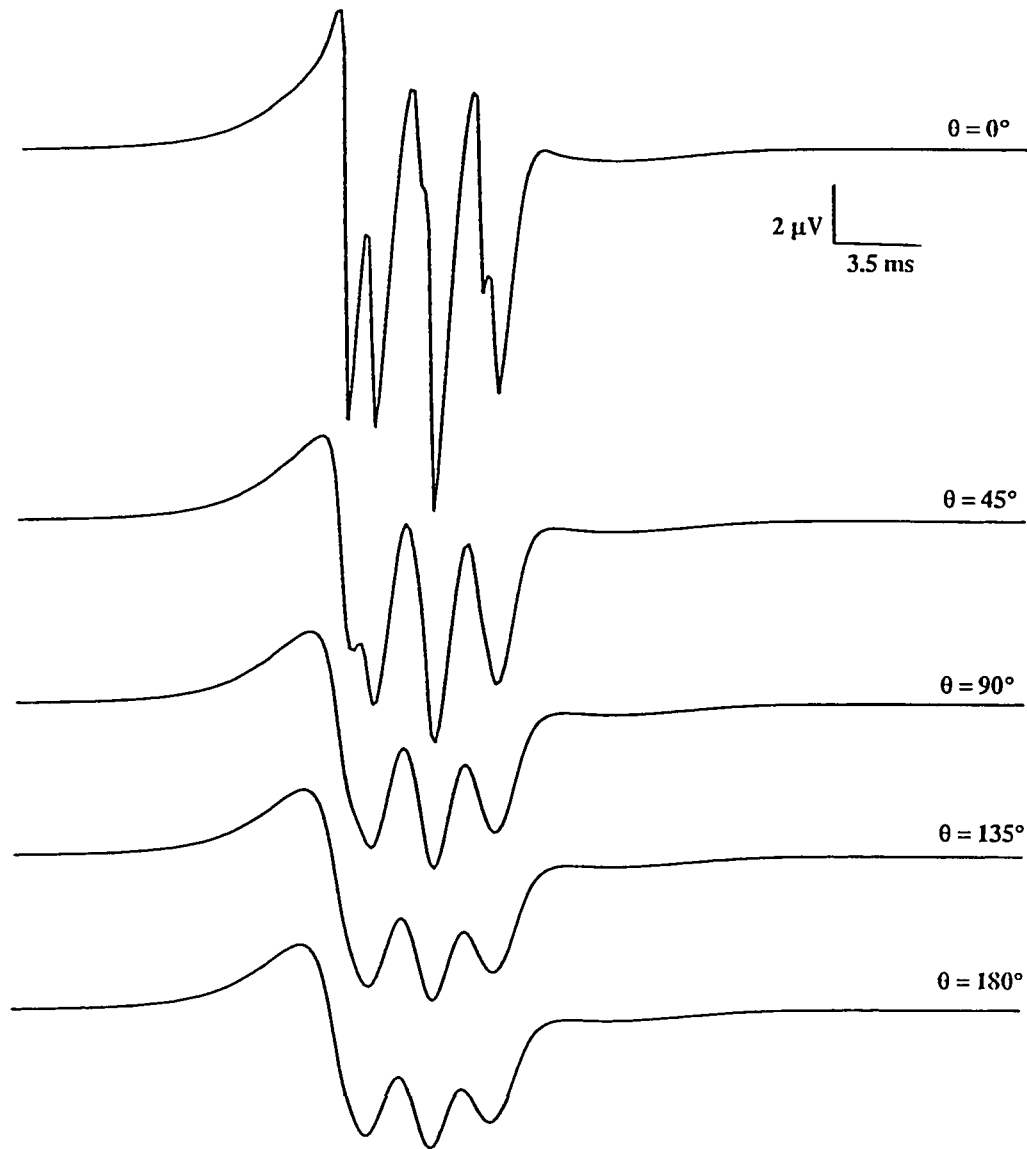


Figure 4.12 b The calculated composite potential waveform at the point P of fig. 3.10 when the stimulus is applied in succession to fiber 0, 1, 2, 3, 4, 5, 6, 7, 8 at 0.75 ms intervals. The muscle is considered to have a radius $b = 2000$ microns and $\lambda = 1.67$.

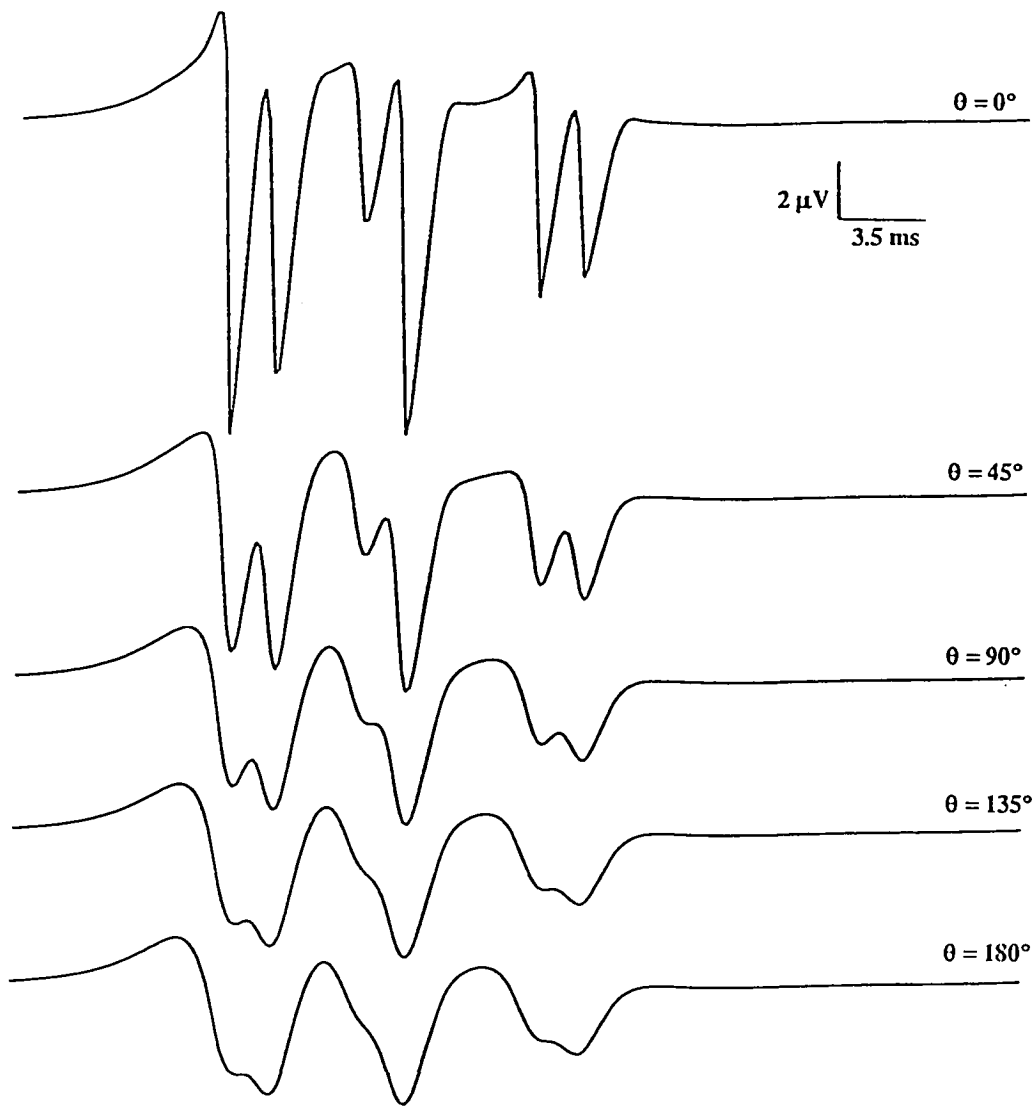


Figure 4.12 c The calculated composite potential waveform at the point P of fig. 3.10 when the stimulus is applied in succession to fiber 0, 1, 2, 3, 4, 5, 6, 7, 8 at 1.5 ms intervals. The muscle is considered to have a radius $b = 2000$ microns and $\lambda = 1.67$.

4.5 Discussion of results

In this chapter a technique for evaluating extracellular potentials from either a single active muscle fiber or an active motor unit, located in a finite, anisotropic volume conductor, has been demonstrated. The method employs a two dimensional Fourier transform technique that allows the active fiber to be located anywhere within the muscle. Although not demonstrated in this work, an advantage of the two dimensional Fourier formulation is the ease with which the filter functions may be utilized to calculate the potential at the membrane surface of the active fiber within the muscle, given the recorded potential at a point on the exterior of the muscle. Computation time for the Fortran 77 simulation of the single fiber problem on a VAX 11-750 employing a 4.2 Berkeley Standard Unix operating system was under thirty seconds. The active motor unit (nine fibers) took approximately two minutes. This represents a considerable savings over the computation time required had a finite difference or a finite element method been employed.

It has also been shown here that it is possible to obtain compound extracellular potential waveforms by allowing the individual muscle fibers to conduct action potentials that are not synchronized to the same stimulus. The model developed here may be used to run simulations useful in gaining an insight into the nature of desynchronized surface EMG waveforms, as well as the more general problem of the decomposition of surface EMG waveforms into fundamental components.

CHAPTER 5

Conclusions and Future Extensions of the Model

In the preceding chapters a mathematical technique has been developed to rapidly compute volume conducted potentials and currents from a variety of excitable cells. The technique that couples a distributed parameter description of a fiber with a field theory description of its environment is completely general. The method does not require a constant propagation velocity of the electrical activity along the fiber, as was necessary in previous work of this nature (Clark and Plonsey, 1968, Greco et al, 1977, Wilson et al, 1985); nor is the field theoretic model in any way restricted by the assumption of axial current flow, as the equivalent core conductor model is. The present technique as it stands is very rapid and efficient. The finite difference method employed to solve the distributed parameter model of the fiber has also been selected with an eye to the rapidity and stability of the numerical integration scheme. The method used here is the Crank-Nicholson integration scheme which is known to be stable for time and spatial step sizes that are several orders of magnitude larger than those permissible for explicit integration schemes (Smith, 1978). The resulting set of equations is fortunately of a form that can be rapidly evaluated using a one step Gauss elimination method (chapter 2). No time consuming iterative schemes or matrix inversion methods are needed anywhere in the entire evaluation process. The time waveforms are also reconstructed using a simple shifting and sampling method, which is considerably faster than using a Green's function description of the time varying current density and potential fields around the fibers. A discussion of results from the application of the method to each problem considered in the thesis is contained within the chapter concerned.

Important extensions of the thesis are to two specific areas :

(a) the development of a more complete mathematical model of the myelinated nerve fiber, for the study of various other aspects of demyelination disease. An initial attempt to develop an expanded, more adequate model, one containing potassium channels in the internodal region as well as, a cleft space between the myelin sheath and the plasma membrane, is shown in Appendix I;

(b) the expansion of the skeletal muscle motor unit model to study the field distribution in the immediate vicinity of the motor unit, considering such topics as muscle fiber interaction and the effect on the local field distribution of having some fibers in the field active, and others inactive. The guide for that study would be the work of Clark and Plonsey (1970).

APPENDIX I

An Improved Source Description of the Active Myelinated Nerve

The complete network equivalent circuit for a small Δz increment of the myelinated fiber is shown in fig. A1.1. The entire fiber consists of several such elements in series. If the series element r_c , which is the resistance per unit length of the cleft region between the myelin sheath and the cell membrane, is considered to be very large, an assumption that is probably justified because of the very small cross section area of the cleft space, the series link interconnecting the consecutive nodes in the cleft space can be approximated by an open circuit. Under these circumstances, the two resistive-capacitive parallel networks, one describing the myelin sheath and the other the cell membrane beneath it, are in series with each other. Typical values for the circuit parameters indicate that the myelin conductance and capacitance are both two to three orders of magnitude lower than the corresponding membrane conductance and capacitance in series with them. To a first approximation therefore the membrane capacitance and conductance can be neglected in comparison to the myelin capacitance and conductance. This results in the network characterization of the myelinated fiber that is used in this study, and is shown in figures 1.3 and 1.4.

The model used will therefore approximate the actual conditions present in a myelinated fiber under normal conditions and for one sweep of an action potential. This model cannot be used to simulate the situation where the myelinated fiber is stimulated repeatedly. This is so because under conditions of repeated stimuli there may quite possibly be a build up of potassium concentration in the cleft region which may have a profound influence on the excitability of the nerve. Under these conditions the full blown network characterization of the myelinated fiber will have to be used coupled with a compartmental system that allows for potassium exchange between the various regions of the model. The general equations that characterize the more complicated network of the myelinated fiber model and the compartmental model that is coupled with it are developed below.

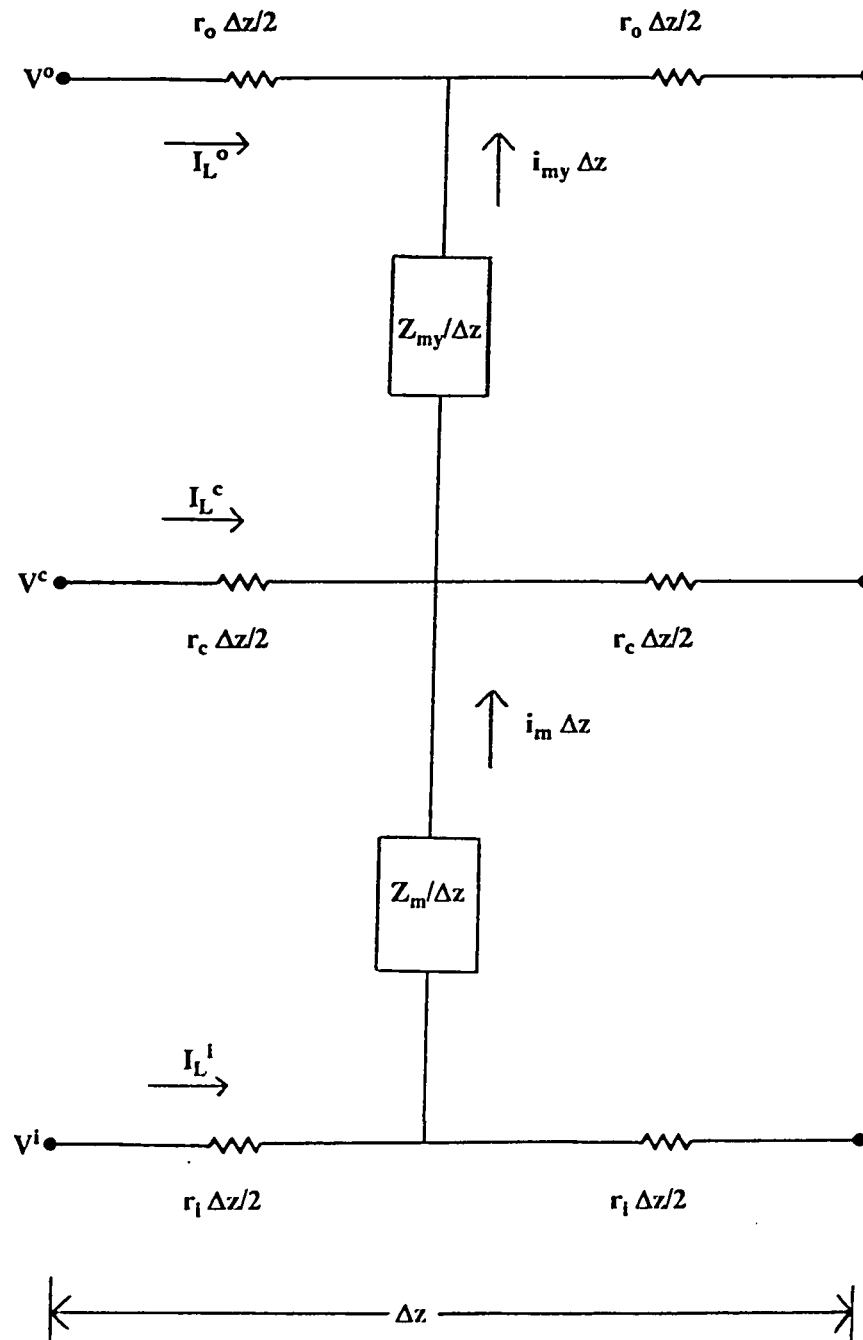


Figure A1.1 The electrical equivalent network of an active myelinated nerve fiber in a homogeneous cylindrical volume conductor, consistent with the classical core conductor model of Hermann (1879).

A1.1 A modified network model for the myelinated fiber

For a single external network branch in fig. A1.1 we have :

$$I_L^o(z) = \frac{V^o(z) - V^o(z + \Delta z)}{r_o \Delta z} \quad (\text{A1.1})$$

In the limit when $\Delta z \rightarrow 0$ we have :

$$I_L^o(z) = - \frac{1}{r_o} \frac{\partial V^o(z)}{\partial z} \quad (\text{A1.2})$$

Similarly for the cleft space current $I_L^c(z)$ and the internal longitudinal current $I_L^i(z)$ the following relations may be obtained.

$$I_L^c(z) = - \frac{1}{r_c} \frac{\partial V^c(z)}{\partial z} \quad (\text{A1.3})$$

and

$$I_L^i(z) = - \frac{1}{r_i} \frac{\partial V^i(z)}{\partial z} \quad (\text{A1.4})$$

Applying Kirchoff's current law at the external node results in the following relation between i_{my} and $I_L^o(z)$.

$$I_L^o(z + \Delta z) = i_{my} \Delta z + I_L^o(z) \quad (\text{A1.5})$$

or

$$i_{my} = \frac{I_L^o(z + \Delta z) - I_L^o(z)}{\Delta z} \quad (\text{A1.6})$$

which reduces to

$$i_{my} = \frac{\partial I_L^o(z)}{\partial z} \quad (\text{A1.7})$$

in the limit when $\Delta z \rightarrow 0$. Similarly analyzing the internal node results in

$$i_m = - \frac{\partial I_L^i(z)}{\partial z} \quad (\text{A1.8})$$

Applying Kirchoff's current law to the central node results in the following expression.

$$i_m \Delta z + I_L^c(z) = i_{my} \Delta z + I_L^c(z + \Delta z) \quad (\text{A1.9})$$

which in the limit when $\Delta z \rightarrow 0$ is given by

$$i_m - i_{my} = \frac{\partial I_L^c(z)}{\partial z} \quad (\text{A1.10})$$

or

$$\frac{\partial I_L^c(z)}{\partial z} = - \frac{\partial I_L^i(z)}{\partial z} - \frac{\partial I_L^o(z)}{\partial z} \quad (\text{A1.11})$$

Defining the potential difference $V_{m1}(z)$ across the element $Z_m/\Delta z$ as

$$V_{m1}(z) = V^i(z) - V^c(z) \quad (\text{A1.12})$$

it follows that

$$\frac{\partial V_{m1}(z)}{\partial z} = \frac{\partial V^i(z)}{\partial z} - \frac{\partial V^c(z)}{\partial z} \quad (\text{A1.13})$$

or, upon rewriting (A1.13) using equations (A1.3) and (A1.4)

$$\frac{\partial V_{m1}(z)}{\partial z} = -r_i I_L^i(z) + r_c I_L^c(z) \quad (\text{A1.14})$$

Differentiating the above equation with respect to z , and substituting equation (A1.11) into it results in

$$\frac{\partial^2 V_{m1}(z)}{\partial z^2} = -(r_i + r_c) \frac{\partial I_L^i(z)}{\partial z} - r_c \frac{\partial I_L^o(z)}{\partial z} \quad (\text{A1.15})$$

or

$$\frac{\partial^2 V_{m1}(z)}{\partial z^2} = (r_i + r_c) i_m - r_c i_{my} \quad (\text{A1.16})$$

Similarly defining the potential difference $V_{my1}(z)$ across the shunt element $Z_{my}/\Delta z$ as

$$V_{my1}(z) = V^c(z) - V^o(z) \quad (\text{A1.17})$$

it follows that

$$\frac{\partial V_{my1}(z)}{\partial z} = \frac{\partial V^c(z)}{\partial z} - \frac{\partial V^o(z)}{\partial z} \quad (A1.18)$$

or, upon rewriting (A1.18) using equations (A1.2) and (A1.3)

$$\frac{\partial V_{my1}(z)}{\partial z} = -r_c J_L^c(z) + r_o J_L^o(z) \quad (A1.19)$$

Differentiating the above equation with respect to z , and substituting equation (A1.11) into it results in

$$\frac{\partial^2 V_{my1}(z)}{\partial z^2} = r_c \frac{\partial I_L^i(z)}{\partial z} + (r_c + r_o) \frac{\partial I_L^o(z)}{\partial z} \quad (A1.20)$$

or

$$\frac{\partial^2 V_{my1}(z)}{\partial z^2} = -r_c j_m + (r_c + r_o) i_{my} \quad (A1.21)$$

Finally the total transmembrane potential $V_m(z)$ is defined as :

$$V_m(z) = V_{my1} + V_{m1} \quad (A1.22)$$

The finite difference forms of equations (A1.16) and (A1.21) are given as follows.

$$\begin{aligned} V_{i-1,j+1}^m - (2 + \alpha_m) V_{i,j+1}^m + V_{i+1,j+1}^m + \beta_{my} V_{i,j+1}^{my} \\ = -V_{i-1,j}^m + (2 - \alpha_m) V_{i,j}^m - V_{i+1,j}^m + \beta_{my} V_{i,j}^{my} + \gamma_m + \gamma_{my} \end{aligned} \quad (A1.23)$$

and

$$\begin{aligned} V_{i-1,j+1}^{my} - (2 + \alpha_{my}) V_{i,j+1}^{my} + V_{i+1,j+1}^{my} + \beta_m V_{i,j+1}^m \\ = -V_{i-1,j}^{my} + (2 - \alpha_{my}) V_{i,j}^{my} - V_{i+1,j}^{my} + \beta_m V_{i,j}^m + \delta_m + \delta_{my} \end{aligned} \quad (A1.24)$$

where V^m and V^{my} denote the discrete forms of the potential differences V_m and V_{my} respectively and the various terms in (A1.23) and (A1.24) are defined as follows

$$\alpha_m \equiv 4\pi a(r_i + r_c) \frac{C_m h^2}{k} \quad (A1.25)$$

$$\alpha_{my} \equiv 4\pi a'(r_c + r_o) \frac{C_{my} h^2}{k} \quad (A1.26)$$

$$\beta_m \equiv 4\pi a r_c \frac{C_m h^2}{k} \quad (A1.27)$$

$$\beta_{my} \equiv 4\pi a' r_c \frac{C_{my} h^2}{k} \quad (A1.28)$$

$$\gamma_m \equiv 4\pi a(r_i + r_c) h^2 i_{ion} \quad (A1.29)$$

$$\gamma_{my} \equiv 4\pi a' r_c h^2 i_{my} \quad (A1.30)$$

$$\delta_m \equiv 4\pi a r_c h^2 i_{ion} \quad (A1.31)$$

$$\delta_{my} \equiv 4\pi a'(r_c + r_o) h^2 i_{my} \quad (A1.32)$$

Here a is the axonal radius and a' is the fiber radius i.e. the radius of the axon and its myelin sheath. The specific capacitance C_m is associated with the axon membrane while the specific capacitance C_{my} is associated with the myelin sheath.

Equations (A1.23) and (A1.24) may be rewritten upon defining certain terms as follows.

$$\theta^m \equiv -(2 + \alpha_m) \quad (A1.33)$$

$$\theta^{my} \equiv -(2 + \alpha_{my}) \quad (A1.34)$$

$$\phi^m \equiv -V_{i-1,j}^m + (2 - \alpha_m)V_{i,j}^m - V_{i-1,j}^m + \beta_{my}V_{i,j}^{my} + \gamma_m + \gamma_{my} \quad (A1.35)$$

$$\phi^{my} \equiv -V_{i-1,j}^{my} + (2 - \alpha_{my})V_{i,j}^{my} - V_{i-1,j}^{my} + \beta_m V_{i,j}^m + \delta_m + \delta_{my} \quad (A1.36)$$

The ends of the fiber are considered to be sealed, representing an infinite resistance to longitudinal current flow. Thus,

$$\frac{\partial V_{m1}}{\partial z}(0,t) = \frac{\partial V_{m1}}{\partial z}(L,t) = 0 \quad (A1.37)$$

$$\frac{\partial V_{m1}}{\partial z}(0,t) = \frac{\partial V_{m1}}{\partial z}(L,t) = 0 \quad (\text{A1.38})$$

and

$$\frac{\partial V_{my1}}{\partial z}(0,t) = \frac{\partial V_{my1}}{\partial z}(L,t) = 0 \quad (\text{A1.39})$$

$$\frac{\partial V_{my1}}{\partial z}(0,t) = \frac{\partial V_{my1}}{\partial z}(L,t) = 0 \quad (\text{A1.40})$$

where L is the length of the fiber. The boundary conditions may be represented in discrete form as follows.

$$-3V_{0,j+1}^m + 4V_{1,j+1}^m - V_{2,j+1}^m = 0 \quad (\text{A1.41})$$

$$-3V_{N,j+1}^m + 4V_{N-1,j+1}^m - V_{N-2,j+1}^m = 0 \quad (\text{A1.42})$$

and

$$-3V_{0,j+1}^{my} + 4V_{1,j+1}^{my} - V_{2,j+1}^{my} = 0 \quad (\text{A1.43})$$

$$-3V_{N,j+1}^{my} + 4V_{N-1,j+1}^{my} - V_{N-2,j+1}^{my} = 0 \quad (\text{A1.44})$$

Therefore, for a cable with N segments a set of N+1 equations exists for each of the potential differences V_{m1} and V_{my1} , which are of the following form.

$$\underline{A} \underline{X} + \underline{C} * \underline{Y} = \underline{b} \quad (\text{A1.45})$$

where

$$\underline{A} = \begin{bmatrix} -2 & 4+\theta^m & 0 & 0 & 0 & 0 & 0 & 0 \\ 1 & \theta^m & 1 & 0 & 0 & 0 & 0 & 0 \\ 0 & 1 & \theta^m & 1 & 0 & 0 & 0 & 0 \\ \cdot & \cdot & \cdot & \cdot & \cdot & \cdot & \cdot & \cdot \\ \cdot & \cdot & \cdot & \cdot & \cdot & \cdot & \cdot & \cdot \\ \cdot & \cdot & \cdot & \cdot & \cdot & \cdot & \cdot & \cdot \\ 0 & 0 & 0 & 0 & 0 & 1 & \theta^m & 1 \\ 0 & 0 & 0 & 0 & 0 & 0 & 4+\theta^m & -2 \end{bmatrix} \quad (\text{A1.46})$$

$$\underline{X} = \begin{bmatrix} V_{0,j+1}^m \\ V_{1,j+1}^m \\ V_{2,j+1}^m \\ \vdots \\ \vdots \\ V_{N-1,j+1}^m \\ V_{N,j+1}^m \end{bmatrix} \quad (\text{A1.47})$$

$$\underline{Y} = \begin{bmatrix} V_{0,j+1}^{my} \\ V_{1,j+1}^{my} \\ V_{2,j+1}^{my} \\ \vdots \\ \vdots \\ V_{N-1,j+1}^{my} \\ V_{N,j+1}^{my} \end{bmatrix} \quad (\text{A1.48})$$

$$\underline{b} = \begin{bmatrix} \phi_{1,j}^m \\ \phi_{1,j}^m \\ \phi_{2,j}^m \\ \vdots \\ \vdots \\ \vdots \\ \phi_{N-1,j}^m \\ \phi_{N-1,j}^m \end{bmatrix} \quad (\text{A1.49})$$

and the constant C is

$$C = \beta_{my} \quad (\text{A1.50})$$

for the potential difference V_{m1} . The set of equations for the potential difference V_{my1} is of the same form where the θ^m in equation (A1.46) is substituted by θ^{my} , V^m in equation (A1.47) is replaced by V^{my} , V^{my} in equation (A1.48) by V^m and ϕ^{my} takes the place of ϕ^m in (A1.49). For the case of the potential difference V_{my1} the constant C is equal to β_m .

The set of simultaneous equations that arise can be uncoupled as follows. The two sets of equations to be solved simultaneously are

$$\underline{A}_1 \underline{V}^m + \beta_{my} \underline{V}^{my} = \underline{b}_1 \quad (\text{A1.51})$$

and

$$\underline{A}_2 \underline{V}^{my} + \beta_m \underline{V}^m = \underline{b}_2 \quad (A1.52)$$

\underline{V}^{my} can be found in terms of \underline{V}^m from equation (A1.51) as

$$\underline{V}^{my} = \frac{1}{\beta_{my}} \left\{ \underline{b}_1 - \underline{A}_1 \underline{V}^m \right\} \quad (A1.53)$$

Substituting \underline{V}^{my} from (A1.53) into (A1.52) we have

$$\left\{ \beta_{my} \beta_m - \underline{A}_2 \underline{A}_1 \right\} \underline{V}^m = \beta_{my} \underline{b}_2 - \underline{A}_2 \underline{b}_1 \quad (A1.54)$$

The product $\underline{A}_2 \underline{A}_1$ is a diagonally dominant matrix given as :

$$\underline{A}_2 \underline{A}_1 = \begin{bmatrix} 2+\theta^{my} & -8+2\theta^m+\theta^{my}\theta^m & 4+\theta^{my} & 0 & 0 & 0 & 0 \\ -2+\theta^{my} & 5+\theta^m+\theta^{my}\theta^m & \theta^{my}+\theta^m & 1 & 0 & 0 & 0 \\ 1 & \theta^{my}+\theta^m & \theta^{my}\theta^m+2 & \theta^{my}+\theta^m & 1 & 0 & 0 \\ 0 & 1 & \theta^{my}+\theta^m & \theta^{my}\theta^m+2 & \theta^{my}+\theta^m & 1 & 0 \\ \cdot & \cdot & \cdot & \cdot & \cdot & \cdot & \cdot \\ \cdot & \cdot & \cdot & \cdot & \cdot & \cdot & \cdot \\ \cdot & \cdot & \cdot & \cdot & \cdot & \cdot & \cdot \\ 0 & 0 & 1 & \theta^{my}+\theta^m & \theta^{my}\theta^m+2 & \theta^{my}+\theta^m & 1 \\ 0 & 0 & 0 & 1 & \theta^{my}+\theta^m & 5+\theta^m+\theta^{my}\theta^m & -2+\theta^{my} \\ 0 & 0 & 0 & 0 & 4+\theta^{my} & -8+2\theta^m+\theta^{my}\theta^m & 2+\theta^{my} \end{bmatrix} \quad (A1.55)$$

Equation (A1.54) may be rewritten in the form $Ax = b$ as :

$$\underline{A}' \underline{V}^m = \underline{b}' \quad (A1.56)$$

where \underline{A}' is the matrix given by

$$\underline{A}' = \beta_{my} \beta_m - \underline{A}_2 \underline{A}_1 \quad (A1.57)$$

and

$$\underline{b}' = \begin{bmatrix} \beta_{my} \phi_{1,j}^{my} - 2\phi_{1,j}^m - \theta^{my} \phi_{1,j}^m \\ \beta_{my} \phi_{1,j}^{my} - \phi_{1,j}^m - \theta^{my} \phi_{1,j}^m - \phi_{2,j}^m \\ \beta_{my} \phi_{2,j}^{my} - \phi_{1,j}^m - \theta^{my} \phi_{2,j}^m - \phi_{3,j}^m \\ \cdot \\ \cdot \\ \cdot \\ \beta_{my} \phi_{N-1,j}^{my} - \phi_{N-2,j}^m - \theta^{my} \phi_{N-1,j}^m - \phi_{N-1,j}^m \\ \beta_{my} \phi_{N-1,j}^{my} - 2\phi_{N-1,j}^m - \theta^{my} \phi_{N-1,j}^m \end{bmatrix} \quad (A1.58)$$

The matrix equation (A1.57) is no longer a simple one where the coefficient matrix \underline{A}' is a tridiagonal matrix. In fact \underline{A}' is not even a sparse matrix that could be easily inverted using some form of an elimination technique. The $(N+1) \times (N+1)$ coefficient matrix has to be explicitly inverted in order to obtain the required solution of the transmembrane potential across the membrane of the equivalent cell characterizing the myelinated fiber. The resulting mathematical modeling technique is neither rapid nor efficient.

A1.2 A compartmental model for the myelinated fiber

The current i_m that flows across the shunt element $Z_m/\Delta z$ is dependent on voltage, time, and ionic concentrations on either side of the fiber membrane. The compartmental model that is needed to characterize the concentration changes of potassium in the region around the cell membrane must include all the three relevant regions namely, the intracellular region, the cleft space and the extracellular region. The model used is shown in fig. A1.2 where the flows between compartments are donor-controlled flows, depending only on the mass or concentration present in the donor compartment. In this figure V denotes the volume of the compartment in cm^3 , C is the concentration in mg/cm^3 and the terms k_{12} , k_{21} etc. are rate coefficients in cm/msec , such that k_{ij} is the rate coefficient for the flow to compartment i from compartment j . The following mass balance equations may be written for each compartment.

$$V_1 \frac{dC_1}{dt} = k_{12}A_{12}C_2 - k_{21}A_{12}C_1 \quad (\text{A1.59})$$

$$V_2 \frac{dC_2}{dt} = k_{21}A_{12}C_1 - k_{12}A_{12}C_2 - k_{32}A_{23}C_2 + k_{23}A_{23}C_3 \quad (\text{A1.60})$$

$$V_3 \frac{dC_3}{dt} = k_{32}A_{23}C_2 - k_{23}A_{23}C_3 \quad (\text{A1.61})$$

where A_{ij} is the area of the membrane between the two compartments i and j . Equations (A1.59) through (A1.61) may be rewritten in conventional form as :

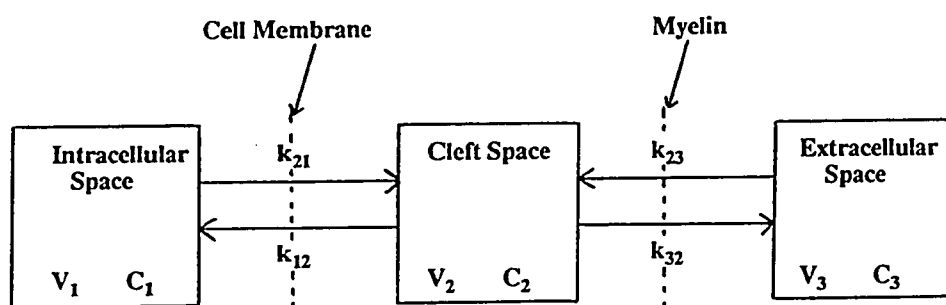


Figure A1.2 A compartmental model to account for potassium ion movement across the membrane and into the cleft space between the cell membrane and the myelin sheath.

$$\frac{dC_1}{dt} = - \left[\frac{k_{21}A_{12}}{V_1} \right] C_1 + \left[\frac{k_{12}A_{12}}{V_1} \right] C_2 \quad (\text{A1.62})$$

$$\frac{dC_2}{dt} = \left[\frac{k_{21}A_{12}}{V_2} \right] C_1 - \left[\frac{k_{12}A_{12} + k_{32}A_{23}}{V_2} \right] C_2 + \left[\frac{k_{23}A_{23}}{V_2} \right] C_3 \quad (\text{A1.63})$$

$$\frac{dC_3}{dt} = \left[\frac{k_{32}A_{23}}{V_3} \right] C_2 - \left[\frac{k_{23}A_{23}}{V_3} \right] C_3 \quad (\text{A1.64})$$

The set of equations (A1.62) through (A1.64) may be rewritten in matrix form upon defining the following terms.

$$\underline{X}(t) = \begin{bmatrix} C_1(t) \\ C_2(t) \\ C_3(t) \end{bmatrix} \quad (\text{A1.65})$$

$$\underline{G} = \begin{bmatrix} -\frac{k_{21}A_{12}}{V_1} & \frac{k_{12}A_{12}}{V_1} & 0 \\ \frac{k_{21}A_{12}}{V_2} & -\frac{k_{12}A_{12} + k_{32}A_{23}}{V_2} & \frac{k_{23}A_{23}}{V_2} \\ 0 & \frac{k_{32}A_{23}}{V_3} & -\frac{k_{23}A_{23}}{V_3} \end{bmatrix} \quad (\text{A1.66})$$

The describing equations of the system are therefore written as

$$\dot{\underline{X}} = \underline{G} \underline{X} \quad (\text{A1.67})$$

which is to be solved for the concentrations in each of the compartments as a function of time, subject to the initial conditions

$$\underline{X}(0) = \begin{bmatrix} C_1(0) \\ C_2(0) \\ C_3(0) \end{bmatrix} \quad (\text{A1.68})$$

where $C_i(0)$ is the initial concentration in the i^{th} compartment.

A1.3 Summary

Since in this study only one action potential is allowed to propagate along the fiber, the simplified model that results in a set of matrix equations that can be solved for rapidly and efficiently is adequate. The neglected potassium channels beneath the myelin sheath may at most cause an error in the propagation velocity of the electrical activity along the myelinated nerve fiber. A thorough investigation is needed of the parameters that characterize the cleft space before the full blown network model can be used in a simulation.

A better source characterization will definitely extend the scope of the present technique but will in no way change the field theory techniques used to compute the extracellular currents and potentials from the myelinated fiber. A better source characterization is also necessary before a study of the effects of different stimulation strengths and patterns can be studied.

APPENDIX II

Source Code of Major Computer Programs

The following is a listing of some of the source code used to simulate the various problems in the thesis.

```

c      The following is a driver program to simulate a propagating
c      action potential using the Frankenhaeuser-Huxley model for
c      the myelinated nerve. Various subroutines are called in
c      the proper succession to calculate the voltages at the nodes
c      along the cable as a function of time and space.
c
c      Subroutines used ::
c          finput :: the subroutine that is used to
c                   input initial values of various
c                   parameters
c          crnknic :: the subroutine that sets up the
c                   partial differential equation
c                   model, solves it and outputs the
c                   results
c
c      Subroutine call formats ::
c          finput :: call finput(par)
c                   where par is the length 36
c                   parameter vector
c          crnknic :: call crnknic(v,par)
c                   where v is the length 190
c                   voltage vector
c                   and par is the length 36
c                   parameter vector
c
c      Input files :: none required
c
c      Output file :: File fort.10 containing the voltage array stored
c                   in the format 5f13.6 as a succession of the
c                   voltages (in millivolts) at all segment nodes
c                   for each time point
c                   File fort.11 containing the ionic current density
c                   stored in the format 5f13.6 as a succession of
c                   the current densities (in microamps per square
c                   centimeter) at all segment nodes for each time
c                   point
c
c      implicit real*8 (a-h,o-z)
c      dimension v(190),par(36)
c
c      call the input subroutine to input the values of the various
c      parameters of the model

```



```

c      call finput(par)
c
c      initialize all the segment voltages to the resting potential
c
c      k=ifix(par(1))+1
c      do 10 i=1,k
10     v(i)=par(4)
c
c      call the subroutine to set up and solve the partial differential
c      equation model and output the results
c
c      call crknkc(v,par)
c
c      the end of the program
c
c      stop
c      end

```

```

c      The following is the subroutine to input various parameter
c      values to the simulation of a propagating action potential
c      in a myelinated nerve
c

```

```

c      Subroutines used :: none
c

```

```

c      Input files :: none required
c

```

```

c      Output files :: none required
c

```

```

c      Calling format of the present subroutine ::
c

```

```

c      finput :: call finput(par)
c      where par is the length 36
c      parameter vector
c

```

```

c      NOTE :: ALL VOLTAGES ARE NORMALIZED WITH RESPECT TO THE RESTING
c      POTENTIAL i.e. RESTING POTENTIAL IS TAKEN TO BE 0. mV
c

```

```

c      Parameters in the program ::
c

```

```

c      par(1) : Number of segments in the cable
c      par(2) : Number of time points used
c      par(3) : Number of myelinated nodes between
c              two active nodes
c      par(4) : Membrane resting potential in
c              microvolts
c      par(5) : Stimulus current strength in microamps
c      par(6) : Stimulus starting time in millisecs
c      par(7) : Stimulus ending time in millisecs
c      par(8) : Node that is to be stimulated
c      par(9) : Step size in time (dt) in millisecs
c      par(10): Step size in space (dx) in centimeters
c      par(11): Node specific capacitance (cm) in
c              millifarads per square centimeter
c      par(12): Outside sodium concentration in

```



```

c          millimoles per litre
c      par(13): Outside potassium concentration in
c          millimoles per litre
c      par(14): Inside sodium concentration in
c          millimoles per litre
c      par(15): Inside potassium concentration in
c          millimoles per litre
c      par(16): Leak potential in millivolts
c      par(17): Leak conductance in millimhos per
c          square centimeter
c      par(18): Sodium permeability constant in
c          centimeters per second
c      par(19): Potassium permeability constant in
c          centimeters per second
c      par(20): Non-specific permeability constant in
c          centimeters per second
c      par(21): Axon radius (a) in centimeters
c      par(22): Myelin sheath thickness (at) in
c          centimeters
c      par(23): Specific resistance of axoplasm i.e.
c          inside cell (Ri) in ohms cm
c      par(24): Specific resistance outside cell
c          (Ro) in ohms centimeter
c      par(25): Myelin specific capacitance (cmy) in
c          millifarads per square cm
c      par(26): Myelin specific conductance (gmy) in
c          millimhos per square centimeter
c      par(27): Node length (nl) in centimeters
c      par(28): Number n2 given as n**2, where the
c          extent of the volume outside the
c          cell is a cylinder of radius n*a
c      par(29): A constant C given as equal to
c           $2*((n2-1)*Ri+Ro)*(dx**2)/((n2-1)*a)$ 
c      par(30): A constant C1 given as equal to
c           $C*(a+at)/a$ 
c      par(31): A constant alpha given as equal to
c           $2*(cm*C*nl+cmy*(dx-nl)*C1)/(dt*dx)$ 
c      par(32): A constant alpha1 given as equal to
c           $2*(cmy/dt)*C1$ 
c      par(33): A constant theta given as equal to
c           $-(2.+alpha)$ 
c      par(34): A constant theta1 given as equal to
c           $-(2.+alpha1)$ 
c      par(35): A number that scales the myelin
c          capacitance and conductance when
c          the myelin thickness is changed
c          by p% and is given as equal to
c           $\ln\{(a+at)/a\}/\ln\{(a+p*at)/a\}$ 
c      par(36): An integer set to 1 if an abnormal
c          central node is desired but is
c          set to 0 otherwise

```

```

subroutine finput(par)

```



```

implicit real*8 (a-h,o-z)
dimension par(36)

c
c      specify the values of the various parameters
c
par(1)=189.
par(2)=800.
par(3)=10.
par(4)=0.0
par(5)=.075
par(6)=0.01
par(7)=0.02
par(8)=189.
par(9)=0.005
par(10)=0.02
par(11)=0.002
par(12)=114.5
par(13)=2.5
par(14)=13.74
par(15)=120.
par(16)=0.026
par(17)=30.3
par(18)=0.008
par(19)=0.0012
par(20)=0.00054
par(21)=0.0005
par(22)=0.0002
par(23)=100.
par(24)=70.
par(25)=0.00000387
par(26)=0.000083308
par(27)=0.0004
par(28)=900.
par(29)=2.0*(((par(28)-1)*par(23))+par(24))*(par(10)**2)
par(29)=par(29)/((par(28)-1)*par(21))
par(30)=par(29)*(par(21)+par(22))/par(21)
par(31)=par(25)*(par(10)-par(27))
par(31)=(par(31)*par(30))+((par(11)*par(27)*par(29)))
par(31)=2.0*par(31)/(par(9)*par(10))
par(32)=2.0*(par(25)/par(9))*par(30)
par(33)=-(2.0+par(31))
par(34)=-(2.0+par(32))
par(35)=dlog((par(21)+par(22))/par(21))
par(35)=par(35)/dlog((par(21)+(0.008*par(22)))/par(21))
par(36)=0
return
end

```

```

c      The following is the subroutine that sets up and solves the
c      partial differential equation model for the simulation of the
c      propagating action potential. It also outputs the solution of
c      the partial differential equation.
c

```



```

c      Subroutines used ::
c
c          fmmodel :: the subroutine that is used to solve
c                      for the membrane model
c          bandmat :: the subroutine that solves the set
c                      of equations of the form  $Ax=b$ 
c                      where A is a tri-diagonal matrix
c
c      Subroutine call formats ::
c          fmmodel :: call fmmodel(v,par,xm,xh,xn,,xp,curden,mode)
c                      where v is the length 190 voltage vector
c                      par is the length 36 parameter vector
c                      xm is the length 20 vector containing
c                          the sodium activation variable
c                          m, for each active node
c                      xh is the length 20 vector containing
c                          the sodium inactivation variable
c                          h, for each active node
c                      xn is the length 20 vector containing
c                          the potassium activation
c                          variable n, for each active node
c                      xp is the length 20 vector containing
c                          the gating variable p for each
c                          active node
c                      curden is the length 190 vector that
c                          has the values of the voltage
c                          due to the ionic current density
c                          at each node
c                      and mode is the value of the time point at
c                          which the evaluation is being
c                          done
c          bandmat :: call bandmat(v,par,phi,mode)
c                      where v is the length 190 voltage vector
c                      par is the length 36 parameter vector
c                      phi is the right hand side of the set
c                          of equations  $Ax=b$ 
c                      and mode is the value of the time point at
c                          which the evaluation is being
c                          done
c
c      Input files :: none required
c
c      Output file :: File fort.10 containing the voltage array stored
c                      in the format 5f13.6 as a succession of the
c                      voltages (in millivolts) at all segment nodes
c                      for each time point
c
c      Calling format of the present subroutine ::
c          crnknic :: call crnknic(v,par)
c                      where v is the length 190
c                          voltage vector
c                      and par is the length 36
c                          parameter vector
c
c

```



```

c      subroutine crnknic(v,par)
c      implicit real*8 (a-h,o-z)
c      dimension v(190),par(36),xm(20),xh(20),xn(20),xp(20)
c      dimension curden(190),phi(190)
c
c      initialize loop variables
c
c      pi=3.141592653589793
c      t=0.
c      k=par(1)
c      l=par(2)
c
c      begin set up and solution of the partial differential equations
c
c      do 30 j=1,l
c          t=t+par(9)
c          mode=j
c          call fmmodel(v,par,xm,xh,xn,xp,curden,mode)
c
c      specify the location of the first active node
c
c      inode=9
c
c      set up the partial differential equations
c
c          do 10 i=2,k
c              xstim=par(5)
c              if(t.lt.par(6)) xstim=0.0
c              if(t.gt.par(7)) xstim=0.0
c              if(i.ne.par(8)) xstim=0.0
c              g1=xstim/(4.0*pi*par(21)*par(10))
c              if(i.ne.inode) go to 2
c              gamma=2.0*(curden(i)-(par(29)*g1))
c
c      check to see if an abnormal central node is desired, if so
c      simulate paranodal demyelination at that node
c
c          if(par(36).eq.1.and.inode.eq.99) go to 11
c          phi(i)=-v(i-1)+(2.0-par(31))*v(i)-v(i+1)+gamma
c          go to 111
11      alpha=par(11)*par(29)*8.d0*par(27)
c          alpha=alpha+par(25)*par(30)*(par(10)-(8.d0*par(27)))
c          alpha=2.d0*alpha/(par(10)*par(9))
c          phi(i)=-v(i-1)+(2.0-alpha)*v(i)-v(i+1)+gamma
111      inode=inode+ifix(par(3))
c          go to 10
2      gamma=2.0*(curden(i)-(par(30)*g1))
c          phi(i)=-v(i-1)+(2.0-par(32))*v(i)-v(i+1)+gamma
10      continue
c
c      divide the voltage by 1000 to put it in units of millivolts
c
c      do 20 i=1,k+1

```



```

20      v(i)=v(i)/1000.d0
c      continue
c
c      write the voltage to the output file
c
c      write(10,1) (v(i),i=1,k+1)
1      format(5f13.6)
c
c      solve the set of partial differential equations to evaluate
c      the voltage at the next time point, except when the last time
c      point is being evaluated
c
c      if(mode.eq.1) go to 30
c      call bandmat(v,par,phi,mode)
30     continue
c     return
c     end

c      The following is a subroutine that solves the membrane model
c      for the myelinated nerve. The model used is the Frankenhaeuser
c      and Huxley model for myelinated nerve.
c
c      Subroutines used ::
c          fgvar :: the subroutine that evaluates the rate
c                  constants associated with the
c                  gating variables of the membrane
c                  model
c
c      Subroutine call formats ::
c          fgvar :: call fgvar(vm,xinf,tinf)
c                  where vm is the membrane voltage at which the
c                        gating variables are to be found
c                  xinf is a length 4 vector that contains
c                        the infinity values of m, h, n,
c                        and p, respectively
c                  and tinf is a length 4 vector that contains
c                        the time constants of the gating
c                        variables
c
c      Input files :: none required
c
c      Output file :: File fort.11 containing the ionic current density
c                  stored in the format 5f13.6 as a succession of
c                  the current densities (in microamps per square
c                  centimeter) at all segment nodes for each time
c                  point
c
c      Calling format of the present subroutine ::
c          fmmodel :: call fmmodel(v,par,xm,xh,xn,xc,curden,mode)
c                  where v is the length 190 voltage vector
c                  par is the length 36 parameter vector
c                  xm is the length 20 vector containing
c                  the sodium activation variable

```



```

c          m, for each active node
c          xh is the length 20 vector containing
c          the sodium inactivation variable
c          h, for each active node
c          xn is the length 20 vector containing
c          the potassium activation
c          variable n, for each active node
c          xp is the length 20 vector containing
c          the gating variable p, for each
c          active node
c          curden is the length 190 vector that
c          has the values of the voltage
c          due to the ionic current density
c          at each node
c          and mode is the value of the time point at
c          which the evaluation is being
c          done
c
c          subroutine fmmodel(v,par,xm,xh,xn,xp,curden,mode)
c          implicit real*8 (a-h,o-z)
c          dimension v(190),par(36),xm(20),xh(20),xn(20),xp(20)
c          dimension curden(190),xinf(4),tinf(4)
c
c          initialize loop variables
c
c          k=par(1)+1
c
c          specify physical constants to be used in the program i.e. R,
c          the universal gas constant in Joules per mole degree Kelvin, and
c          F, Faraday's constant in Coulombs per gram equivalent; the
c          temperature, Te is in degree Kelvin (nominal value of which is
c          293 deg K or 20 deg C)
c
c          F=96487.
c          R=8.31
c          Te=273.0+20.0
c          frt=F/(R*Te)
c          f2rt=(F**2)/(R*Te)
c
c          check to see if routine is called for the first time, if so
c          initialize everything to the resting values, otherwise do not
c          initialize
c
c          if(mode.ne.1) go to 11
c          vm=par(4)/1000.
c          call fgvar(vm,xinf,tinf)
c          do 10 i=1,20
c             xm(i)=xinf(1)
c             xh(i)=xinf(2)
c             xn(i)=xinf(3)
c             xp(i)=xinf(4)
10      continue
c

```



```

c      evaluate the gating variables by integrating their differential
c      equations using Rush-Larsen approximations and evaluate the
c      current density at each node whether it be an active node or
c      a passive node due to the myelin sheath, after specifying the
c      location of the first active node
c
11      inode=9
      ig=0
      do 20 i=1,k

c
c      check to see if the node is active or not, if the node is
c      passive then evaluate the constant current density, otherwise
c      solve the membrane model to evaluate the current density and the
c      voltage due to it (the current density is calculated after
c      correcting the various permeability constants for the nodal area
c      being used i.e. the constants get multiplied by nl/dx where nl
c      is the node length and dx is the segment length)
c
      vm=v(i)/1000.
      if(i.ne.inode) go to 12
      call fgvar(vm,xinf,tinf)
      ig=ig+1
      xm(ig)=xinf(1)-(xinf(1)-xm(ig))*exp(-par(9)/tinf(1))
      xh(ig)=xinf(2)-(xinf(2)-xh(ig))*exp(-par(9)/tinf(2))
      xn(ig)=xinf(3)-(xinf(3)-xn(ig))*exp(-par(9)/tinf(3))
      xp(ig)=xinf(4)-(xinf(4)-xp(ig))*exp(-par(9)/tinf(4))

c
c      evaluate the various currents using the absolute membrane
c      voltage, e, (in volts) and vm, the membrane voltage normalized
c      with respect to the resting potential
c
      e=(vm-70.0)/1000.
      expo=exp(e*frt)
      denom=1.-expo
      prod=e*f2rt
      pna=par(18)*(par(27)/par(10))*(xm(ig)**2)*xh(ig)
      pk=par(19)*(par(27)/par(10))*(xn(ig)**2)
      pp=par(20)*(par(27)/par(10))*(xp(ig)**2)
      cna=(pna*prod*(par(12)-(par(14)*expo)))/denom
      ck=(pk*prod*(par(13)-(par(15)*expo)))/denom
      cp=(pp*prod*(par(12)-(par(14)*expo)))/denom
      cl=par(17)*(par(27)/par(10))*(vm-par(16))
      cmy=(par(26)*(par(10)-par(27))/par(10))*vm

c
c      check to see if an abnormal central node is desired, if so
c      simulate paranodal demyelination at that node
c
      if(par(36).eq.1.and.inode.eq.99) go to 15
      go to 16
15      ck=8.d0*ck
      cp=8.d0*cp
      cmy=cmy*(par(10)-(8.d0*par(27)))/(par(10)-par(27))
16      curden(i)=(par(29)*(cna+ck+cp+c1))+(par(30)*cmy)
      inode=inode+ifix(par(3))

```



```

c
c      store the value of the ionic current density at each node in the
c      appropriate output file
c
c          curtot=cna+ck+cp+cl+cmy
c          write(11,*) curtot
c          go to 20
c
c      evaluate constant current density for the passive node and the
c      voltage due to it
c
c      12          curden(i)=par(30)*par(26)*vm
c
c      store the value of the ionic current density at each node in the
c      appropriate output file
c
c          curtot=curden(i)/par(30)
c          write(11,*) curtot
20      continue
      return
      end

c      The following is the subroutine that evaluates the rate
c      constants of the various gating variables associated with the
c      Frankenhaeuser-Huxley myelinated nerve model
c
c      Subroutines used :: none
c
c      Input files :: none required
c
c      Output files :: none required
c
c      Calling format of the present subroutine ::
c          fgvar :: call fgvar(vm,xinf,tinf)
c                  where vm is the membrane voltage at which the
c                        gating variables are to be found
c                  xinf is a length 4 vector that contains
c                        the infinity values of m, h, n,
c                        and p, respectively
c                  and   tinf is a length 4 vector that contains
c                        the time constants of the gating
c                        variables
c
c
c      subroutine fgvar(vm,xinf,tinf)
c      implicit real*8 (a-h,o-z)
c      dimension xinf(4),tinf(4)
c
c      rate equations for the model
c
c      am=(.36*(22.-vm))/(exp((22.-vm)/3.)-1.)
c      bm=(.4*(13.-vm))/(1.-exp((vm-13.)/20.))

```



```

ah=(.1*(-10.-vm))/(1.-exp((vm+10.)/6.))
bh=4.5/(exp((45.-vm)/10.)+1.)
an=(.02*(35.-vm))/(exp((35.-vm)/10.)-1.)
bn=(0.05*(10.-vm))/(1.-exp((vm-10.)/10.))
ap=(0.006*(40.-vm))/(exp((40.-vm)/10.)-1.)
bp=(0.09*(-25.-vm))/(1.-exp((vm+25.)/20.))
tinf(1)=1.0/(am+bm)
tinf(2)=1.0/(ah+bh)
tinf(3)=1.0/(an+bn)
tinf(4)=1.0/(ap+bp)
xinf(1)=am*tinf(1)
xinf(2)=ah*tinf(2)
xinf(3)=an*tinf(3)
xinf(4)=ap*tinf(4)
return
end

```

c The following is the subroutine that solves a set of equations
c of the form $Ax=b$ when A is a tri-diagonal matrix. The method
c used is backward substitution

c
c Subroutines used :: none

c Input files :: none required

c Output files :: none required

c Calling format of the present subroutine ::

c bandmat :: call bandmat(v,par,phi,mode)
c where v is the length 190 voltage vector
c par is the length 36 parameter vector
c phi is the right hand side of the set
c of equations $Ax=b$
c and mode is the value of the time point at
c which the evaluation is being
c done

c
c subroutine bandmat(v,par,phi,mode)
c implicit real*8 (a-h,o-z)
c dimension v(190),par(36),phi(190),c(190),d(190)

c initialize loop variables

c k=par(1)
c j=mode

c the value of theta for the node with paranodal demyelination

c
c alpha=par(11)*par(29)*8.d0*par(27)
c alpha=alpha+par(25)*par(30)*(par(10)-(8.d0*par(27)))
c alpha=2.d0*alpha/(par(10)*par(9))


```

      theta=-(2.d0+alpha)
c
c      evaluate the constants c and d
c
      c(1)=(4.0+par(33))/(-2.0)
      d(1)=phi(2)/(-2.0)
c
c      specify the location of the first active node
c
      inode=9
      do 10 i=2,k
c
c      check to see if the node being evaluated is active, passive or
c      abnormal and use the appropriate value of the constants
c
          if(i.ne.inode) b=par(34)
          if(i.eq.inode) b=par(33)
          if(i.eq.inode.and.inode.eq.99.and.par(36).eq.1) b=theta
          if(i.eq.inode) inode=inode+ifix(par(3))
          c(i)=1.0/(b-c(i-1))
          d(i)=(phi(i)-d(i-1))/(b-c(i-1))
10      continue
      c(k+1)=0.0
c
c      use the correct value of the constant for passive or active
c      node
c
      if((k+1).eq.inode) b=par(33)
      if((k+1).ne.inode) b=par(34)
      d(k+1)=(phi(k)-(4.0+b)*d(k))/(-2.0-c(k)*(4.0+b))
c
c      evaluate the voltages at the various nodes at the next time
c      point
c
      v(k+1)=d(k+1)
      do 20 ii=1,k
          kk=k+1-ii
          v(kk)=d(kk)-c(kk)*v(kk+1)
20      continue
      return
      end

c      This is the program to calculate the field potentials.
c      The model is a eccentric one with one boundary.
c
c      Subroutines used ::
c          ibessel :: the subroutine that returns the I
c                      besel functions of all orders needed
c                      and their derivatives
c          kbessel :: the subroutine that returns the K
c                      besel functions of all orders needed
c                      and their derivatives
c          dfft2d :: the two dimensional Fast Fourier

```



```

c                                     Transform routine
c
c
c      Subroutine call formats ::
c          ibessel :: call ibessel(arg,x,n,array,m1,m2,rlt)
c                      where arg is the argument of the
c                          bessel function
c                      x is the parameter in arg
c                          with respect to which
c                          the first and second
c                          derivatives are found
c                      n is the maximum order of
c                          bessel function needed
c                      array is the array into
c                          which the bessel
c                          functions and their
c                          derivatives are returned
c                      m1 is the first dimension
c                          of array
c                      m2 is the second dimension
c                          of array
c                      and rlt is the array column for
c                          I function insertion
c      kbessel :: same format as ibessel and similar
c                  routine parameters
c      dfft2d :: call dfft2d(array,x,y,i,m1,j,m2,id,iw)
c                  where array is the complex array
c                      in which the input is
c                      passed to the routine
c                      and the output returned
c                      from the routine
c                      x and y are work space
c                      real vectors, dimension
c                      i or j which ever is
c                      larger
c                      i is the first dimension
c                          of the complex array
c                      m1 is the power to which 2
c                          must be raised to get i
c                      j is the second dimension
c                          of the complex array
c                      m2 is the power to which 2
c                          must be raised to get j
c                      id is a positive integer
c                          if a forward fft is
c                          desired and negative
c                          otherwise
c                      and iw is the dimension of the
c                          work vectors x and y
c
c
c
c

```

```

implicit real*8 (a-h,p-z)
implicit complex*16 (o)
dimension ohw(32,256),x(4100),y(4100),alri(19,3),alrk(19,3)
dimension fx(2050),ohws(32,256),alak(1,3),albi(19,3),albk(19,3)

```



```

dimension rk(19,3),bk(19,3),alrsk(19,3),alrsi(19,3)
pi=3.141592653589793
c
c      input the various electrical and geometrical parameters of the model
c
      read(5,12) npts,nstage,mpts,mstage
      read(5,10) ra,delz,delt,rr,rb
      read(5,10) rs,anise,anisr,sigoz,sige
      read(5,10) sigsh,csh,delr
10      format(5f13.6)
12      format(4i6)
c
c      compute various multiples of the input integers
c
      nh=npts/2
      nhp1=nh+1
      n4p1=4*npts+1
      n8=8*npts
      n8p2=n8+2
      np2=npts+2
      np1=npts+1
      n2=2*npts
      n2p2=n2+2
      nm1=npts-1
      nm40=npts-40
      np40=npts+40
      mh=mpts/2
      mhp1=mh+1
      mhp2=mh+2
      mp1=mpts+1
      mp2=mpts+2
      m2=2*mpts
      m2p1=m2+1
      m2p2=m2+2
c
c      calculate the anisotropy ratios and other constants
c
      alam=dsqrt(anisr)
      sigo=sigoz/anisr
      vel=delz/delt
      zt=delz*float(npts)
      zt8=8.d0*zt
      tpi=2.d0*pi
      cshv=csh*vel
c
c      read in the input source potential
c
      read(5,10) (fx(i),i=1,n2)
c
c      remove dc component from source potential
c
      avem=0.d0
      l=1
      do 121 i=nm40,npts

```



```

                avem=avem+fx(i)
                if(l.gt.npts) go to 122
121      l=l+1
122      avem=avem/float(l)
          do 125 i=1,n2
125      x(i)=fx(i)
          xm=0.d0
          do 130 i=1,n2
130      xm=xm+x(i)
          xm=xm/dfloat(n2)
          do 135 i=1,n2
135      x(i)=x(i)-xm
          do 150 i=1,n2
150      y(i)=0.d0
c
c      calculate the Fourier transform of the source potential
c
          do 160 i=1,n2
160      ohws(1,i)=dcmplx(x(i),y(i))
          call dfft2d(ohws,x,y,32,5,256,8,1,256)
c
c      find fir filter for medium potential filter
c
          do 275 i=2,np1
              arg=pi*dfloat(i-1)/(zt*2.d0)
              rarg=arg*rr
              call kbessel(rarg,rr,mp2,rk,19,3,1)
              alrarg=alam*arg*rr
              call ibessel(alrarg,rr,mp2,alri,19,3,1)
              call kbessel(alrarg,rr,mp2,alrk,19,3,1)
              alrsarg=alam*arg*rs
              call ibessel(alrsarg,rs,mp2,alrsi,19,3,1)
              call kbessel(alrsarg,rs,mp2,alrsk,19,3,1)
              alaarg=alam*arg*ra
              call kbessel(alaarg,ra,0,alak,1,3,1)
              barg=arg*rb
              call kbessel(barg,rb,mp2,bk,19,3,1)
              albarg=alam*arg*rb
              call ibessel(albarg,rb,mp2,albi,19,3,1)
              call kbessel(albarg,rb,mp2,albk,19,3,1)
              cter=-cshv*arg
              osig=dcmplx(sigsh,cter)
c
c      form complex filter function for all values of theta for each k
c
          do 250 j=1,mp1
              ad1=sige*sigo*bk(j,2)*albi(j,2)
              oad2=sigo*osig*bk(j,1)*albi(j,2)
              oad3=sige*osig*bk(j,2)*albi(j,1)
              adxp=bk(j,3)+albi(j,3)
              oad=ad1-oad2+oad3
              if(rr.ge.rb) go to 222
c
c      form the filter function inside the volume conductor medium

```



```

c
    at1=sige*sigo*bk(j,2)*alrsi(j,1)*albk(j,2)*alri(j,1)
    oat2=sigo*osig*bk(j,1)*alrsi(j,1)*albk(j,2)*alri(j,1)
    oat3=sige*osig*bk(j,2)*alrsi(j,1)*albk(j,1)*alri(j,1)
    atxp=bk(j,3)+alrsi(j,3)+albk(j,3)+alri(j,3)
    oat=-at1+oat2-oat3
    ow1=oat/oat3
    w1xp=atxp-adxp
    w3=alak(1,1)
    w3xp=-alak(1,3)

c
c    filter function when field radius is less than source radius
c
    if(rr.ge.rs) go to 1111
    w2=alrsk(j,1)*alri(j,1)
    w2xp=alrsk(j,3)+alri(j,3)
    go to 1222

c
c    filter function when field radius is greater than source radius
c
c
1111    w2=alrk(j,1)*alrsi(j,1)
        w2xp=alrk(j,3)+alrsi(j,3)
1222    if(w1xp.gt.w2xp) wxp=w1xp
        if(w2xp.gt.w1xp) wxp=w2xp
        ohw(j,i)=(ow1*dexp(w1xp-wxp))+(w2*dexp(w2xp-wxp))
        ohw(j,i)=(ohw(j,i)/w3)*dexp(wxp+w3xp)
        go to 250

c
c    form filter function outside the volume conductor medium
c
c
222    bt1=albk(j,2)*albi(j,1)
        bt2=albk(j,1)*albi(j,2)
        btxp=albk(j,3)+albi(j,3)
        bt=bt1-bt2
        ow1=sigo*osig*bt*alrsi(j,1)*rk(j,1)/(oat*alak(1,1))
        w1xp=alrsi(j,3)+rk(j,3)+btxp-adxp-alak(1,3)
        ohw(j,i)=ow1*dexp(w1xp)

250    continue
275    continue
c
c    form the product of Fso and the filter function
c
    do 300 i=1,np1
    do 300 j=1,mp1
300    ohw(j,i)=ohw(j,i)*ohws(j,i)
c
c    fill in the filter function array
c
    do 350 j=1,mp1
    do 350 i=2,npts
350    ohw(j,n2p2-i)=dconjg(ohw(j,i))
    do 375 j=2,mpts
    do 375 i=1,n2
375    ohw(m2p2-j,i)=ohw(j,i)

```



```

c
c      find the best estimate of the field potential
c
c      call dfft2d(ohw,x,y,32,5,256,8,-1,256)
c
c      print output
c
c      do 450 j=1,m2
c          do 400 i=1,n2
400      x(i)=1000.d0*dreal(ohw(j,i))
c          write(6,10) (x(i),i=1,n2)
450      continue
1000     stop
c      end

```

```

c .....
c
c      Subroutine IBESSEL
c
c      Purpose
c      To compute the modified bessel functions i and their first
c      derivatives for orders 0 to n and arguments > 0
c
c      Usage
c      call ibessel(arg,x,n,array,m1,m2,rlt)
c
c      Description of Parameters
c      arg - argument of the bessel functions i which is assumed
c            to be in the form arg = alpha*x, REAL*8 (input)
c      x    - parameter in ARG with respect to which the first and
c            second derivatives are to be found, such that
c            arg = alpha*x. If x=arg, derivatives are with
c            respect to the argument itself. REAL*8 (input)
c      n    - maximum order of bessel functions i INTEGER (input)
c      array - array into which bessel functions and derivatives
c            are to be inserted. This array is REAL*8 dim(m1,m2)
c            and insertion is down columns for increasing orders
c            of bessel function. The mantissa of I(p,arg) is in
c            ARRAY(p+1,rlt); of I'(p,arg) in ARRAY(p+1,rlt+1);
c            and the exponent in ARRAY(p+1,rlt+2) such that the
c            bessel function value is MANTISSA*exp(EXPONENT).
c      m1    - 1st dimension (# rows) of ARRAY, >= n+1. INTEGER
c      m2    - 2nd dimension (# cols) of ARRAY, >= 3. INTEGER
c      rlt    - ARRAY column for I function insertion. INTEGER.
c
c      Modifications
c      The basis of this routine was obtained from the IBM SSP
c      package programs I0 and INUE. These routines were combined
c      and extensively modified by O.B. Wilson, Rice University,
c      1985 to enhance readability and to extend the range of
c      argument which can be used. This extension is by means of
c      the "mantissa-exponent" notation, whereby the actual value
c      of any bessel function evaluation is expressed as a mantissa

```



```

c      plus exponent. Use of this notation removes all practical
c      restrictions on the argument range.
c
c      Subroutines Required
c      None.
c
c      Method
c      Values of the bessel functions are obtained by a
c      backward recurrence relation. Starting with the highest
c      order required, the ratio  $i(n+1,arg)/i(n,arg)$  is obtained
c      from a continued fraction. The zeroth order terms is then
c      found explicitly. (Forward recursion fails because the
c      I functions are an increasing family and the error term
c      would grow without bound. Consequently, a backward
c      relationship is used to obtain the relationship between the
c      different function orders; then multiplication by  $i_0$  gives
c      actual function values.) For reference see
c      G. Blanch, "Numerical Evaluation of Continued Fractions,"
c      SIAM Review, Vol. 6, no.4, 1964 383-421.
c      Evaluation of first and second derivatives of orders 0
c      through n is obtained by means of the formulae:
c       $I'(n,z) = I(n-1,z) - nI(n,z)/z$ 
c       $I''(n,z) = I'(n-1,z) - nI'(n,z)/z + nI(n,z)/z^2$ 
c      These formulae may be derived from the general derivative
c      expression for Bessel functions. See eg.
c      Abramowitz & Stegun, "Handbook of Math. Functions," Dover
c      Press. The I" values are not computed or output, but the
c      arithmetic is correctly implemented in commented-out lines.
c
c      Error handling:
c      The following conditions lead to a diagnostic and halt
c      execution. No other conditions are tested for.
c      n < 0      (Function order may not be negative)
c      arg <= 0   (Argument may not be 0 or negative)
c      x <= 0     (Parameter may not be 0 or negative)
c      m1 < n+1   (Col. length of array may not be < n+1)
c      m2 < rlt+2 (Row length may not be < RLT+2 )
c
c      .....
c
c      subroutine ibessel(arg,x,n,array,m1,m2,rlt)
c
c      integer n,m1,m2,rlt
c      implicit real*8 (a-h)
c      implicit real*8 (o-z)
c      dimension array(m1,m2)
c
c      test for invalid input parameters--automatic program abort in
c      case of errors. No argument range testing is performed.
c      if (n) 10,20,20
c      10  write(6,*) "I Bessel function order ",n," should be positive"
c          write(6,*) "Program aborted by routine IBESSEL"
c          stop
c      20  if (arg) 30,30,40

```



```

30  write(6,*) "I Bessel argument ",arg," should be positive"
    write(6,*) "Program aborted by routine IBESSEL"
    stop
40  if (x) 50,50,60
50  write(6,*) "I Bessel parameter ",x," should be positive"
    write(6,*) "Program aborted by routine IBESSEL"
    stop
60  if (m1 - (n+1)) 70,80,80
70  write(6,*) "Array too small for ",n," Bessel function orders"
    write(6,*) "Program aborted by routine IBESSEL"
    stop
80  if (m2 - (n+2)) 90,99,99
90  write(6,*) "Not enough columns in Array, dimension",m2
    write(6,*) "Program aborted by routine IBESSEL"
    stop

c  evaluate zeroth order function mantissa ri0, exponent xi0, used
c  in determining all other orders
99  xi0 = 0.0
    if (arg - 3.75) 100,100,200
100 z = arg*arg*7.11111e-2
    ri0 = (((((4.5813e-3*z + 3.60768e-2)*z + 2.659732e-1)*z
1    + 1.206749e0)*z + 3.089942e0)*z + 3.515623e0)*z + 1.0
    go to 1

200 z = 3.75/arg
    xi0 = arg
    ri0 = 1.0/dsqrt(arg)*(((((((3.92377e-3*z - 1.647633e-2)*z
1    + 2.635537e-2)*z - 2.057706e-2)*z + 9.16281e-3)*z
2    - 1.57565e-3)*z + 2.25319e-3)*z + 1.328592e-2)*z
3    + 3.989423e-1)

c  select either small or large argument approximation regime for
c  determining backward ratios of functions starting at nth order
1  fn = 2.0*dfloat(n)
    q1 = arg/fn
    if (arg - 5.0e-4) 6,6,2

2  a0 = 1.0
    a1 = 0.0
    b0 = 0.0
    b1 = 1.0
    fi = fn
3  fi = fi + 2.0
    an = fi/arg
    a = an*a1 + a0
    b = an*b1 + b0
    a0 = a1
    b0 = b1
    a1 = a
    b1 = b
    q0 = q1
    q1 = a/b
    if (dabs((q1-q0)/q1) - 1.0e-6) 6,6,3

```



```

c Ratios of  $I(k, \arg)/I(k-1, \arg)$  are placed in ARRAY(k,RLT),  $k > 0$ 
c If n orders of I are required, n ratios must be found
6 k = n
7 q1 = arg/(fn+arg*q1)
  array(k+1,rlt) = q1
  fn = fn - 2.0
  k = k - 1
  if (k) 8,8,7

c forward substitution of zero function into series relationship
c to obtain correct function values for all orders through n.
c commented line calculates 2nd derivative, zeroth order.
8 const = arg/x
  array(1,rlt) = ri0
  array(1,rlt+2) = xi0
  array(1,rlt+1) = const*ri0*array(2,rlt)
c array(1,**) = const*const*ri0*(1 - array(2,rlt)/arg)
  if (n .eq. 0) return

c last two commented statements calculate 2nd derivative, ith order
do 9 i=1,n
  fli = dfloat(i)
  fi = array(i,rlt)*array(i+1,rlt)
  temp = dlog(fi)
  array(i+1,rlt) = 1.0
  array(i+1,rlt+2) = array(i,rlt+2) + temp
  array(i+1,rlt+1) = const*( array(i,rlt)*dexp(-temp) - fli/arg )
c array(i+1,**) = const*( array(i,rlt+1)*dexp(-temp)
c z - fli*array(i+1,rlt+1)/arg + fli*const/(arg*arg) )
9 continue

  return
end

c .....
c
c Subroutine KBESSEL
c
c Purpose
c To compute the modified bessel functions K and their first
c derivatives for orders 0 to n and arguments > 0
c
c Usage
c call kbessel(arg,x,n,array,m1,m2,rlt)
c
c Description of Parameters
c arg - argument of the bessel functions k which is assumed
c to be in the form  $\arg = \alpha * x$ . REAL*8 (input)
c x - parameter in ARG with respect to which the first and
c second derivatives are to be found, such that
c  $\arg = \alpha * x$ . If  $x = \arg$ , derivatives are with
c respect to the argument itself. REAL*8 (input)

```


c n - maximum order of bessell functions k. INTEGER (input)
 c array - array into which bessell functions and derivatives
 c are to be inserted.
 c Insertion is down columns for increasing orders
 c of bessell function. The mantissa of K(p,arg) is in
 c ARRAY(p+1,rlt); of K'(p,arg) in ARRAY(p+1,rlt+1);
 c A common exponent of K,K' such that the value of the
 c bessell function is MANTISSA*exp(EXPONENT) is in
 c ARRAY(p+1,rlt+2). dim(m1,m2). REAL*8
 c m1 - 1st dimension (# rows) of ARRAY, >= n+1. INTEGER.
 c m2 - 2nd dimension (# cols) of ARRAY, >= 3. INTEGER.
 c rlt - ARRAY column for insertion of K functions. INTEGER.

Modifications

c The basis of this routine was obtained from the IBM SSP
 c package program BESK. This routine was extensively
 c modified by O.B. Wilson, Rice University, 1985, to enhance
 c readability and to extend the range of argument which can
 c be used. This extension is by means of the "mantissa-
 c exponent" notation, whereby the actual value of any bessell
 c function evaluation is expressed as a mantissa plus
 c exponent. Use of this notation removes all practical
 c restrictions on the argument range.

Subroutines Required

c None.

Method

c Values of the bessell function are obtained by a forward
 c series relationship after explicit evaluation of the
 c zeroth and first order functions using recurrence relations
 c or polynomial approximation techniques. Reference:
 c A.J.M. Hitchcock, "Polynomial Approximations to Bessel
 c Functions of Order Zero and One and to Related Functions,"
 c MTAC, v11, 1957, pp86-88, and G.N. Watson,
 c "A Treatise on the Theory of Bessel Functions," Cambridge
 c University Press, 1985, p62.

c Evaluation of first and second derivatives of orders 0
 c through n is obtained by means of the formulae:

$$K'(n,z) = -K(n-1,z) - nK(n,z)/z$$

$$K''(n,z) = -K'(n-1,z) - nK'(n,z)/z + nK(n,z)/(z*z)$$

c These formulae may be derived from the general derivative
 c expressions for Bessel functions. See eg.

c Abramowitz & Stegun, "Handbook of Math. Functions," Dover
 c Press. The second derivatives are evaluated correctly
 c in commented-out lines, and are not output.

Error handling:

c The following conditions lead to a diagnostic and halt
 c execution. No other conditions are tested for.

c n < 0 (Function order may not be negative)

c arg <= 0 (Argument may not be 0 or negative)

c x <= 0 (Parameter may not be 0 or negative)

c m1 < n+1 (Col. length of array may not be < n+1)


```

c          m2 < rlt+2      (Row length may not be < RLT+2 )
c
c  .....

subroutine kbessel(arg,x,n,array,m1,m2,rlt)

integer n,m1,m2,rlt
implicit real*8 (a-h)
implicit real*8 (o-z)
dimension t(12),array(m1,m2)

c  test for invalid input parameters--automatic program abort in
c  case of errors. No argument range testing is performed.
if (n) 10,11,11
10  write(6,*) "K Bessel function order ",n," should be positive"
    write(6,*) "Program aborted by routine KBESSEL"
    stop
11  if (arg) 12,12,13
12  write(6,*) "K Bessel argument ",arg," should be positive"
    write(6,*) "Program aborted by routine KBESSEL"
    stop
13  if (x) 14,14,15
14  write(6,*) "K Bessel parameter ",x," should be positive"
    write(6,*) "Program aborted by routine KBESSEL"
    stop
15  if (m1 - (n+1)) 16,17,17
16  write(6,*) "Array columns too short for",n,"Bessel orders"
    write(6,*) "Program aborted by routine KBESSEL"
    stop
17  if (m2 - (rlt+2)) 18,20,20
18  write(6,*) "Not enough columns in Array, dimension",m2
    write(6,*) "Program aborted by routine KBESSEL"
    stop

c  select small or large argument approximation regime
20  if (arg - 1.0) 36,36,25

c  compute K0 and K1 using larger argument approximation
25  b = 1.0/arg
    c = dsqrt(b)
    t(1) = b
    do 26 l=2,12
        t(l) = t(l-1)*b
26  continue

c  compute K0 using polynomial approximation
    xg0 = -arg
    g0 = (1.2533141-0.1566642*t(1)+0.08811128*t(2)-0.09139095*t(3)
2  +0.1344596*t(4)-0.2299850*t(5)+0.3792410*t(6)-0.5247277*t(7)
3  +0.5575368*t(8)-0.4262633*t(9)+0.2184518*t(10)-0.06680977*t(11)
4  +0.009189383*t(12))*c

c  compute K1 using polynomial approximation
    g1 = (1.2533141+0.4699927*t(1)-0.1468583*t(2)+0.1280427*t(3)

```



```

2  -0.1736432*t(4)+0.2847618*t(5)-0.4594342*t(6)+0.6283381*t(7)
3  -0.6632295*t(8)+0.5050239*t(9)-0.2581304*t(10)+0.07880001*t(11)
4  -0.01082418*t(12))*c

c  skip over small argument approximation: go to nth order iterations
   go to 100

c  small argument evaluation: series expansion, first for k0
36  b = arg/2.0
    a = 0.5772157 + dlog(b)
    c = b*b
    g0 = -a
    xg0 = 0.0
    x2j = 1.0
    fact = 1.0
    hj = 0.0
    do 40 j=1,6
        rj = 1.0/dfloat(j)
        x2j = x2j*c
        fact = fact*rj*rj
        hj = hj+rj
        g0 = g0 + x2j*fact*(hj - a)
40  continue

c  compute k1 using series expansion
    x2j = b
    fact = 1.0
    hj = 1.0
    g1 = 1.0/arg + x2j*(0.5 + a - hj)
    do 50 j=2,8
        x2j = x2j*c
        rj = 1.0/dfloat(j)
        fact = fact*rj*rj
        hj = hj + rj
        g1 = g1 + x2j*fact*(0.5 + (a-hj)*dfloat(j))
50  continue

c  Compute the derivatives of K0 and K1; set loop variables for
c  iterative procedure for Kn and derivatives. 2nd derivative values
c  are calculated in commented lines.
100 const = arg/x
    array(1,rlt) = g0
    array(1,rlt+2) = xg0
    dg0 = -const*g1
    array(1,rlt+1) = dg0
c  array(1,**) = const*const*(g0 + g1/arg)
    if (n .eq. 0) return

    array(2,rlt) = g1
    array(2,rlt+2) = xg0
    dg1 = -const*(g0 + g1/arg)
    array(2,rlt+1) = dg1
c  array(2,**) = const*const*(g1 + g0/arg + 2.0*g1/(arg*arg))

```



```

if (n .eq. 1) return

c  Compute Kn and derivatives. Throughout this loop, the current jth
c  order function (gj), current order derivatives (dgj and ddgj) and
c  the previous order function and its first derivative (g1,dg1)
c  are maintained. The exponent for all these
c  the same, and is modified once per iteration only for those
c  functions which will survive into the next iteration.
c  Note that dg1 and dgj incorporate a factor CONST already; this
c  is accounted for in the calculation of ddgj. Calculations of the
c  2nd derivatives are commented out.
do 35 j=2,n
  dflj = dfloat(j)
  gj = 2.0*(dflj - 1.0)*g1/arg + g0
  dgj = -const*(g1 + dflj*gj/arg)
c  ddgj = const*(-dg1 - dflj*dgj/arg + const*dflj*gj/(arg*arg))
  test = dlog(gj)
  exptest = dexp(-test)
  gj = 1.0
  dgj = dgj*exptest
c  ddgj = ddgj*exptest
  g1 = g1*exptest
  xg0 = xg0 + test
  g0 = g1
  g1 = gj
  dg1 = dgj
  array(j+1,rlt) = gj
  array(j+1,rlt+2) = xg0
  array(j+1,rlt+1) = dgj
c  array(j+1,**) = ddgj
35 continue

return
end

c
c  This program evaluates a two dimensional fft by performing a
c  one dimensional fft row by row and then column by column. If id
c  is a positive number then the forward fft is evaluated otherwise
c  the inverse fft is found. Double precision is used throughout.
c
c  The complex*16 array array(i,j) contains the complex signal
c  whose fft is to be found. Real*8 arrays x and
c  y are for work space and have dimension equal to the
c  greater of i and j. m1 is the power to which 2 has to
c  be raised to get i and m2 is the power to which 2 has to be
c  raised to get j. The output is returned in array(i,j). iw is
c  the dimension of the work arrays x and y and must be greater
c  than either i or j whichever is larger.
c
c  Subroutines used ::
c      fftd2 :: the one dimensional fft routine
c

```



```

c      Subroutine call format ::
c      ffd2 :: call ffd2(x,y,n,n2,id)
c      where x is the real part of the
c      input data and the
c      Fourier transform
c      y is the imaginary part of
c      the input data and the
c      Fourier transform
c      n the fft length
c      n2 is the power to which 2
c      must be raised to obtain
c      n
c      and id is a positive integer if
c      the forward fft is
c      desired and is negative
c      otherwise
c
c      subroutine dfft2d (array,x,y,i,m1,j,m2,id,iw)

c      integer i,m1,j,m2,id,iw
c      complex*16 array(i,j)
c      real*8 x(iw),y(iw)
c      implicit real*8 (b-h,o-z)

c      Perform row by row ffts working from (i,1) to (i,j)
do 5 k=1,i
  do 10 l=1,j
    x(l) = dreal(array(k,l))
    y(l) = dimag(array(k,l))
10    continue
    call ffd2(x,y,j,m2,id)
    do 15 l=1,j
      array(k,l) = dcmlpx(x(l),y(l))
15    continue
5    continue

c      Perform col by col ffts working from (1,j) to (i,j)
do 20 k=1,j
  do 25 l=1,i
    x(l) = dreal(array(l,k))
    y(l) = dimag(array(l,k))
25    continue
    call ffd2(x,y,i,m1,id)
    do 30 l=1,i
      array(l,k) = dcmlpx(x(l),y(l))
30    continue
20    continue
  return
end

c      subroutine to compute n point complex dft for n=2**m.
c      the algorithm is the radix 2 common factor with decimation

```



```

c      in frequency.
c      the maximum value of n is 8192.
c
c      Subroutines used :: None required
c
c      the call is fftd2(x,y,n,mi,inv)
c          where x is the real part of the input array
c          y is the imaginary part of the input array
c          n is the length of the fft
c          mi is the power to which 2 is raised to get n
c          inv is the flag which is negative for an inverse
c              fft and positive otherwise
c      the output is returned in arrays x and y.
c
c
c      subroutine fftd2(x,y,n,mi,inv)
c      implicit real*8 (a-h,o-z)
c      dimension fcos(4100),x(n),y(n)
c      fn=n
c      confn=1.d0/float(n)
c      fm=dlog(fn)/dlog(2.d0)
c      m=ifix(fm+.1)
c      nt=2**m
c      if(nt.ne.n) go to 1000
c      if(mi.ne.m) go to 1000
c
c      calculate table of sines and cosines
c
c      pi=3.14159265
c      angle=2.d0*pi*confn
c      if(inv.lt.0) angle=-angle
c      n3q=(3*n)/4
c      do 10 i=1,n3q
c          angk=angle*float(i-1)
c          fcos(i)=dcos(angk)
10  continue
c
c      start fft computation
c
c      use l as counter for stages 1-m
c      do 100 l=1,m
c      ***** define parameters that change with l
c          l21=2**l
c          n21=n/l21
c          l212=2**(l-1)
c          n212=n/l212
c      ***** use j counter for each sub-stage of consecutive
c          butterflies.
c          do 200 j=1,l212
c      ioffse will define number of indices to jump from one
c          sub-stage to another.
c          ioffse=(j-1)*n212
c      use k counter for consecutive butterflies in sub-stage j.
c          do 300 k=1,n21

```



```

c      define both indices for input to butterfly.
          index1=k+ioffse
          index2=index1+n21
c      calculate index indw for accessing sines and cosines.
          indw=1+(k-1)*1212
          indw1=indw+(n/4)
c
c      start butterfly
c
          tr=x(index1)-x(index2)
          ti=y(index1)-y(index2)
          x(index1)=x(index1)+x(index2)
          y(index1)=y(index1)+y(index2)
          if(inv.lt.0) go to 333
          x(index2)=tr*fcos(indw)-ti*fcos(indw1)
          y(index2)=ti*fcos(indw)+tr*fcos(indw1)
          go to 300
333      x(index2)=tr*fcos(indw)+ti*fcos(indw1)
          y(index2)=ti*fcos(indw)-tr*fcos(indw1)
300      continue
200      continue
100      continue
c
c      scale by 1/n if inverse fft is being found
c
          if(inv.ge.0) go to 390
          do 350 k=1,n
              x(k)=x(k)*confn
              y(k)=y(k)*confn
350      continue
c
c      start bit reversing
c
390      do 400 k=1,n-1
          km=k-1
c      get bit reversed value of counter (minus 1) k
          l=nbitre(km,m)+1
          if(l.le.k) go to 400
c      interchange if above condition is not satisfied
          tr=x(l)
          ti=y(l)
          x(l)=x(k)
          y(l)=y(k)
          x(k)=tr
          y(k)=ti
400      continue
c
          return
1000     write(6,1010) n
1010     format(' error in fftd2 size n =',i5)
          stop
          end

```



```
c      function to calculate bit reverse value of k for m bit
c      representation.
c      integer function nbitre(k,m)
c      initialize sum to 0
      kbr=0
      io=k
      do 10 j=1,m
c      get least significant bit
          ibit=io-2*(io/2)
c      shift to the right for next time
          io=io/2
c      add contributions of this bit to total
          kbr=kbr+ibit*2**(m-j)
10      continue
      nbitre=kbr
      return
      end
```


References

- [1] Abramowitz, M. and I.A. Stegun, *Handbook of Mathematical Functions*, Dover Publications, Inc., N.Y., 1965.
- [2] Adrian, R. and L. Peachey, "Reconstruction of the action potential of frog sartorius muscle", *J. Physiol.*, **235**, 103-121, 1973.
- [3] Andreassen, S. and A. Rosenfalck, "Relationship of intracellular and extracellular action potentials of skeletal muscle fibers", *CRC Critical Reviews in Bioengineering*, 267-306, 1981.
- [4] Bernstein, J., *Untersuchungen über den Erregungsvorgang im Nerven- und Muskelsystem*, Heidelberg, 1-240, 1871.
- [5] Bostock, H. and T.A. Sears, "The internodal axon membrane: electrical excitability and continuous conduction in segmental demyelination", *J. Physiol.*, **280**, 273-301, 1978.
- [6] Brismar, T., "Potential clamp analysis of membrane currents in rat myelinated nerve fibers", *J. Physiol.*, **313**, 301-315, 1980.
- [7] Buchthal, F., C. Guld and P. Rosenfalk, "Volume conduction of the spike of the motor unit potential investigated with a new type of multielectrode", *Acta. physiol. scand.*, **38**, 331-354, 1957a.
- [8] Buchthal, F., C. Guld and P. Rosenfalk, "Multielectrode study of the territory of a motor unit", *Acta. physiol. scand.*, **39**, 83-104, 1957b.
- [9] Buchthal, F. and P. Rosenfalk, "Evoked action potentials and conduction velocity in human sensory nerves", *Brain Research*, **3**, 1-122, 1966.
- [10] Buchthal, F. and P. Rosenfalk, "Spontaneous electrical activity of human muscle", *Electroenceph. clin. Neurophysiol.*, **20**, 321-336, 1966.
- [11] Burger, H.C. and R. van Dongen, "Specific electric resistance of body tissues", *Physics Med. Biol.*, **5**, 431-447, 1960-61.
- [12] Chiu, S.Y., J.M. Ritchie, R.B. Rogart and D. Stagg, "A quantitative description of membrane currents in rabbit myelinated nerve", *J. Physiol.*, **292**, 149-166, 1979.
- [13] Clark, J.W. and R. Plonsey, "A mathematical evaluation of the core conductor model," *Biophysical J.*, **6**, 95-112, 1966.
- [14] Clark, J.W. and R. Plonsey, "The extracellular potential field of the single active nerve fiber in a volume conductor," *Biophysical J.*, **8**, 842-864, 1968.
- [15] Clark, J.W. and R. Plonsey, "A mathematical study of nerve fiber interaction", *Biophysical J.*, **10**, 937-957, 1970.

- [16] Craib, W.H., "A study of the electrical field surrounding skeletal muscle", J.Physiol., 66, 95-112, 1928.
- [17] Craib, W.H. and R. Canfield, "A study of the electrical field surrounding active heart muscle", Heart, 14, 71-106, 1927.
- [18] Crank, J. and P. Nicholson, "A practical method for the numerical evaluation of solutions of partial differential equations of the heat conduction type", Proc. Camb. Philo. Soc. (Math. Phy. Sci.) 43, 50-67, 1947.
- [19] Elmqvist, D., T. Johns and S. Thesleff, "A study of some electrophysiological properties of human intercostal muscle", J. Physiol., 154, 602-607, 1960.
- [20] Frankenhaeuser, B. and A.F. Huxley, "The action potential in the myelinated nerve fiber of *Xenopus Laevis* as computed on the basis of voltage clamp data", J. Physiol. 171, 302-315, 1964.
- [21] Ganapathy, N., J.W. Clark, O.B. Wilson and W. Giles, "Forward and Inverse Potential Field Solutions for Cardiac Strands of Cylindrical Geometry", IEEE Trans. BME., 32, 566-577, 1985.
- [22] Geddes, L.A. and L.E. Baker, "The specific resistance of biological material -- a compendium of data for the biomedical engineer and physiologist", Med. & biol. Engg., 5, 271-293, 1967.
- [23] Goldman, L. and J.S. Albus, "Computation of impulse conduction in myelinated fibers; theoretical basis of the velocity-diameter relation", Biophysical Journal 8, 596-607, 1968.
- [24] Greco, E. C., J. W. Clark and T. L. Harman, "Solution of the forward and inverse problems associated with the potential field of a single active nerve fiber in a volume conductor", Mathematical Biosciences 33, 235-256, 1977.
- [25] Green, R.M., *A translation of Luigi Galvani's De Viribus Electricitatis In Motu Musculari Commentarius. Commentary on the effect of electricity on muscular motion*, E. Licht. Publ., Cambridge, Mass., 1-97, 1953.
- [26] Hermann, L. *Handbuch der Physiologie*, Leipzig, Vogel, 2, 1879.
- [27] Hodgkin, A. L. and A. F. Huxley, "A quantitative description of membrane current and its application to conduction and excitation in nerve", J. Physiol. 117, 500-544, 1952.
- [28] Horakova, M., W. Nonner and R. Stampfli, "Action potentials and voltage-clamp currents of single rat Ranvier nodes", Proc. int. Union. physiol. Sci., 7, 198, 1968.
- [29] Kocsis, J.D. and S.G. Waxman, "Absence of potassium conductance in central myelinated axons", Nature, 287, 348-349, 1980.
- [30] Lipicky, R., S. Bryant and J. Salmon, "Cable parameters, sodium, potassium, chloride and water content and potassium efflux in isolated external intercostal muscle of normal volunteers and patients with myotonia congenita", J. Clin. Invest., 50, 2091-2103, 1971.

- [31] Lorente de No, R., "A study of nerve physiology, Chapter XVI, Analysis of the action currents of nerve in volume conductors", *Studies from the Rockefeller Institute for Medical Research*, 132, 384-477, 1947a.
- [32] Lorente de No, R., "Action potential of the motoneurons of the hypoglossus nucleus", *J. cell. comp. Physiol.*, 29, 207-288, 1947b.
- [33] Oppenheim, A.V. and R.W. Schaffer, *Digital Signal Processing*, Englewood Cliffs, NJ, Prentice Hall, 1975.
- [34] Paintal, A.S., "Effects of temperature on conduction in single vagal and saphenous myelinated nerve fibers of the cat", *J. Physiol.*, 180, 20-49, 1965.
- [35] Paintal, A.S., "The influence of diameter of medullated nerve fibers of cats on the rising and falling phases of the spike and its recovery", *J. Physiol.*, 184, 791, 1966.
- [36] Rasminsky, M. and T.A. Sears, "Internodal conduction in undissected demyelinated nerve fibers", *J. Physiol.*, 227, 323-350, 1972.
- [37] Rosenfalck, P. and F. Buchthal, "Volume conducted action potentials and their correlation to the intracellular potentials", *Acta. physiol. scand.*, 42, 118-119, 1957.
- [38] Rosenfalck, P. and F. Buchthal, "Studies on the fibrillation potentials of denervated human muscle", *Electroenceph. clin. Neurophysiol.*, 130-132, 1962.
- [39] Rosenfalck, P., "Intra- and Extracellular potential fields of active nerve and muscle fibers", *Acta Physiol. scand.*, 75 : suppl (321), 1-68, 1969.
- [40] Smith, G.D., *Numerical Solution of Partial Differential Equations*, Clarendon Press, Oxford, 1978.
- [41] Stalberg, E. and J.V. Trontelj, *Single Fiber Electromyography*, Mirvalle Press Ltd., Old Woking, Surrey, U.K., 1979.
- [42] Tasaki, I., and N. Tasaki, "The electrical field which a transmitting nerve fiber produces in the fluid medium", *Biochim. Biophys. Acta*, 5, 335-342, 1950.
- [43] Wilson, O.B., J.W. Clark, Jr., N. Ganapathy and T.L. Harman, "Potential field from an active nerve in an inhomogeneous, anisotropic volume conductor", *IEEE Trans. BME*, 32, 1032-1041, 1985.